THE MECHANICAL ROLE OF GAGS IN THE AORTIC VALVE

Liyong Jia

Submitted for the degree of Doctor of Philosophy,

Queen Mary, University of London

School of Engineering and Materials Science

Queen Mary, University of London

2015

Statement of originality

I, Liyong Jia, confirm that the research included within this thesis is my own work or that where it has been carried out in collaboration with, or supported by others, that this is duly acknowledged below and my contribution indicated. Previously published material is also acknowledged below.

I attest that I have exercised reasonable care to ensure that the work is original, and does not to the best of my knowledge break any UK law, infringe any third party's copyright or other Intellectual Property Right, or contain any confidential material.

I accept that the College has the right to use plagiarism detection software to check the electronic version of the thesis.

I confirm that this thesis has not been previously submitted for the award of a degree by this or any other university.

The copyright of this thesis rests with the author and no quotation from it or information derived from it may be published without the prior written consent of the author.

Signature: *Liyong JIA*

Date: 12 August 2016

Abstract

Aortic valve (AV) dysfunction accounts for ~43% of all valvular disease. There is huge demand for improved prosthetic valves, but to develop such replacements, it is first critical to understand structure-function mechanics of the native valve, to provide insight into how we can replicate these functions. The AV is composed of three layers, namely the fibrosa, spongiosa, and ventricularis, each with a distinct matrix composition and organisation. The central spongiosa is rich in glycosaminoglycans (GAGs) and thought to be critical in facilitating valve flexion and maintaining structural integrity during loading. This study focuses on the effects of GAGs on AV mechanics and micromechanics, comparing native AV leaflets, with leaflets treated with Chondroitinase ABC and hyaluronidase to remove GAGs. GAG digestion had no effect on gross quasi-static tensile properties of leaflets. However, micro-mechanical analysis highlighted the importance of GAGs in modulating stiffness across the width of a leaflet in the radial direction. Native AV leaflets were stiffest free edge region, with stiffness correlating to spongiosa thickness. Digesting GAGs led to homogenous strains across the leaflet, suggesting GAGs may play a critical role in modulating stiffness of AV leaflets in a localized manner, to control AV micro-mechanics for optimal mechanical function.

Table of Contents

Acknowledgements

Firstly, I would like to acknowledge the China Scholarship Council for their generous funding of this project.

I would like to thank my primary supervisor Prof Hazel Screen for her invaluable support and guidance over the last four years.

I am also very grateful to Prof Wang for his advice and support.

I would also thank all my colleagues and friends at the School of Engineering and Materials Science, QMUL. In particular my thanks go to Dr Chavaunne Thorpe for his assistance with the rig setting and stain methods.

I would like to thank George from Barts and The London School of Medicine and Dentistry for his assistance with histology.

I would like to thank my dear friend, Xiaojing, Zhao, and Huihui for helps over the last four year in London.

Finally, I would like to thanks my parents and wife for their support and encouragement while completing my thesis.

List of Figures

List of Tables

Chapter One

Literature Review

1.1. Heart Valve function, haemodynamics and structure

1.1.1. The heart and heart valves

The heart is an organ of particularly complicated configuration, composed of four chambers, which fill alternately to deliver blood to both the lungs for oxygenation and the systemic circulation and organs for metabolic nutrition and exchange [1, 2]. There are 2 primary circulatory loops in the human body: the pulmonary circulation loop and the systemic circulation loop [1, 2]. Pulmonary circulation transports deoxygenated blood from the right side of the heart to the lungs, where the blood picks up oxygen, to return to the left side of the heart. The pumping chambers of the heart that support the pulmonary circulation loop are the right atrium and right ventricle. Systemic circulation carries highly oxygenated blood from the left side of the heart to all of the tissues of the body (with the exception of the heart and lungs). Systemic circulation removes waste from body tissues and returns deoxygenated blood to the right side of the heart. The left atrium and left ventricle of the heart are the pumping chambers for the systemic circulation loop [3]. Undoubtedly, this indispensable function is crucially important for our health. To maintain this function, heart valves are necessary as they play a vital role in maintaining the unidirectional flow of blood during the cardiac cycle [4, 5].

There are four different valves in the heart: tricuspid valve (TV); pulmonary valve (PV); mitral valve (MV); and aortic valve (AV) [5, 6]. Two views of these four valves are shown in **Fig.1- 1**. Depending on their anatomical positions in the heart, these four heart valves are divided into two types: the semilunar valves and the atrio-ventricular valves.

The PV and AV are termed semilunar valves, due to the half-moon shape of their leaflets [5, 7-9], and they lie between the ventricle and the great vessel on each side of the heart from which their name derives (**Fig.1- 1**). The TV and MV are termed atrio-ventricular valves as they lie between the atrium and ventricle on both the right and left sides of the heart, respectively (**Fig.1- 1**).

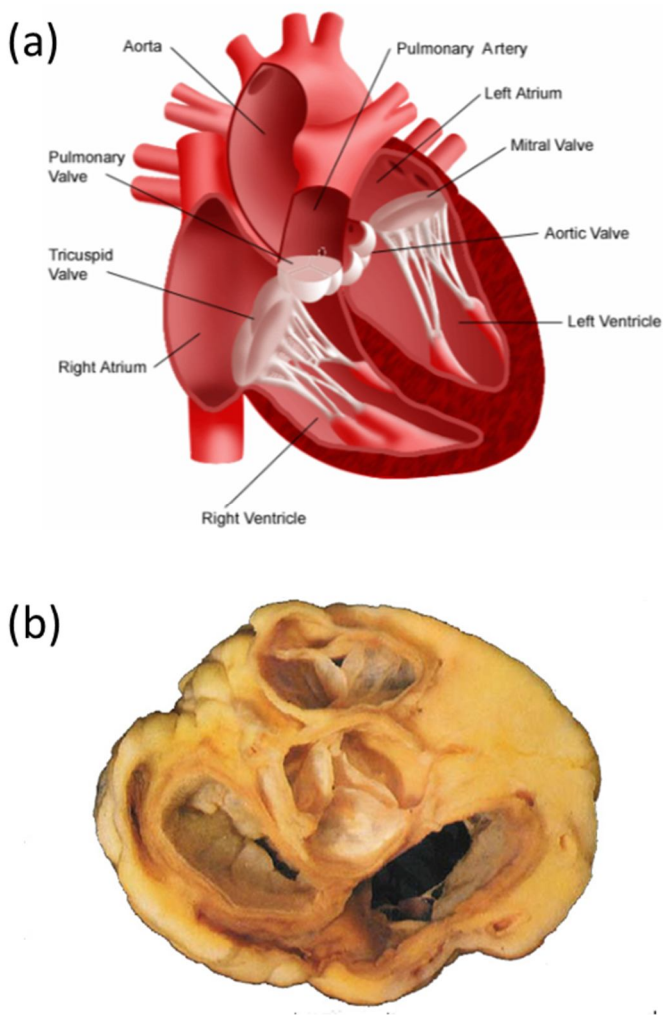

Fig.1- 1. Anatomic structure of heart (a) (adapted from http://nyp.org/health/cardiac-valves.html and view of the four heart valves (b), viewed from above (adapted from [4]).

1.1.2. Function and haemodynamics

The most important physiological role of a heart valve is to regulate the direction of blood flow. The tricuspid and pulmonary valves on the right side of the heart regulate the flow of blood that is returned from the body to the lungs for oxygenation, whereas the mitral and aortic valves on the left side of the heart control the flow of oxygenated blood to the body. The aortic and pulmonary valves allow blood to be pumped from the ventricles into the arteries on the left and right sides of the heart, respectively. Similarly, the mitral and tricuspid valves regulate blood flow between the atria and ventricles of the left and right sides of the heart, respectively. The aortic and pulmonic valves open during systole when the ventricles are contracting and close during diastole when the ventricles are filling through the opening of mitral and tricuspid valves. During isovolumic contraction and relaxation, all four valves are closed [10]. The directional flow of blood and opening-closing periods of heart valves are shown within the cardiac cycle in **Fig.1- 2**. The time period for one complete cycle is about 0.8 seconds. Blood flows from the aorta to the major arteries, small arteries, arterioles, capillaries, venioles, and veins throughout the body, finally returning through the tricuspid valve to the top right chamber of the heart (**Fig.1- 2**). Heart valves have the ability to allow between 1 and 20 litres of blood per minute to run through them during rest, exercise, or other physiological or pathological conditions [4]. The cardiac cycle permits blood to circulate and transport nutrients (such as amino acids and electrolytes), oxygen, carbon dioxide, hormones, and blood cells to and from the

cells in the body to provide nourishment and help in fighting diseases, stabilize temperature and pH, and maintain homeostasis.

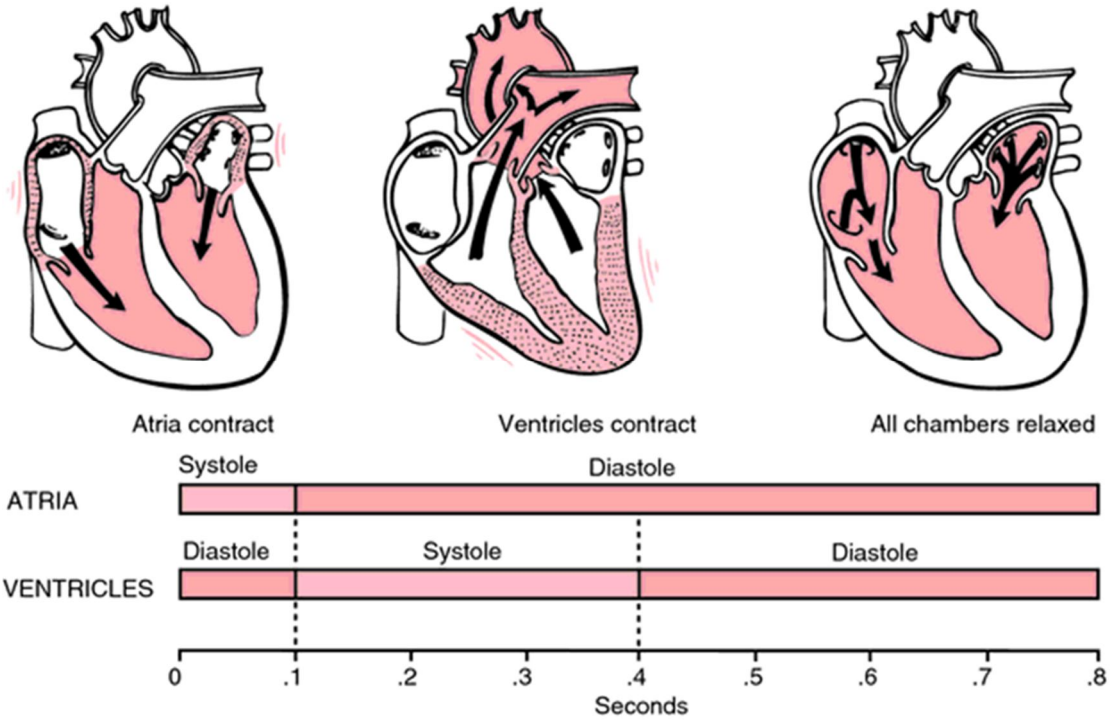

Fig.1- 2. Cardiac cycle (adapt from Applegate, 2000).

Heart valves are passive cardiac structures, i.e. opening and closure is controlled by the surrounding haemodynamic environment [5, 7]. Although the four heart valves each have different anatomies (**Fig.1- 1**), and different opening/closing characteristics (described in followed text), they are classified together as they all have the same key function of ensuring the unidirectional flow of blood while maximizing flow rate and minimizing resistance to flow. During diastole, when the right and left ventricles are filling [10], the TV and the MV are open to allow blood to pass from the atria into the ventricles. To keep pressure in the ventricles low enough, the PV and AV are closed.

Once the ventricles are full, they contract opening the semilunar valves (AV and PV), ejecting the blood into the great vessels. To prevent retrograde blood flow into the atria, the MV and TV close during systole. The opening and closing of the valves during diastole/systole is shown in **Fig.1- 2**. This is essential for two reasons: 1) it allows the heart to generate contractile forces sufficient to propel the blood to either the lungs or the systemic circulation; 2) it allows the myocardial muscle tissue of the heart to receive the necessary metabolic nutrients it needs during diastole [7, 10].

In healthy individuals, blood flow through the AV accelerates to a peak value of 1.35 ± 0.35 m/s [5]. The normal physiological transvalvular pressure on the AV is 80 mmHg [10-12], about 8-times higher than the pressure on the PV [10]. The AV and PV close near the end of the deceleration phase of systole (**Fig.1- 2** and **Fig.1- 3**). When closed, the free edges of the three leaflets coapt to prohibit back flow of blood into the ventricle. They must replicate this feat with each heart-beat. Over a typical lifetime, the valves will open and close an average of 3×10^9 times [5, 6]. The higher pressures on the right side of the heart mean that the AV is much more prone to damage than the PV, and there has been considerable research focused on establishing its physiological environment. From the fully open situation, closure of the AV takes about 50ms [5], during which the AV leaflets experience in vivo strains of approximately 10.1% and 30.8% in the circumferential and radial directions, respectively [13]. The in vivo strain rates have been reported to be 440% ± 80% s^{-1} circumferentially, and 1240% ± 160% s^{-1} radially [13], resulting in overall typical stresses in the AV in the range of 250-400 kPa [9, 12]. The AV closes near the end of

the deceleration phase of systole with very little reverse flow through the valve [5-7, 14]. The small amount of reverse flow that does occur is thought to facilitate movement of the AV leaflets away from the sinus wall and towards the closed position. When this force is coupled with the vortices that push the leaflet surfaces towards the closed position, a very efficient and fast closure is obtained. Studies indicated that the coronary sinuses contribute to the function of the AV as they enhance the reverse flow [5-7, 14]. Indeed in vitro studies have shown that the axial pressure difference alone is sufficient to close the valve [5, 6], but, without the vortices in the sinuses and reverse flow, the closure is not as efficient.

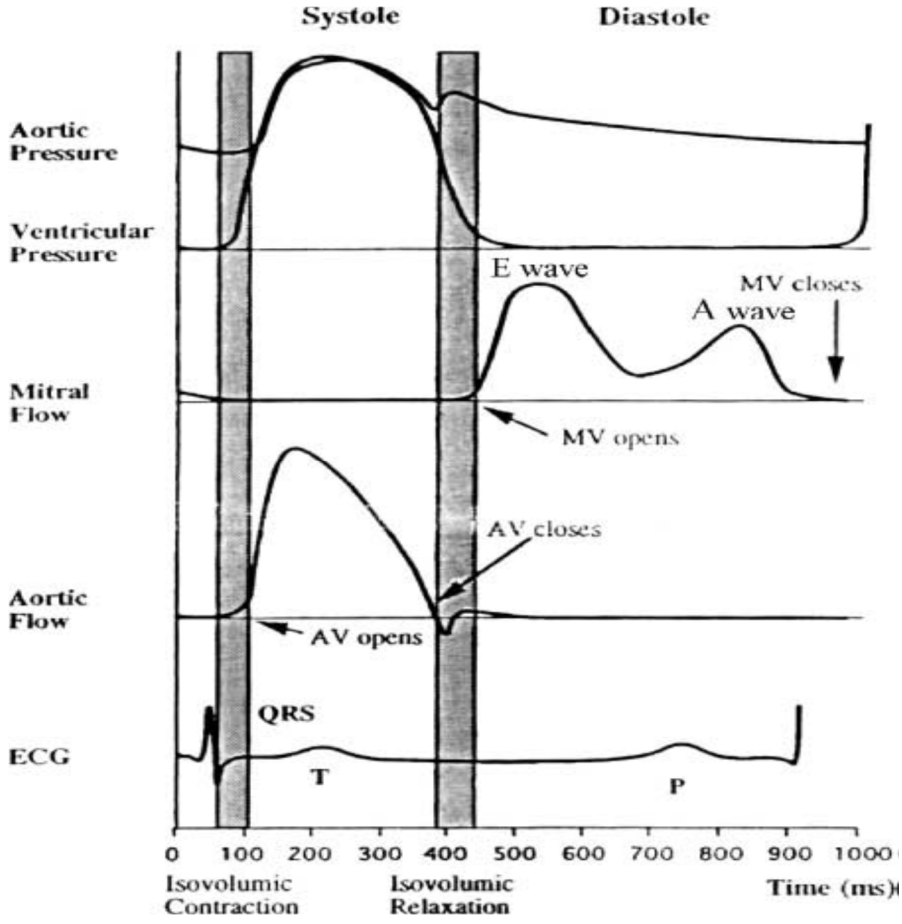

Fig.1- 3. Typical pressure and flow curves for the aortic and mitral valves (adapted from [10]).

During the cardiac cycle, a number of heart sounds can be heard. The sounds emitted by a human heart during a single cardiac cycle consists of two dominant events, known as the first heart sound S1 and the second heart sound S2. S1 relates to the closing of the mitral and tricuspid valves whilst S2 is generated by the closing of the aortic and pulmonary valves leaflets [8, 9]. Specifically, the sounds reflect the turbulence created when the heart valves snap shut. In cardiac auscultation, an examiner may use a stethoscope to listen for these unique and distinct sounds that provide important auditory data regarding the condition of the heart. In addition to these normal sounds, a variety of other sounds may be present, including heart murmurs, adventitious sounds, and gallop rhythms S3 and S4 [10]. Heart murmurs are generated by the turbulent flow of blood, which may occur inside or outside the heart [15, 16]. Murmurs may be physiological (benign) or pathological (abnormal). Abnormal murmurs can be caused by stenosis restricting the opening of a heart valve [17], resulting in turbulence as blood flows through it. Abnormal murmurs may also occur with valvular insufficiency (regurgitation), where incompetent valve closure allows some backflow of blood. Different murmurs are audible in different parts of the cardiac cycle, depending on the cause of the murmur.

1.2. Composition and structure

The quantity, quality, and architecture of the extracellular matrix (ECM), particularly collagen, elastin, and GAGs, in addition to the cells in the valve, are the major determinants of not only the short-term function but also the long-term (lifetime) durability of a valve.

1.2.1. The cells of the aortic valve

The AV cusps contain two cell types: aortic valve endothelial cell (AVEC) and aortic valve interstitial cells (AVICs). The AVICs make up the majority of cells within the valve, while the AVECs form single cell monolayers on the valve surface (

Fig.1- 4

) [18, 19].

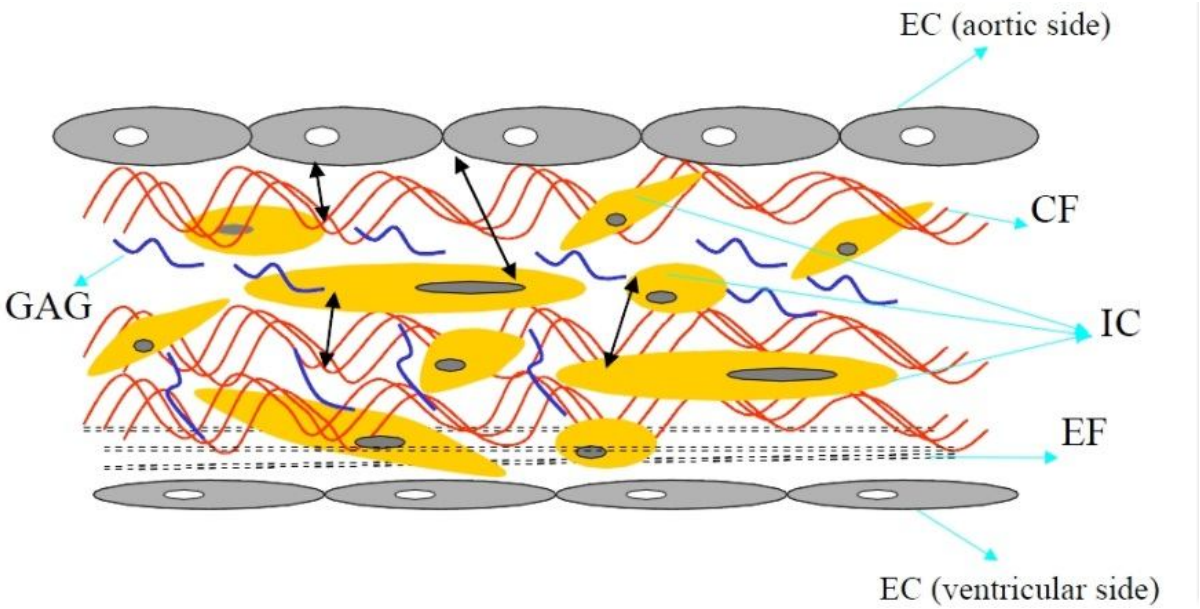

Fig.1- 4. Schematic showing the leaflet structure, EC: endothelial cells, IC: interstitial cells, CF: collagen fibers, EF: elastic fibers, GAG: glycoaminoglycans, ⟷ : cell-cell, cell-matrix interactions (adapt from Yun Xing, 2005).

1.2.1.1. Aortic valve endothelial cell

AVECs, along with the basement membrane, form the endothelium surrounding the valve surface, serving as a barrier between the bloodstream and the tissue [20]. The

AVECs align perpendicularly to flow [21, 22].

AVECs play a key role in protecting the leaflet from inflammatory and thrombotic factors, and maintaining leaflet homeostasis [23-26]. Their dysfunction is a key factor in the etiology of calcific aortic valve disease (CAVD) [27, 28], where it is believed that endothelial dysfunction leads to infiltration of low-density lipoprotein (LDL) and starts the progression towards inflammation, AVIC activation, and calcific stenosis [29, 30].

AVECs are also responsive to their mechanical environment, particularly side-specific flow patterns. On the outflow side, blood moves in a low magnitude oscillatory pattern, whereas on the inflow side, blood moves in a high magnitude laminar pattern [31-36]. In the leaflet, the outflow side calcifies preferentially to the inflow side, suggesting that the flow pattern on the outflow side influences endothelial dysfunction and calcification [29, 30]. An altered hemodynamic profile on the outflow side of leaflets has been shown to induce cell adhesion molecules, bone morphogenic protein-4 (BMP-4), and transforming growth factor (TGF-β1) [37]. Recent studies suggests that the AVEC on the two sides of the AV leaflet show differential gene expression profiles due to the differences in flow pattern between the two sides of the valve [38, 39].

1.2.1.2. Aortic valve interstitial cells

The AVICs are a heterogeneous population of cells that make up the interior of the leaflet (

Fig.1- 4

) [40, 41], and constitute 30% of the volumetric density of the leaflet [41, 42]. Phenotypic studies suggest the presence of at least three distinct populations of cells within the matrix [41, 43]: 1) a quiescent vimentin-positive fibroblast phenotype, whose role is homeostatic matrix remodeling [41, 44-46]; 2) a smooth muscle a-actin (SMA)-positive population of cells, which are thought to be involved in proliferation and migration [41, 43]; 3) fetal-like smooth muscle cells located in the fibrosa with an unclear role [44, 47]. Valve interstitial cells represent a dynamic population of cells and the phenotype of valve cells is influenced by both complex genetic programming as well as the local hemodynamic factors [25, 48, 49]. AVICs can move from one phenotype to another during the lifespan of a cell, allowing them to adapt to their environment [45, 46].

The AVICs are believed to play a critical role in normal functioning of the valve and in the initiation and progression of valve pathology [18]. The main function of AVICs is to maintain the extracellular matrix of the AV leaflet [41]. AVICs have been shown to synthesize collagen, elastin, fibronectin, and chondroitin sulfate [50, 51]. AVICs produce MMPs and prolyl-4-hydxoylase (P4H), indicating a role in matrix synthesis, and matrix remodeling [41, 45, 51]. Other studies shown that AVICs can regulate

vascular tone, inflammation and thrombosis, and are also responsive to their mechanical environment [52]. Their dysfunction has been linked with multiple disorders [32, 53].

1.2.2. Extracellular matrix

The main cellular and extracellular matrix components of the aortic valve are shown in **Table 1- 1**.

Table 1- 1 Key cellular and extracellular matrix components of the aortic valve (modified from [54]).

Component	Location	Putative Function
Endothelial cells	Lining inflow and outflow valve surfaces	Provides thromboresistance, mediation of inflammation
Interstitial cells	Deep to surface, throughout all layers	Synthesis and remodeling matrix elements
Elastin	Concentrated in the ventricularis layer	Extends in diastole, recoils in systole
GAGs	Concentrated in the spongiosa layer	Absorbs shear of relative movements and cushions shock between the ventricularis and fibrosa during cyclical valve motion
Collagen	Concentrated in the fibrous layer	Provides strength and stiffness to maintain

1.2.2.1. Collagen

In our body, collagens are ubiquitous, and found in skin [55, 56], bone [57, 58], tendon [59-62], intervertebral disc [63, 64], ligaments [65, 66] , blood vessels [67-69], eyes [70] and heart valves [71, 72]. The role of collagen in the AV is to provide strength and stiffness to maintain coaptation during diastole [54, 71].

The structure of fibrillar collagens is hierarchical, with the most basic structure being the tropocollagen molecule, which is formed by the hydroxylation and folding of α-chains and the subsequent removal of amine and carboxyl groups [73]. Tropocollagen molecules then assemble into 20-400 nm diameter fibrils, which are stabilized by lysyl oxidase (LOX) cross-links between lysine residues on the α-chains. Fibrils further bundle and organize into 0.2-12 μm diameter fibers [73, 74]. At this level, collagen exhibits a planar, wavy configuration known as crimp, which is a result of compressive forces from the surrounding ECM that buckle the collagen fibers (**Fig.1-5**). The unfolding of crimp under tension is the primary source of extensibility in collagenous tissues [74].

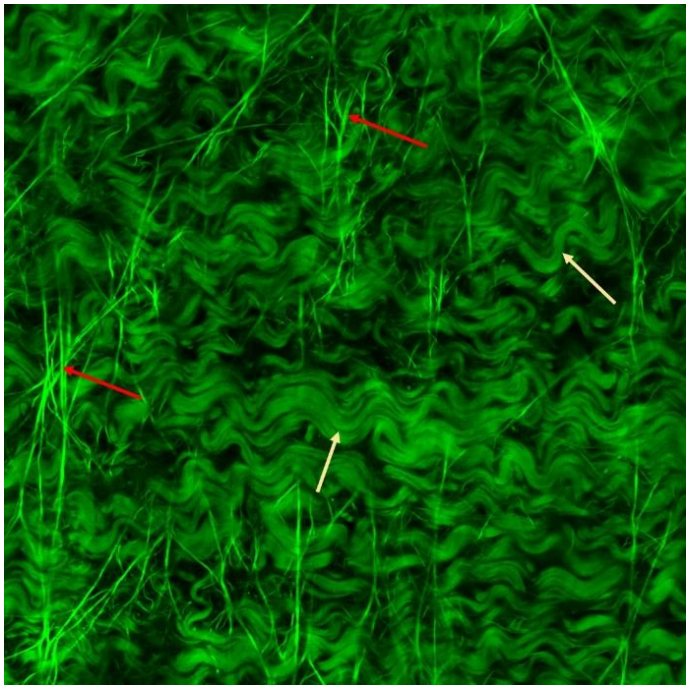

Fig.1- 5. Aortic valves tissue stained with 5-DTAF showing the collagen (yellow arrow) and elastin (red arrow).

1.2.2.2. Elastin

Elastin is very important in the lungs [75-77], elastic ligaments [78] intervertebral disk [78], skin [77, 79, 80], bladder [81-83], aorta [84, 85] and heart valves.

Elastin consists of the more basic molecule tropoelastin, which is made of alternating proline-rich hydrophobic and lysine-rich cross-link domains [86, 87]. Tropoelastin is aligned into fibers so that cross-linking domains are adjacent and crosslinked by LOX [86]. Elastin is then surrounded by a sheath of microfibrils to form the elastic fiber [86, 87]. Microfibrils are a collection of proteins that regulate elastic fiber assembly, with fibrillin being the most important, as it binds to elastin and maintains fiber integrity.

In the heart valve, these elastin fibers are further organized into dense continuous sheets [86-88].

Elastic fibers are hypothesized to have multiple roles in aortic valves [88]. First, the compliant elastic fibers permit radial stretch, which allows the leaflet to extend in diastole to close the valve [89, 90]. Second, elastin ensures recoil in the leaflets, to return the structure to its original unloaded configuration [9, 89-92]. It has also been found that elastin takes a role in connecting elastic fibers in one layer of the valve to collagen in another, coupling the two layers and distributing stress between collagen and elastic fibers [9, 93, 94].

1.2.2.3. Glycosaminoglycans

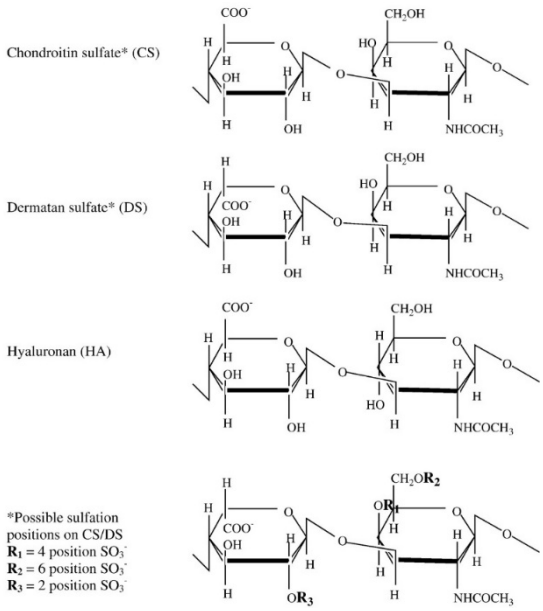

Fig.1- 6. Repeating disaccharide units and possible sulfation positions of the glycosaminoglycan chains found in aortic valve proteoglycans (adapt from [95])

GAGs are composed of linear long chains of repeating disaccharide units[96]. Each disaccharide consists of a uronic acid and an amino sugar. Depending on the GAG type, the uronic acid could be either glucuronic or iduronic acid (**Table 1- 2**), and the amino sugar could be either either N-acetylglucosamine or N-acetylgalactosamine, which can then be sulfated at the 2, 4, or 6 position (**Fig.1- 6**) [95, 96]). Four families of GAGs have been defined: 1) hyaluronan (HA), 2) heparin/heparan sulfate (HS), 3) chondroitin sulfate (CS)/ dermatan sulfate (DS), and 4) keratan sulfate (KS). When GAGs are attached to a protein core through a covalent linkage, the unit is called a proteoglycan. All GAGs existed as part of a proteoglycan *in vivo* expect hyaluronan [95, 96]).

Table 1- 2 The Proteoglycans/GAGs of human aortic valves adapt from [95, 96])

Glycosaminoglycan	Uronic acid	Hexosamine	Proteoglycans
Hyaluronan	**Glucuronic**	**N-acetylglucosamine**	**Hyaluronan**
Chondroitin sulfate	**Glucuronic**	**N-cetylgalactosamine**	**Versican/ Decorin/Biglycan**
Dermatan sulfate	**Glucuronic** / Iduronic	**N-cetylgalactosamine**	**Decorin /Biglycan**

The negatively charged glycosaminoglycans (GAGs) are important in the ECM of aortic valves as they can absorb shear and cushion shock as the valve flexes and strains. The roles of GAGs in the aortic valve, especially their influence on AV mechanical properties is a main area of investigation in this thesis.

1.2.3. Structure

As shown in **Fig.1- 1**(a), the aortic valve is compose of three half-moon shaped leaflets [5, 7-9]. Each leaflet of the aortic valve has a structure divided into the three sublayers, namely the fibrosa, spongiosa, and ventricularis. The three layered structure of the aortic valve is shown in **Fig.1- 7** [6, 9, 97-100]. As shown in **Table 1- 3**, each layer has a different composition of ECM components. Although overall the GAGs were are predominantly found exit in the spongiosa, some specific types of GAGs are more prevalent in other layers (**Table 1- 3**).

Table 1- 3 Distribution of ECM components within the aortic valve leaflet indicating in which layer the majority of each component is found (adapt from [101] and [102]). f = fibrosa, sp = spongiosa, v = ventricularis.

ECM	Component
Collagen	**f > v > sp**
Elastin	**v > sp > f**
Decorin	**v > sp,f**
Biglycan	**v >> sp > f**
Versican	**sp > v > f**
Hyalurona	**sp > v > f**
fibrillin	**sp > v > f**

1.2.3.1. Fibrosa

The fibrosa, which is the thickest of the three layers, at approximately 317.1μm, faces the aorta [9]. When the valve is relaxed, the fibrosa exhibits corrugations along the circumferential direction (fig.1-4 (b) and (f)), which enable the fibrosa to expand radially during diastole. The fibrosa consists primarily of a dense network of type I collagen fibres [9, 103, 104]. Collagen fibres can withstand high tensile forces, but have low torsional and flexural stiffness, making the fibrosa the strongest and stiffest layer of the valve. Functionally, it is the main loading bearing layer and provides a collagen network extending over the entire leaflet surface [5, 6, 8, 105]. The fibrosa also contains elastic fibres. Elastic fibres store energy by stretching as the valve is loaded, releasing it to facilitate efficient recoil during unloading, thus allowing the valve to return to its resting position [89, 106].

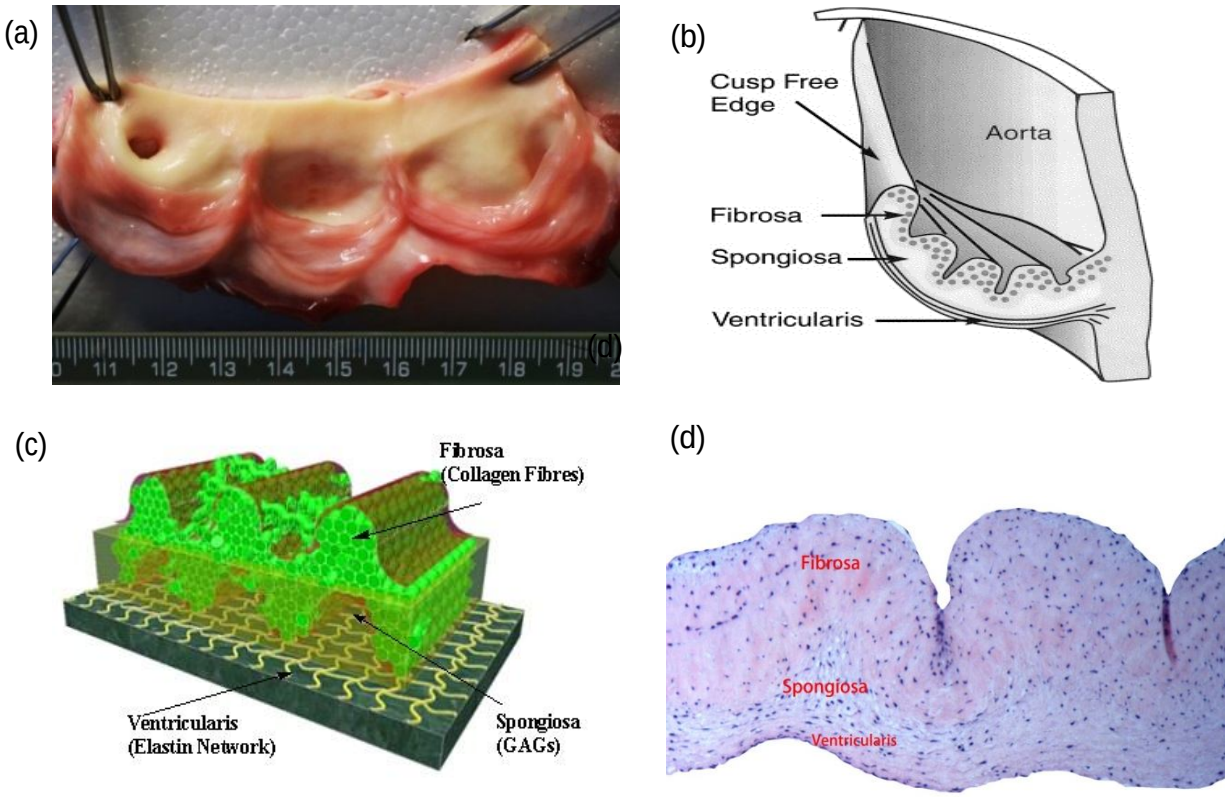

Fig.1- 7. Aortic valve structure and composition: (a) a view of the three leaflets of the AV in a longitudinal cut from the aortic root; (b) Cross section of the leaflet showing the organization of the three layers [89]; (c) schematic diagram of the layers of the AV leaflet [107]; (d) histology of the cross section of a valve leaflet showing the three layers, fibrosa, spongiosa, and ventricularis.

1.2.3.2. Spongiosa

The centrally located spongiosa layer primarily contains a high concentration of highly hydrated glycosaminoglycans (GAGs) and proteoglycans (PGs) [5, 88], with a loosely arranged collagen and elastin fibre structure coupling it to the two outer layers [9, 105]. The negatively charged GAGs have the ability to bind water molecules [108],

meaning, the GAG rich spongiosa layer acts as a damper, to reduce the impact created by sudden changes in pressure gradient at systole. It also allows for relative movement of the outer two layers of the valve as it opens or closes through internal shearing [6, 99, 109]. This is critical as the loading environment includes tension, flexion, pressure, and shear stress [5, 6, 99]. The biomechanical properties of GAGs in aortic valves are still not clear, however, there is evidence that the spongiosa, as a result of its GAG content, is responsible for much of viscoelastic behaviour of the AV, but has minimal effect on tensile biomechanics of the AV [104, 108].

1.2.3.3. Ventricularis

As the name implies, the ventricularis layer faces the left ventricle chamber, and has a mean thickness of 158.2 μm [9]. It is composed of a dense network of collagen and elastin fibres [13, 89], in which the elastin creates a network of radially aligned fibres visible in a radial cross-section [9, 110]. The elastin network in this layer is thought to function as a 'return-spring mechanism', assisting in facilitating the large radial strains that occur during maximum forward flow when the valve is fully opened [6, 87, 89]. The ventricularis also contains some collagen fibres, but they are sparser than in the fibrosa. The ventricularis is thought to contribute to the load bearing response of the valve at lower levels of tissue strain and stress [5, 6, 9].

The complex and anisotropic layered structure of the native aortic valve enables it to exhibit different mechanical behaviours during loading and unloading, in order to meet the necessary hemodynamic conditions. Each of these layers differs in mechanical properties and plays a different role in response to mechanical stretch due to the variation in their ECM components [6, 90, 106]. However, it should be noticed that the overall mechanical behavior of the AV is a summation of the mechanics of each of the individual layers within the valve leaflet.

1.3. Aortic valve dysfunction and aetiology

Aortic valve dysfunction will cause serious problems to human health, even death. Globally, heart valve dysfunction constitutes a large portion of cardiovascular disease (CVD), based on the database of the American Heart Association. It was reported that cardiovascular disease accounts for one in three deaths in the United States each year [111] and a total of 65,000 aortic-valve replacements were performed in the United States in 2010 [112]. There is also a progressive increase in the number and age of patients in need of surgical interventions for heart valve dysfunction each year [111, 113]. Aortic stenosis (AS) was the most frequent single-valve disease (43%), followed by mitral regurgitation (MR) (32%), aortic regurgitation (AR) (13%), and mitral stenosis (MS) (12%) [114].

1.3.1. Structural changes

There are two types of AV disease: congenital or acquired [54, 112, 113]. Congenital disease is an abnormality that develops before birth, in which valves may be the wrong size, have malformed leaflets or have leaflets that are not attached to the annulus correctly [6]. Bicuspid aortic valve (BAV) is the most common congenital cardiac malformation [115] and has been identified with a prevalence of 4.6 cases per 1000 live births [116], with strong male predominance [117, 118]. Instead of the normal three leaflets or cusps in the valve, the bicuspid aortic valve has only two (**Fig.1- 8**) [117, 119]. Individuals may have a normally functioning BAV, and may be unaware of its presence and the potential risk of impending complications for many years. They may typically remain asymptomatic until the third or fourth decade of life, when the valve becomes dysfunctional. Such patients then require close follow-up, and valve replacement may be warranted [6, 116, 120, 121].

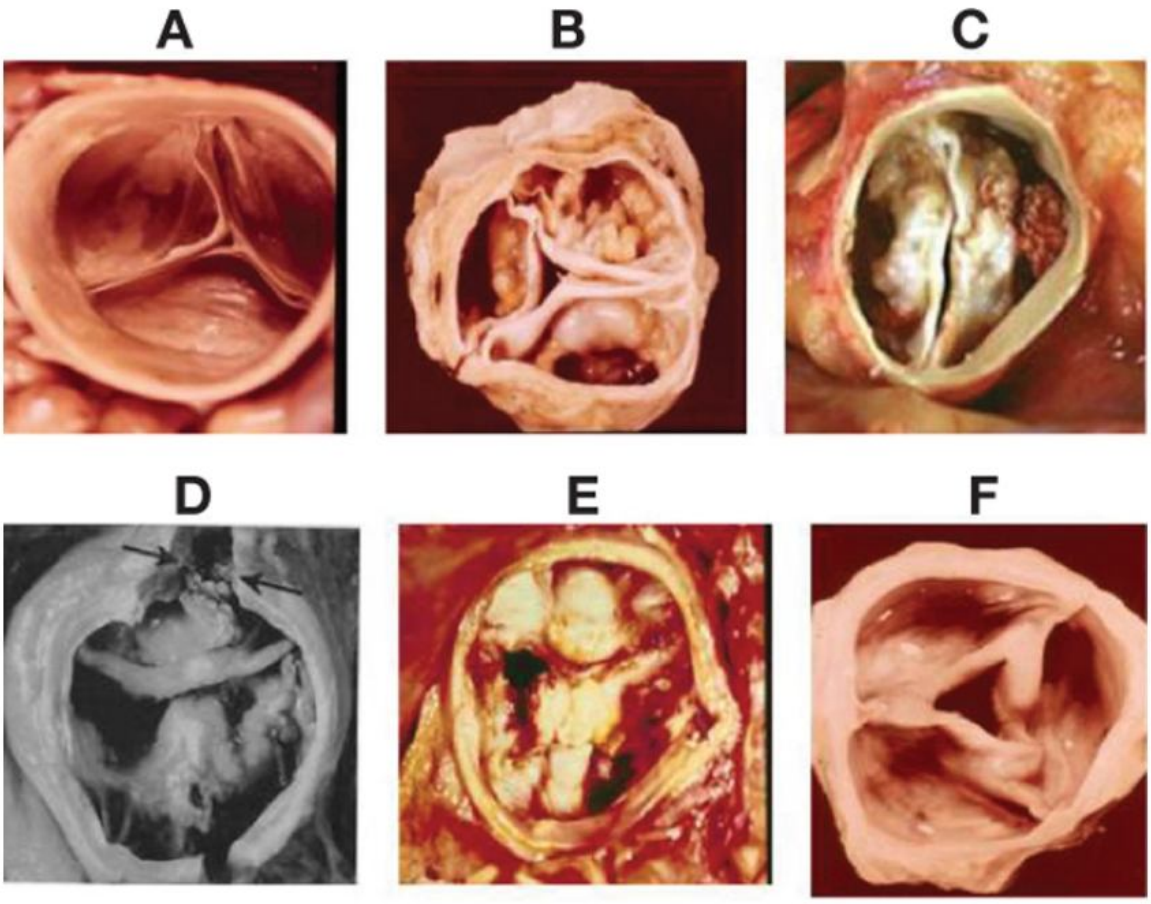

Fig.1- 8. Images depicting aortic stenosis at different stages (adapt from [119]). (A) Normal tricuspid valve. (B) Moderately severe calcific aortic stenosis. (C) Calcific stenosis of a congenital bicuspid aortic valve. (D) Severe calcific aortic stenosis with left main coronary impingement (arrows). (E) Severe calcific aortic stenosis. (F) Rheumatic aortic stenosis with commissural fusion but no calcification of annulus or leaflets.

Acquired diseases are the AV pathologies that develop within the valve over time. They are typically referred to as age-related degenerative valve diseases [112, 113, 117, 122]. These AV diseases develop in an escalating fashion particularly after the age of 65 [114, 122], with approximately 50% of the population having some form of acquired AV disease by the age of 85 [123]. Stenosis and insufficiency are the main acquired pathologies. Stenosis is the failure of a valve to open completely, thereby impeding forward flow. Insufficiency, by contrast, results from failure of a valve to

close completely, thereby allowing reversed flow. These abnormalities can be either pure, when only stenosis or regurgitation is present, or mixed, when both stenosis and regurgitation coexist in the same valve, but in most cases, only one of these two is present. Anatomical, genetic, and clinical factors all contribute to the pathogenesis of aortic stenosis. Calcification occurs in many patients with a normal trileaflet aortic valve, but the presence of a congenital bicuspid valve accounts for 60% of the patients younger than 70 years of age who undergo valve replacement for severe aortic stenosis and for 40% of those 70 years of age or older [112, 115, 124, 125]. **Fig.1- 8** shows images of aortic stenosis at different stages of disease.

Aortic insufficiency (AI) is also known as aortic valve regurgitation or aortic incompetence. In aortic insufficiency, the pressure in the left ventricle falls below the pressure in the aorta, and the aortic valve is not able to completely close. This causes a leaking of blood from the aorta into the left ventricle, meaning that some of the blood that was already ejected from the heart falls back into the heart. Degenerative etiology is the leading cause of AI and it should be considered a disease of the aortic root rather than of the valve. It might combine all degrees of enlargement of the ascending aorta and of leaflet involvement [114]. About 50% of the cases of aortic insufficiency are due to dilatation of the aortic root [18], about 15% of stem from BAV, while about 15% of the cases are due to retraction of the cusps as part of the post-inflammatory processes of endocarditis in rheumatic fever and various collagen

vascular diseases [18, 126]. Other cases may result from aging, or diseases such as syphilitic aortitis or osteogenesis.

1.3.2. Processes of AV dysfunction

The structural changes seen in aortic valve disease were believed initially to be due to progressive degeneration of the valve or “wear and tear”. However, it is now accepted that the onset and progression of aortic valve disease is an active process [19, 112, 114, 122, 127]. As an AV tissue becomes stiffer with age, aortic valve endothelial cells (AVECs) on the surface of the leaflets are exposed to higher levels of strain in each cardiac cycle, causing damage to the cell’s membrane, and eventually haemolysis [127-129]. Calcium is generally present in the solution surrounding the cells, since the membrane of healthy cells pump calcium ions out [130]. However when cells become damaged, the phosphorus which is highly concentrated in the cell membrane will react with those calcium ions, forming calcium phosphate crystals that can deposit on the leaflets [129, 130]. In diseased valves, aortic valve interstitial cells (AVICs) differentiate into myofibroblast type cells, expressing the marker alpha-smooth muscle actin (α-SMA). These activated AVICs are likely to play a key role in the pathogenesis of human clinical disease when the response to injury becomes excessive, leading to disruption of the cusps with excessive remodelling, scarring, and calcification through unknown mechanisms [122, 129]. Progression of

calcific aortic valve disease is marked by the formation of calcific nodules (CNs), which are cellular aggregates characterized in humans by a mixture of calcium phosphate phases [131]. Research has shown that the pathogenesis involves active cell and tissue processes that occur as a tissue response to injury, including inflammation, neovascularization, oxidative stress, activation of the renin–angiotensin system, matrix remodelling, calcification and osteogenesis [129]. In a study of human valves, 83% of the group demonstrated evidence of dystrophic calcification and 13% of those valves had mature lamellar bone and evidence of active bone remodelling [132]. It is unclear whether these processes occur simultaneously or sequentially. Two well-established hypothetical mechanisms of CN formation exist [122]: 1) transforming growth factor β1 (TGF-β1) mediates activation of myofibroblasts, causing calcification via apoptotic mechanisms, and 2) a population of myofibroblasts spontaneously transdifferentiate into osteoblast-like cells and these cells regulate mineralization (**Fig.1- 9**) [133, 134].

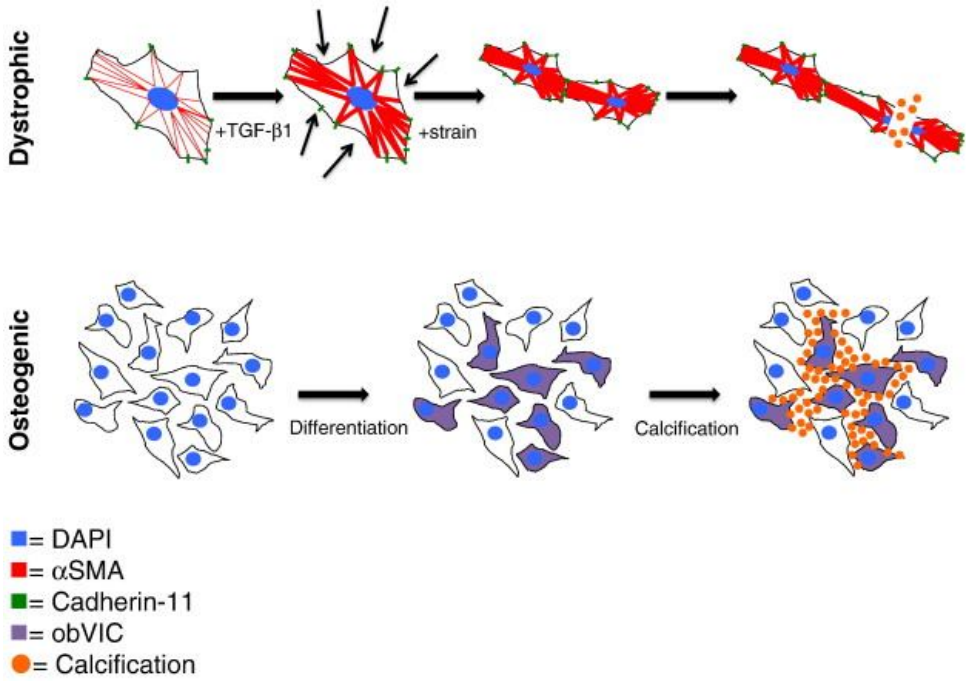

Fig.1- 9. Cartoons depicting proposed mechanisms of valve calcification [122].

Further studies have shown:

1) Inflammation is at the centre stage of mineralization. During mineralization of VICs, IL-6 was a key signal promoting the production of bone morphogenetic protein-2 [135].

2) Inflammatory cells produce different cytokines, such as TNF-α , IL-1 and MMPs, that might promote the mineralization of the AV[127, 135].

3) Low-density lipoprotein (LDL) cholesterol is a risk factor for the development of calcific aortic valve disease (CAVD). Oxidized- LDL and its derived reactive lipid species are strong promoters of mineralization when assessed in isolated VICs [136].

4) Phosphate is a crucial regulator of aortic valve mineralization and ectonucleotidases play roles in CAVD by regulating the levels of phosphate [137, 138].

5) Inflammation stimuli make VICs transform into osteoblast-like cells during the development of CAVD [132].

6) TGF-β1 and Smad signalling is activated in stenotic aortic valves and might play an important role in driving a profibrotic response [127, 139].

7) The endothelium modifies the mechanical microenvironment of VICs to try and prevent the mineralization of VICs [128].

As evident from the extensive list, it is thought that CAVD is caused by multiple different stimuli, with many pathways interacting during the development of CAVD. Further research is needed to fully understand the mechanisms of aortic valve diseases.

1.3.3. Treatment

The most common treatment for end stage of AV dysfunction is surgical replacement of the native valve with a substitute. Approximately 90 000 valve substitutes are now implanted in the United States and 280 000 worldwide per year [140].There are two types of replacement valves available to the patients: (1) mechanical valves; and (2) bioprosthetic valves. In practice, approximately half of replacements utilise

mechanical valves while the other half are bioprosthetic valves [140]. **Fig.1- 10** shows some different types of mechanical and bioprothetic valves.

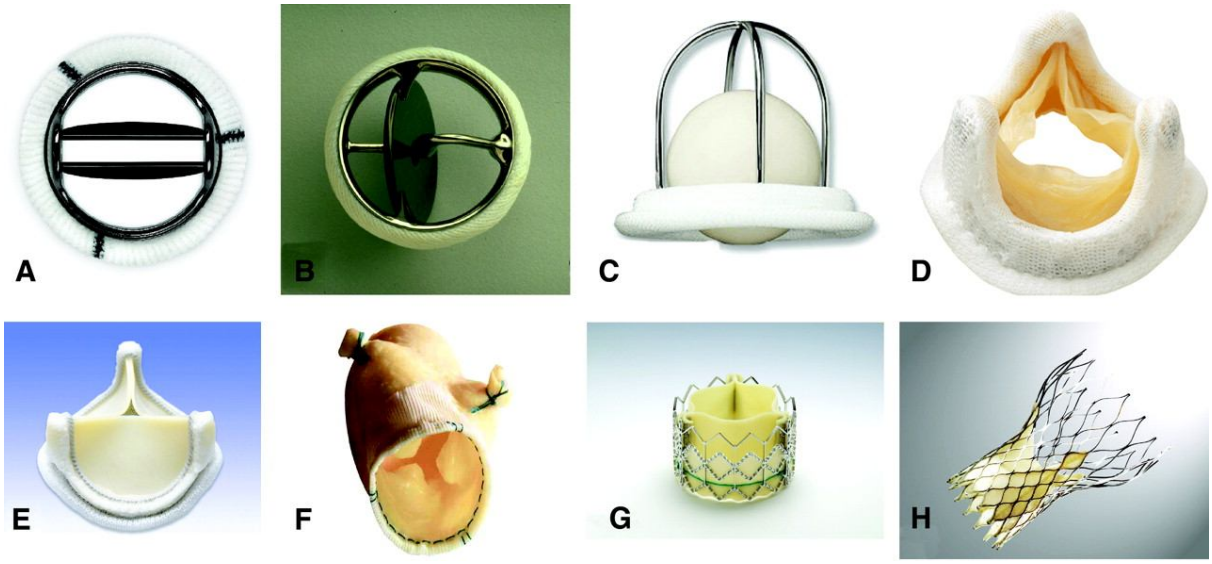

Fig.1- 10. Image of different types of (A-C) mechanical and (D-H) bioprosthetic valves. A) Bileaflet mechanical valve (St Jude); B) monoleaflet mechanical valve (Medtronic Hall); C) caged ball valve (Starr-Edwards); D) stented porcine bioprosthesis (Medtronic Mosaic); E) stented pericardial bioprosthesis (Carpentier-Edwards Magna); F) stentless porcine bioprosthesis (Medtronic Freestyle); G) percutaneous bioprosthesis expanded over a balloon (Edwards Sapien); H) self-expandable percutaneous bioprosthesis (CoreValve). (adapt from [140])

Mechanical heart valves (MHVs, **Fig.1- 10** (A-C)) are made of synthetic materials (e.g., polymers, metals or carbon), whereas bioprosthetic heart valves (BHVs, **Fig.1- 10** (D-H)) are made of biologic tissues which are mounted on a fabric covered plastic frame, called a stent. MHVs are more durable, but their thrombogenicity and need for long-term anticoagulant therapy make them unsuitable for patients in some age groups especially older age groups [54, 140]. In contrast, BHVs are safe to implant,

functionally similar to the native aortic valve, and do not require long-term anticoagulant therapy, hence are associated with reduced risk of haemorrhage. Since their introduction in the mid-1960s, BHVs have gone through many modifications, in their handling from time of harvesting to availability for implantation. Many different tissues and the AVs of different animal species have been tried with varying results. Today, the most commonly used BHVs are derived from porcine aortic valves or from calf pericardium [141]. However, whilst the prosthetic valve has a decreased risk of thromboembolism, it is less durable, hence the risk of reoperation is 25% for a bioprosthetic valve compared with 3% for a mechanical valve [142].

The ideal prosthetic valve, that combines excellent hemodynamic performance and long-term durability without increased thromboembolic risk or the need for long-term anticoagulation, does not exist. Tissue-engineered heart valves attempt to overcome the limitations of mechanical and bioprosthetic valves. The patient's own cells, are isolated and expanded using standard cell culture techniques, and seeded onto an appropriate carrier, termed the scaffold, manufactured in the shape of a heart valve [143, 144]. Subsequent stimulation, transmitted via the culture medium (biological stimuli) or via physiological loading (mechanical stimuli), promotes tissue development [145]. In addition to biocompatibility, biodegradability and reproducibility, the scaffolds ideally possess appropriate cell adhesion and mechanical properties, matched to the native tissue [143, 146]. The key vision of tissue-engineered valves is to develop a living implant, with the potential to grow and

last a lifetime, rather than using external devices implanted inside the heart with numerous associated complications. However, to date it seems that “tissue engineering has promised much more than it has delivered” and there has yet to be a successful clinical implantation of a tissue engineered valve [143].

1.4. Aortic Valve mechanobiology

Although valves were originally thought to be passive pieces of tissue, it is now acknowledged that the mechanisms ensuring the proper structure and function of the heart valves are essentially controlled by the interaction between the valve, its cells, and the surrounding hemodynamic or mechanical environment [18, 34]. During each cardiac cycle, the aortic valve will open and close with structure changes (**Fig.1- 11**). The AV experiences a complex mechanical environment due to blood flow during each cardiac cycle, incorporating tension, flexion, pressure, and shear stress (**Fig.1- 12**) [18, 34, 48]. Several decades of study have been devoted to understanding these varied mechanical stimuli and how they might induce valve pathology [18]. A primary goal of many heart valve mechanobiology studies is to better understand normal valve function and disease progression. This requires a multiscale analysis of the AV mechanical environment, to first establish the hemodynamic forces experienced by the aortic valve in vivo, and then the propagation of these strains through the tissue to the cells, investigating the AV structure and function relationships.

(a)

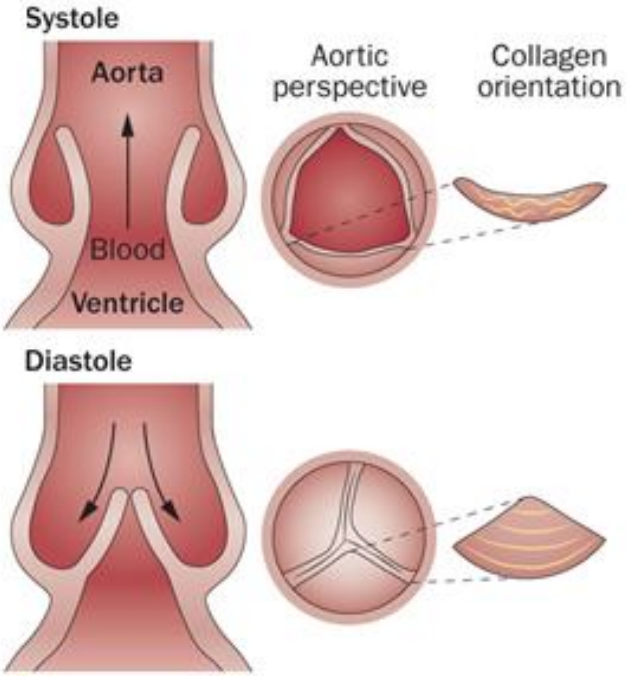

(b)

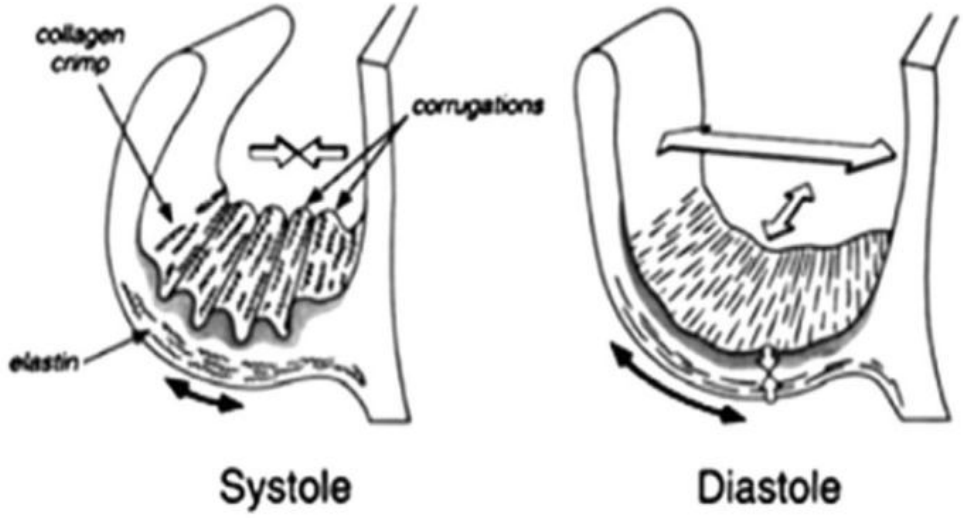

Fig.1- 11. The opening and closing of the aortic valve viewed from in two different schematics [106, 147];

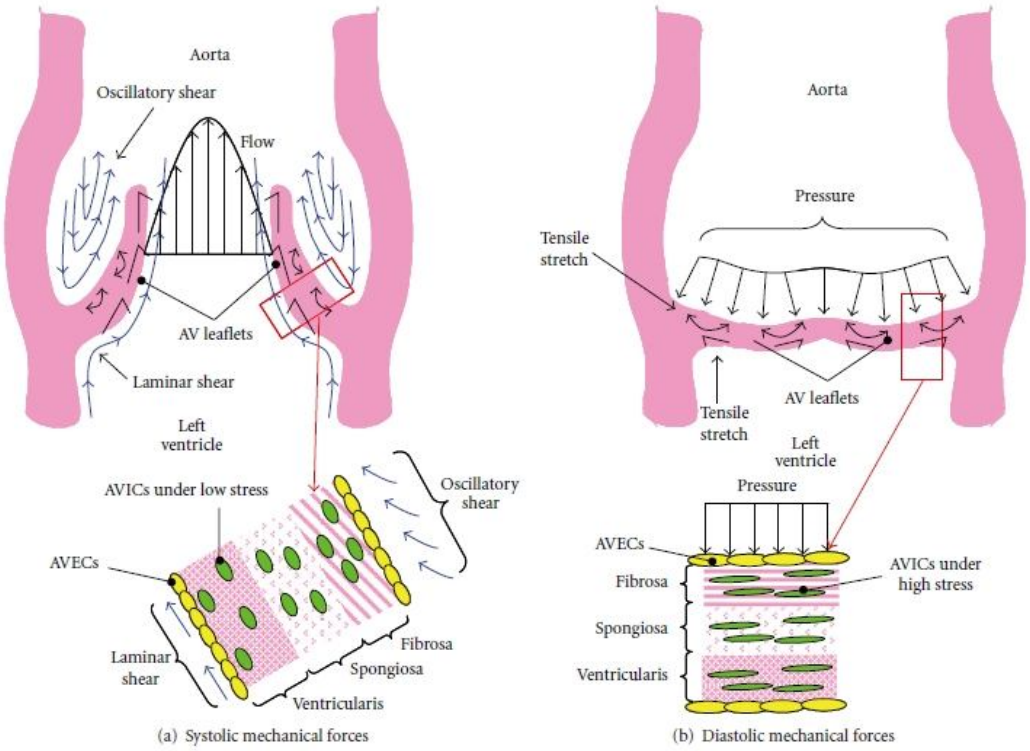

Fig.1- 12. Schematic of the mechanical forces experienced by the aortic valve during peak systole (a), and peak diastole (b). Insets depict qualitatively the effect of these forces on valve cells (adapt from [34]).

1.4.1. In vivo AV Mechanical environment

Pressure: At the beginning of diastole, the AV leaflets close, to stop blood flow back to the left ventricle. The AV pressure reaches a peak value of 80-120 mmHg acting perpendicular to the leaflet area [34, 148, 149]. This stress is resisted predominantly by the fibrosa layer of the leaflet and collagen fibers. The transvalvular pressure gradient depends on the whether the valve is open or closed, is stenotic or healthy. In healthy individuals, the pressure drop across the valve is under a few mmHg during systole [18, 21], in mild stenosis case, the mean pressure drop is

around 20 mmHg, while in severe case, it can reach higher than 40mmHg [18, 150]. With systemic hypertension, the transvalvular pressure gradient can reach as high as 180-200 mmHg [18, 21, 149].

Table 1- 4 Valve hemodynamic/mechanical parameters (summarized in [34]).

Mechanical parameter	Normal	Abnormal
Pressure	120/80 mmHg	Hypertensive: >120/>80mmHg
Membrane stress	Systole: 0.167 kPa Diastole: 2.4 kPa	
Shear stress	Aortic side: peak 20 dyn/cm^2 Ventricular side: peak 64–71 dyn/cm^2	
Peak flow velocity	1.20m/s	7.0m/s (Jet-like flow)
Bending strain and stress	Systole: 14.5% and 1.22MPa Diastole: 8.3% and 0.71MPa	
Tensile strain and stress	Circumferential: 9–11% Radial: 13–25%	Circumferential: >15% Radial: 15–31%

Shear stress Shear stresses occurs across the surface of the AV leaflet due to friction with flowing blood, and are an important factor modulating the synthetic activity of the valvular cells [32, 34, 37, 118, 151, 152]. Shear stress is experienced by the ventricular surface of the leaflets when blood flows past the leaflets during systole, and on the aortic surface when blood pools into the sinuses during diastole (**Fig.1- 12**).

Many techniques, such as laser Doppler velocimetry, hot film anemometry, and doppler ultrasound, as well as computational modelling, have been used to quantify the shear stresses on the leaflets. This studies have reported that the shear stress on the aortic and ventricular sides of the aortic valve leaflet differ greatly (**Table 1- 4**). Shear stress regulates the expression of proteins in AVECs that control many opposing functions, such as vasodilation and vasoconstriction, thrombo-resistance and thrombogenesis, as well as normal cell morphology and the development of atherosclerosis [18].

Bending Stress: The natural deformation mode of the valve in vivo is flexion, occurring as the leaflets open and close in each cardiac cycle (**Fig.1- 12**). Bending stress is both tensile and compressive, with the leaflet on the convex side experiencing tensile stress while the concave side experiences compressive stress [6, 153]. The maximum bending stresses in vitro were found to be 1.22MPa during systole and 0.71MPa during diastole, respectively (**Table 1- 4**) [34, 154]. The bending stress increases with an increase in leaflet stiffness causing early failure of some bioprosthetic valves [34].

Axial strains: The AV is also exposed to large, highly non-linear multi-axial strains. The ability for the valve leaflets to stretch is important, as it allows each cusp to extend and form a coaptive seal with the other two cusps during diastole. The AV

leaflets exhibit anisotropic strains because the collagen is predominantly aligned in the circumferential direction, providing greater tensile strength circumferentially than in the radial direction. Aligned in the radial direction are mainly elastic fibres [9, 98, 155]. As collagen fibre diameters increase with age, the tissue becomes stiffer and less extensible [18, 34].

Close correlations between the mechanical stresses on the valve and the resulting cell biology have been documented by clinical observations and animal studies [34]. The cellular and molecular events involved in these processes, however, still remain unclear. However, there is no doubt that the structure and function of the AV is influenced by its surrounding hemodynamics and mechanical microenvironment [34], and several studies have proved this point [18, 32, 34, 118, 127, 156]. Yoganathan et al reviewed the mechanical environment and resulting mechanobiology relationships of the aortic valve, and summarized the cellular and molecular events involved in these relationships.

Due to the complex loading on the leaflet, the leaflet experiences regionally varying loading [100]. The hinge flexes as the leaflet opens and closes. In the belly, the leaflet is stretched biaxially as blood pressure presses against the leaflet. The coaptation region experiences both flexion and compression. At the free edge, uniaxial tension in the circumferential direction is the dominant load as blood pressure stretches the leaflet (**Fig.1- 12**)[4]. This regional variation in loading has implications for calcific

aortic valve disease (CAVD), as calcific deposits tend to form in areas of flexion, particularly the hinge and coaptation regions [100, 157]. As shown in **Fig.1- 12**, there are also side-specific variations in the flow and shear experienced by the leaflet, where the ventricularis/inflow side experiences high magnitude laminar flow (64-71 dyn/cm^2), while the fibrosa/outflow side experiences low magnitude disturbed flow (20 dyn/cm^2) [31-36]. This side-dependent flow pattern correlates with CAVD, as the outflow side preferentially calcifies, suggesting that the low magnitude shear and the disturbed flow patterns are positively correlated with CAVD [18, 30, 34, 158].

1.4.2 In vitro mechanical behaviour of aortic valve

The successful design of tissue-engineered heart valves, that could closely mimic the native valve's characteristics, first requires a detailed analysis of the mechanical properties of the native AV. Such analysis is also critical to provide the experimental data needed to model AV mechanics. Studies of AV mechanical properties have been mainly divided into 1) tensile properties, investigated using quasi-static uniaxial and/or biaxial loading protocols [9, 99, 155, 159-162]; 2) flexural/bending properties, investigated using three-point bending and/or cantilever bending [104, 153, 163]; 3) viscoelastic properties, manifested by creep and stress-relaxation phenomena and investigated using uniaxial or biaxial loading protocols [98, 104, 108, 164-166]. Although there are significant differences in the material properties of human and animal aortic tissues [159], due to the limited availability of fresh human heart valves,

most studies used animal heart valves, such as porcine [9, 98, 99, 155, 161, 165, 166], ovine [167-169] and bovine[169, 170], to investigate the biomechanical behaviour of heart valves more generally.

1.4.2.1. Uniaxial tensile studies

Uniaxial tensile testing is perhaps the most common means of measuring the mechanical properties of heart valves [106, 171]. A typical uniaxial tensile stress-strain curve for an AV is shown in **Fig.1- 13**. The tensile stress σ, is defined as, $\sigma=F/A$, where F is the applied force and A is the cross sectional are in the released state. The tensile strain, ε, is defined as, $\varepsilon=\Delta L/L_0$, where ΔL is the change in the length of the specimen, and L_0 is its initial length. The elastic modulus, also known as the Young's modulus, is defined by the ratio of stress and strain, given as, $E=\sigma/\varepsilon$ [106]. From **Fig.1- 13**, it can be seen that the tensile stress–strain curve of the AV can be split into a number of regions or phases, whose characteristics are thought to be associated with specific physiological functions [172]. The main phases of the curve are: (i) the low stress–low strain pre-transition phase, which can be linked to the straightening of the crimped fibers of collagen and the elongation of the elastin fibers; (ii) the highly non-linear transition phase that might be related to the transfer of force from the elastin to the collagen fibers; and (iii) a post-transition linear elastic region, linked with the elongation of elastic and collagen fibers [172].

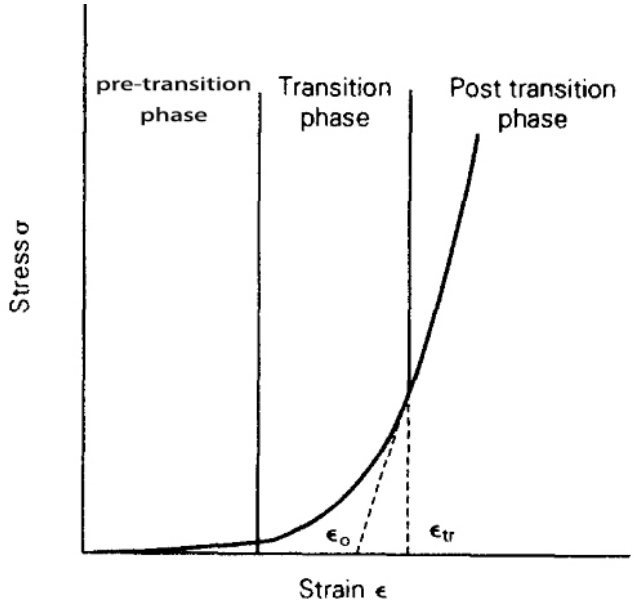

Fig.1- 13. The three defined regions of the stress-strain curve of AV leaflets (adapted from [172]).

The initial attempts to characterize AV leaflet mechanics were carried out in the early 1970's, utilizing quasi-static uniaxial tensile tests performed on fresh and frozen human AVs, reporting a marked anisotropy[1] in the mechanical behaviour of the tissue [173]. The samples withstood large deformations in the radial direction, whilst showing less extensibility and higher stiffness circumferentially. Missirlis and Chong (1978) looked further at variations in strain across porcine AV samples, imaging the movement of ink marks along circumferential and radial strips of porcine AV leaflets under uniaxial strain. Their results confirmed the anisotropy of the tissue properties reported in [173], but also demonstrated that the middle region of a leaflet was the stiffest, particularly in the radial direction [174].

[1] Anisotropy is the property of being directionally dependent, which implies different properties in different directions

Table 1- 5 Reported mechanical properties of human AV samples.

Authors	Orientation	Strain Rate	Sample Size	E (MPa)	Strain at failure (%)	Stress at failure (MPa)
Stradins et al [175]	Circumferential	-	Up to 20mm × 3mm	15.34±3.84	18.35±7.61	1.74±0.29
	Radial			1.98±0.15	23.92±3.94	0.32±0.04
Balguid et al [8]	Circumferential	100%/min	3 mm Wide	15.6±6.4	21.9±10.6	2.6±1.2
	Radial			2.0±1.5	29.8±13.9 %	0.42±0.24
Mavrilas and Missirlis [172]	Circumferential	2-3 s^{-1}	3 mm Wide	14.55±3.7	-	-
	Radial			1.57±0.18	-	-

Table 1- 6 Reported mechanical properties of porcine AV samples.

Authors	Orientation	Strain Rate	Sample Size	E (MPa)	Strain at failure (%)	Stress at failure (MPa)
Anssari-Benam and Screen [99]	Circumferential	6%min	5×10mm	20.4 ± 0.86	45.07 ± 1.25	3.44 ± 0.57
		60%/min		34.07 ± 1.98	31.54 ± 1.69	3.68 ± 0.12
		600%min		37.54 ± 1.45	27.56 ± 1.96	4.45 ± 0.13
	Radial	6%min		0.71 ± 0.8	87.6 ± 1.78	0.34 ± 0.03
		60%/min		1.21 ± 0.09	77.15 ± 0.03	0.50 ± 0.03
		600%min		3.36 ± 0.10	61.11 ± 0.63	0.84 ± 0.05
Sauren et al [166]	Circumferential	0.069 s^{-1}	10 to 20 x 3 mm	28	-	-
		0.08 s^{-1}			-	-
		0.8 s^{-1}			-	-
	Radial	0.008 s^{-1}		-	-	-
		0.32 s^{-1}		1.33	-	-
Rousseau et al [165]	Circumferential	10mms^{-1}	3 mm Wide	6.6	-	-
Mavrilas and Missirlis [172]	Circumferential	2-3 s^{-1}	3 mm Wide	7.78±1.7	-	-
	Radial			1.28±0.34	-	-
Missirlis and Chong [174]	Circumferential	2mm/min	10 x 2 mm	3.35	-	-
	Radial		6 x 2.4 mm	1.09	-	-

The observed non-linear stress-strain curve, has been attributed to the structural re-organization of the extracellular matrix (ECM). In the pre-transition phase, where the tissue offers negligible resistance to elongation, the collagen fibres are mainly crimped, thus the transmission of tensile force is provided mainly by the elastin component, so that this phase is often denoted as the elastin phase [166, 172]. Through the transition phase, gradually more collagen fibres become aligned and uncoiled with the increasing applied load. As they are uncoiled, they become oriented in the loading direction and gradually become straight, increasingly contributing to stress transmission so the tissue increasingly becomes stiffer [166, 172]. By the post transition phase, the collagen fibres have become predominantly aligned and uncrimped, acting as the main load bearing element of the tissue [166, 172]. The post transitional phase has generally been assumed to be linear and elastic, as the slope of the load-elongation curve is steep and almost constant [166, 172], mainly reflecting the material properties of the collagen fibres [166, 172]. As such, the gradient of the line in this region has been typically used to calculate the elastic modulus. **Table 1- 5** and **Table 1- 6** summarize the mechanical characteristics of the AV reported across a number of studies, using human or porcine aortic valves.

The variation in the data provided in **Table 1- 5** and **Table 1- 6** indicates that the test conditions may drastically influence the observed mechanical behaviour of the AV and its reported properties. Factors such as loading protocols, gripping methods, sample geometry and size, and pre-conditioning of the samples may all contribute to

the variation of the results, and there remains no widely accepted standard testing protocol, with experimental setups different and lab specific. Sauren et al (1983) reported that the mechanical properties of the AV were slightly influenced by strain rate [166]. Anssari-Benam and Screen make further studies [99]. They stretched porcine aortic valves at 6%/min, 60%/min, and 600%/min respectively, and found that increasing strain rate leads to an associated increase in failure stress and decrease in failure strain in both the radial and circumferential directions (**Fig.1- 14** and and **Table 1- 6**).

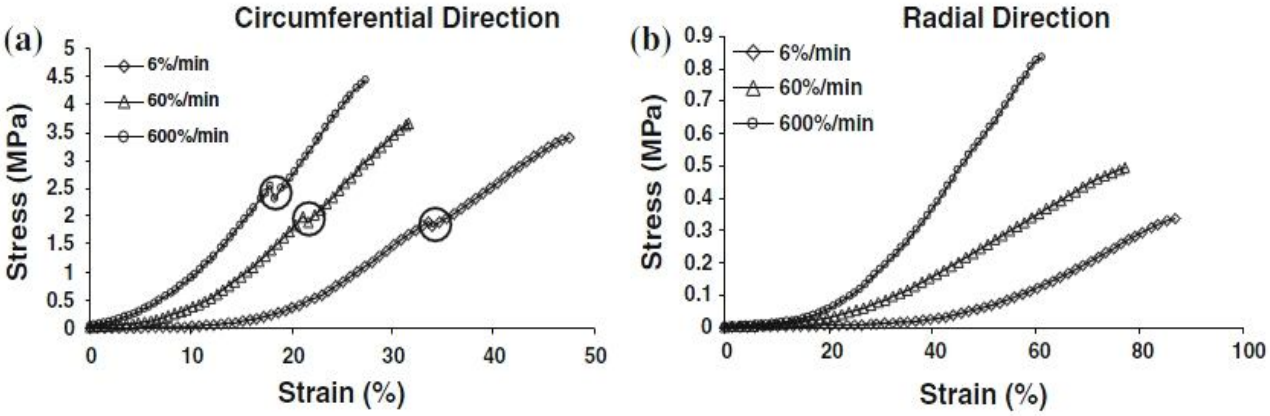

Fig.1- 14. Typical σ −ε curves for the AV strips loaded different strain rates (adapt from [99]) .

In order to investigate their specific roles, Vesely et at (1992) investigated the micromechanical properties of the fibrosa and ventricularis of the aortic valve leaflet [90]. They separated the fibrosa and the ventricularis in fresh leaflets via manual micro dissection and tested them individually. Comparing the fibrosa and the ventricularis directly in a given test direction, circumferentially the fibrosa was almost twice as stiff as the ventricularis (13.02 kPa vs. 7.41 kPa), while there were no

significant differences in stiffness in the radial direction. For extensibility, no difference was found circumferentially while radially the ventricularis was more than twice as extensible as the fibrosa (62.7% vs. 27.8%) [90]. Additional scanning electron microscopy data [90], showed that while the ventricularis contains a large amount of elastin, the amount of radially oriented collagen in the ventricularis is similar to that in the fibrosa. The fibrosa, by itself, has the same extensibility in both directions (about 23% strain), but can extend much more radially when connected to the rest of the leaflet because it is attached to the ventricularis in a highly folded configuration [90].

Additional uniaxial studies regarding the mechanical behaviour of the AV tissue have attempted to investigate the structural reorganisation of the ECM under tensile deformation. Scott and Vesely (1995) performed a histological analysis of samples fixed under varying degrees of uniaxial tension [87]. They observed that the waviness of the collagen fibres allowed the structure to strain to approximately 17%, before the collagen became straightened and loaded. In addition, macroscopic crimping of collagen fibre bundles visible in the fibrosa layer allowed additional strains of up to approximately 23%, and the collagen fibre reorientation facilitated even larger deformations [87]. Based on their study, they proposed that the mechanism that returned the collagen fibre structure to its rest geometry when unloaded was the surrounding elastin matrix, which interconnects the collagen fibres and provides them with a return spring mechanism (**Fig.1- 15**). In this model, elastic springs run from one collagen crimp to the next. As the tissue is initially stretched, the elastin

undergoes tension while the collagen develops small bending forces as the bundles straighten. Once straight, the stiff collagen fibres take up a larger proportion of the load in tension. When the load is released, the elastin acts to return the collagen to its undeformed geometry [87].

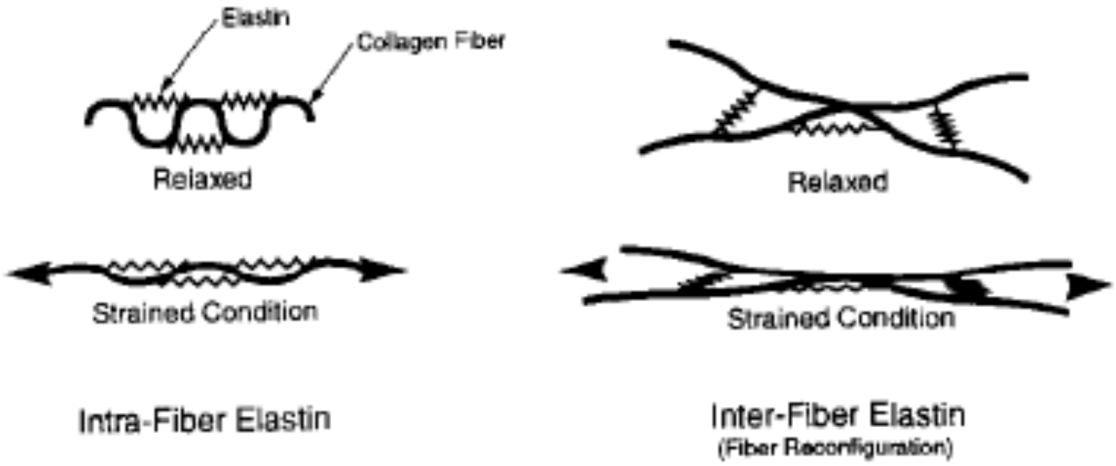

Fig.1- 15. Collagen and elastin linkage model proposed in [87].

1.4.2.2. Biaxial tests

Uniaxial tensile tests have traditionally provided the primary basis for the study and understanding of the mechanical behaviour of the AV leaflets. However, these tests can not reflect the complex multi-axial physiological loading conditions of the native functioning AV [5, 34, 54] as outlined in 1.4.1. In order to further understanding of AV mechanical behaviour under somewhat more physiological and complex loading

conditions, biaxial mechanical testing has been adopted. Biaxial testing methods have not been standardized and methodologies vary widely, due to the complex mechanical behavior of soft tissues and the general difficulty in performing biaxial tests [176, 177]. The most generally accepted protocol for biaxial experiments has been to dissect a square sample from the belly region of an AV leaflet, and to transfer uniformly distributed loading to each of its four sides via surgical sutures [5, 178]. Samples can either be loaded equi-biaxially (i.e. equal levels of tensile load applied to each loading axis) or specific load ratios between the circumferential and radial axes selected. The method of sample gripping affects the constraint on the extracellular fibers at the boundaries of the sample. This applied constraint not only affects how the load is transferred to the sample, but also how the load is transmitted throughout the rest of the material, thereby influencing the resulting mechanical behavior of the tissue [179, 180]. Sutures are preferentially used to secure the valves, as this method of gripping samples minimizes the constraints on sample deformation with applied load [176]. The most commonly used biaxial tensile test of valve leaflets was described in detail by Sacks' group [106]. It was recommended that during the tests, specimens should be immersed in PBS solution at physiological temperature. The tensile loads were applied to the specimen through sutures connected along the specimen edges [106].

Christie and Barratt-Boyes (1995) were pioneers in carrying out biaxial loading experiments on AV and PV leaflets, applying equi-biaxial loading to the valve leaflets

[181]. In this study, the mechanical behaviour of pulmonary and aortic valves, from both fresh and fixed porcine tissues was compared. As shown in **Fig.1- 16**, the aortic valve is stiffer than the pulmonary valve, and fixed samples of both valves behaved in a less complaint manner than fresh samples; data in good agreement with previously reported uniaxial results [165, 166, 172]. However, comparing stress-strain magnitudes with those from previous uniaxial loading tests, highlighted smaller strains for the same applied stress in both the circumferential and radial directions under biaxial loaded conditions, suggesting less extensible mechanical behaviour of the AV leaflet when exposed to biaxial deformation [166].

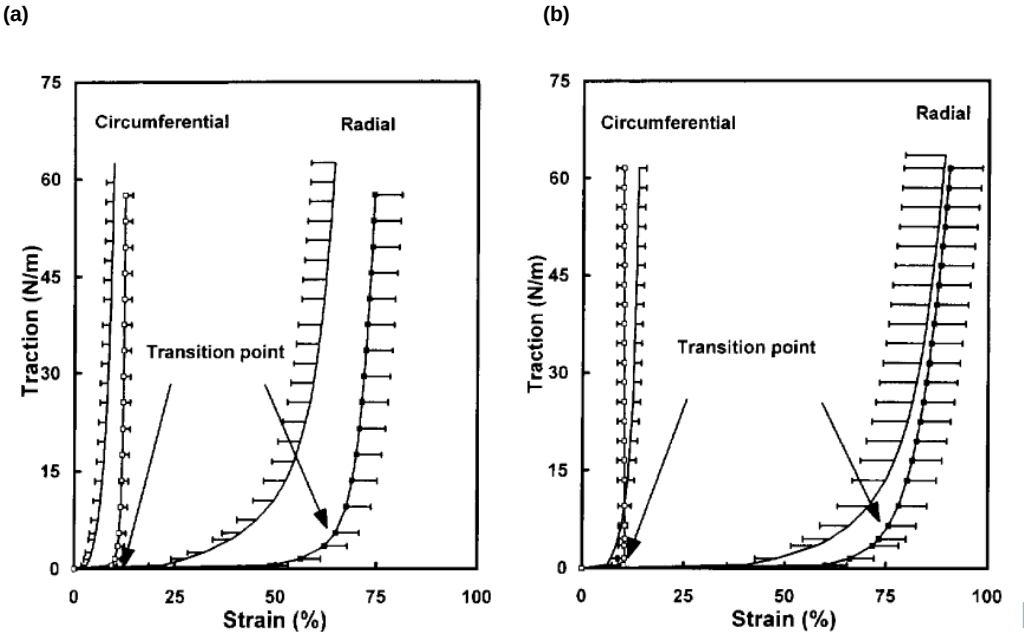

Fig.1- 16. Stress-strain curves from biaxial loading tests (Adapted from [181]): (a) fresh and fixed porcine aortic leaflets. (b) Fresh and fixed porcine pulmonary leaflets. The curves with symbols are the mean results for the 24 fresh samples (closed symbols = radial direction; open symbols = circumferential direction). The curves with no symbols are the corresponding curves for the fixed samples. The error bars show the standard deviation.

The leaflets demonstrated a complex, highly anisotropic mechanical behaviour [106].

Under biaxial loading, the collagen fibers were stretched circumferentially and the circumferential stresses rose rapidly with a minor increase in strain [106, 153]. The leaflet response in the radial direction took place in two stages. In the first, toe region stage, a small change in tensile stress caused a large deformation [106, 153]. In the second stage, the tensile stress rose steeply until the tissue attained its ultimate extensibility. The toe region in the initial stage was explained by the fact that the valvular leaflets did not have many fibers aligned along their radial direction [106, 153]. Such anisotropic properties of the valve leaflets are important for proper valve functioning. The high radial compliance of the leaflet allows leaflets to stretch during diastole and fully seal the valve against the backflow of blood. Circumferential stiffness is important for supporting the high transvalvular pressures to keep the valves closed during diastole.

Christie and Barratt-Boyes, have also investigated age-related changes in the deformation behaviour of AV leaflets [182] and the biaxial mechanical properties of explanted aortic allograft leaflets [183]. They reported that the AV tissue stiffens with increasing age, observing a nearly 50% decrease in extensibility for subjects aged 60 compared with those aged 20 [182, 183].

Sacks and coworkers carried out a series of seminal studies, investigating biaxial mechanical properties of AVs, and characterizing the micro-structural response of the valve to loading [6, 162, 184]. Using small angle X-ray scattering (SAXS) the authors

probed the dependence of AV mechanical properties on the kinematics of collagen fibrils under biaxial stress, by monitoring the change in collagen fibre orientation at different levels of loading [162, 184]. The most interest result was the surprising negative strains in the circumferential direction with increased loading in the radial direction, when the tissue subjected to non-equibiaxial loads (**Fig.1- 17**)[184].

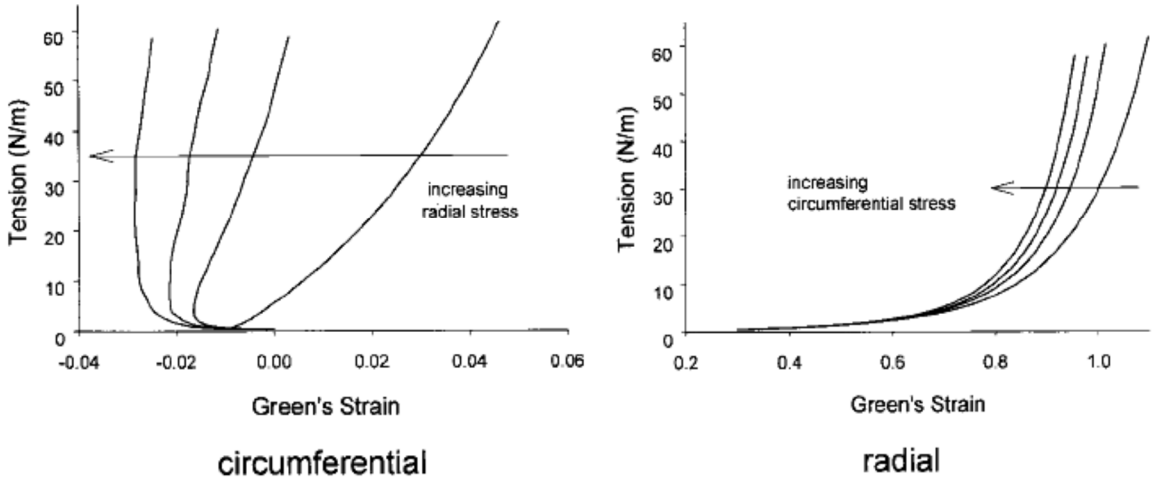

Fig.1- 17. Stress–strain data for AV test specimens under a range of non-equibiaxial loading (adapted from [184]): (a) circumferential; and (b) radial directions.

This complex behaviour of the tissue under biaxial loading was reported to be due to the tight angular distribution of collagen fibres [184]. As the radial axis is loaded, fibres are forced to rotate, which in turn causes a contraction along the circumferential axis. This effect will become more pronounced as the radial loads become larger with respect to the circumferential loads. **Fig.1- 18** shows the process schematically. This effect illustrates that negative strains can be generated even though the stress magnitude is the same along both axes and no buckling of the tissue is observed. Thus, radial loads are ultimately resisted by the highly circumferentially aligned collagen

fibres mainly present in the fibrosa layer, whose rotation into the loading direction facilitates very large strains prior to providing structural resistance [184]

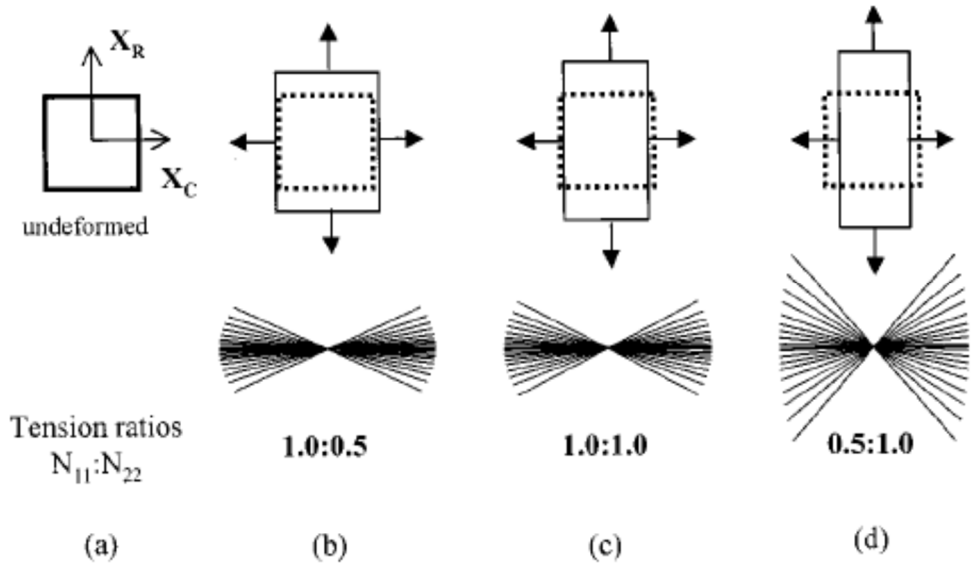

Fig.1- 18. A schematic of a biaxial test specimen, with the fibrous structure of the cusp depicted as collagen cords, which undergo large rotations with loading (a). As the radial loads become larger with respect to the circumferential loads, the collagen fibres undergo large rotations (b-d). This causes contraction along the circumferential axis without buckling and allows for large strains (Adapted from [184]).

More recently the mechanical behaviour of the separate valve layers has been investigated under equi-biaxial loading, and the behaviour of the isolated ventricularis and fibrosa layers compared with the intact tissue [9]. The stress-strain curves for the individual layers and the intact valve are shown in **Fig.1- 19**. The study demonstrated that each AV leaflet exhibits a preloaded status: the fibrosa was observed to elongate after separation of the layers, while the ventricularis contracted. This was in agreement with the uniaxial test results by Vesely's group [90, 91], where the same phenomena upon dissection of the three layers of the AV leaflet was observed.

Several additional interesting results were observed in the behavior of the isolated fibrosa and ventricularis: (i) the separated layers were very compliant at low strains; (ii) each of the separated layers exhibited significant anisotropic responses; (iii) the fibrosa in isolation behaved in a similar manner to the intact valve, with the exception that it was slightly less extensible in the radial direction; (iv) by contrast, the ventricularis exhibited extremely compliant equi-biaxial behaviour, with a very large toe region in the radial direction [9].

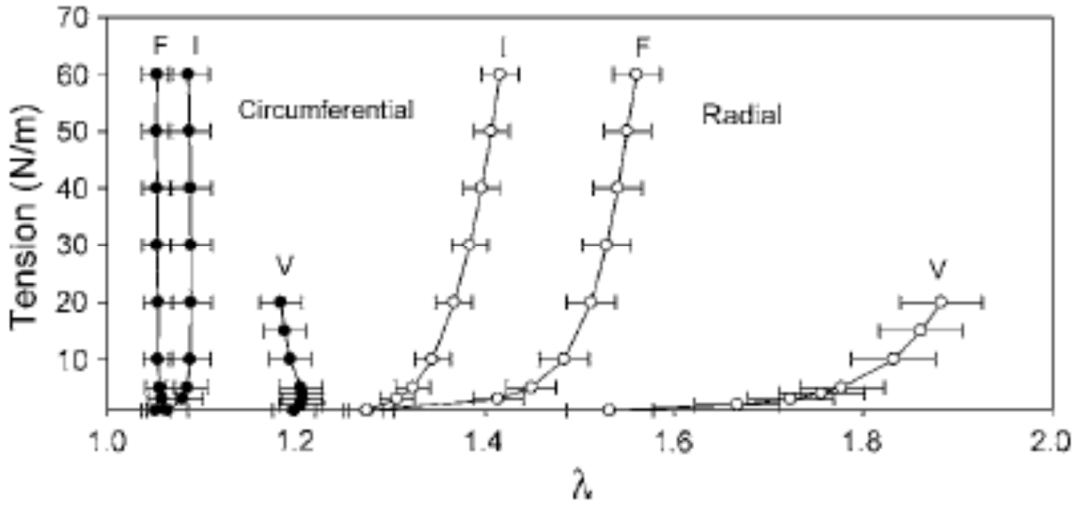

Fig.1- 19. Mean equi-biaxial tissue responses of the intact AV, and the isolated fibrosa and ventricularis layers: I= intact, F = fibrosa, V = ventricularis (adapted from [9]).

1.4.2.3. Flexion tests

Although uniaxial and biaxial tensile tests dominate documented studies [5, 6, 87, 89, 90, 99, 106, 155, 174, 185] and have elucidated valuable data on the in-plane mechanical behaviour of the AV tissue, these tests do not fully represent the physiological deformation of the valves. The natural deformation mode of the valve *in vivo* is extremely complex but incorporates flexion, occurring as the leaflets open and

close in each cardiac cycle [153, 186]. Flexion tests enable the analysis of this loading mode, and have the added advantage of allowing for the quantification of strains at comparatively low stresses [106].

Flexion tests were first conducted on heart valve leaflets in the 1980s when Thubrikar and coworkers (1980) performed in vivo experiments on canine aortic valves [13]. Radiopaque markers were placed on the left coronary leaflet in the circumferential direction, and then tracked to determine the changes in leaflet length occurring during each cardiac cycle. The pressure changes were also measured and recorded using catheter pressure transducers. They reported the changes in pressure around the AV, and the resulting change in the length of the leaflet during the systolic and diastolic phase, calculating the elastic modulus of the AV based on the linear elasticity theory of thin cylindrical shells (Laplace law). The bending modulus was calculated to be 0.24 MPa at systole [13]. In another study by these authors, an analytical model was also proposed to correlate the radius of curvature of the leaflet to the applied stresses [187]. During valve opening, the leaflets bend, producing tensile stresses on the outer surface of the bend and compressive stresses on the inner surface. Flexural stresses are thought to have important links with calcification of aortic valves [188].

In vitro flexion test experiments performed on heart valve leaflets can largely be classified into three categories: three-point bending tests [153, 186, 188], cantilever bending tests [163] and macro-indentation tests [189]. Cantilever and three-point

bending are typically conducted on excised strips of tissue, while macro-indentation tests are performed on the entire valve leaflet [106].

More recently, 3-point bending tests have been performed on rectangular strips cut circumferentially from AV leaflets. In their physiological unloaded position, the AV leaflets have a natural curvature (**Fig.1- 20** a). During tests, specimens can be bent either with the natural curvature or against it, by holding specimens stationary with two supporting posts, while a bending bar is applied to the centre of the tissue (**Fig.1-20** b).

A considerable volume of work on the three-point bending properties of aortic valve leaflets has been reported by Sacks and coworkers. In their study, the bending stiffness, EI, was obtained using the linear beam theory, according to the formula:

$$EI = \frac{FL^3}{48y_{max}}$$

where F is the applied force, L is the span length between the two supports, and y_{max} is the maximum depth of indentation [186].

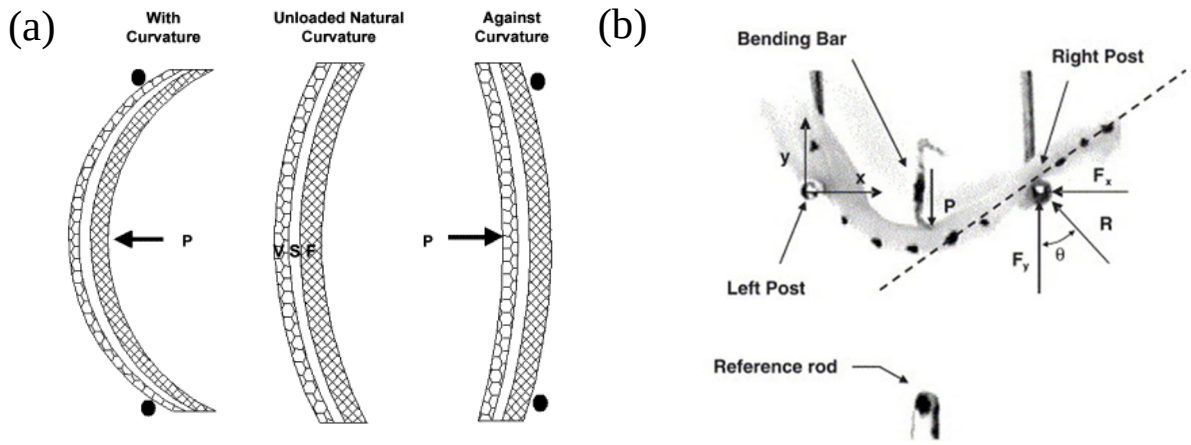

Fig.1- 20. (a) Bending directions of the AV leaflet. (V = Ventricularis layer, F = Fibrosa); (b) Schematic of a leaflet specimen in a 3-point bending test configuration. P = applied load (Adapted from [153]).

By this method, Gloeckner et al. (1999) investigated the effects of fatigue on aortic valve bending properties [186]. The authors reported the experimental results in terms of a bending stiffness index (BSI), meant to serve as a basis for comparison of bending stiffness among samples. A mean BSI of 4.0×10^{4} N m² was obtained in the circumferential direction, while a mean BSI four times lower was obtained in the radial direction, both for bending along the physiological direction of curvature. The BSI value almost doubled for bending against curvature in the circumferential direction, while no significant difference was noted in the radial direction. These variations in BSI value were attributed to the complex structure of the valve tissue, where the preferential orientation of the collagen fibers along the circumferential direction was responsible for the higher BSI in this direction. Also, when bending the leaflet against the natural curvature direction, the fibrosa was stretched and the ventricularis was compressed (opposed to the bending in the curvature direction in

which fibrosa is compressed and ventricularis is stretched). Being thicker and composed primarily of dense collagen fibers, the fibrosa contributes the most to circumferential bending properties and thus increases bending stiffness in the adverse direction.

In a similar study, the flexural properties of the commissural region (where the upper portion of the leaflet joins the aortic root) were investigated, using the Bernoulli-Euler criteria [163]. The relationship between flexion angle (φ) and bending stiffness (*E*) was determined for angles up to φ = 40°, and reported to be linear in both the curvature and against-the-curvature directions. The slope of the φ-*E* line was shown to be negative, indicating that the bending stiffness decreased as the flexion angle increased. The value of *E* at a flexion angle of φ = 30° was taken as the 'representative' value, reporting $E = 42.63 \pm 4.44$ KPa in the curvature direction and $E = 75.01 \pm 14.53$ KPa in the direction against the curvature [163]. Their results showed that the commissural region is approximately 50% stiffer when bending against the natural curvature direction, suggesting the commissural region is functionally adapted for uni-directional physiological flexion.

1.4.2.4. Time-dependant tests

Similar to other collagenous connective tissues such as tendons and ligaments, the AV

also exhibits time-dependent behaviour when subjected to specific loading conditions. Such behaviour can be realised through either stress-relaxation or creep tests. The former reflects a decrease in load (stress) which occurs when the tissues are subjected to a constant elongation, while creep describes the increasing elongation of the tissue under constant load (stress) [164]. Hysteresis is also observed during cyclic loading [99]. As valve leaflets are viscoelastic, their stress–strain characteristics are strain rate dependent. However, although both stress relaxation and creep phenomena are present, studies have indicated the creep is not significant [106].

In contrast to other soft tissues such as skin and tendon, the time-dependant behaviour of the AV has been the subject of very few studies. The early contributions include the study of stress-relaxation in fresh AV tissue [166] and the comparison of stress-relaxation in fresh and glutaraldehyde fixed AV samples [165]. Sauren et al (1983) performed relaxation tests on circumferentially cut samples [166]. By fitting their experimental data to the quasi-linear viscoelasticity (QLV) model, they reported that most of the relaxation occurs within the first 120s of the experiment, and the amount of relaxation is not significant thereafter [166]. 25% relaxation at an initial stress level of 0.8 MPa was reported in that study [166]. However they also argued that the QLV model was not able to accurately describe the experimental data. In a later study, Sauren and Rousseau (1983) performed a sensitivity analysis of the QLV model, and showed that there are some stress (strain) levels at which the QLV model will produce erroneous results [190]. Furthermore, they showed that as the tissue

tends to a more viscous-like behaviour, the errors of the model would increase, until a limit was reached, at which point QLV could not determine the relaxation times [190].

Rousseau et al. (1983) compared the stress-relaxation behaviour of fresh and fixed AV tissue samples, and reported less relaxation in fixed tissue [165]. Fixation under pre-loading also affected the relaxation behaviour, as the samples fixed under 0.3 N preload were reported to relax by only approximately 60% of the relaxation seen in fresh samples. The inaccuracy of using QLV to model stress-relaxation of the AV was again underlined in this study, reflected in the high standard deviations in the parameters calculated by the QLV model [165].

Other studies regarding the stress-relaxation behavior of the AV have investigated the effects of pre-conditioning and strain rates on the relaxation behaviour [191, 192]. It was shown that preconditioning AV samples resulted in less variation in stress-relaxation curves and relaxation parameters, irrespective of the applied strain rate [192]. The proposed optimal protocol was at least 5 loading cycles up to a loading level of 600g. However, this study highlighted that the lack of a standard preconditioning protocol for stress-relaxation tests means a direct comparison between different test data may prove problematic. In another study, it was suggested that strain rate does not have significant effects on AV relaxation, as the QLV parameters were only ‘moderately’ affected by strain-rate [191].

Another constitutive model used to describe the time-dependant behaviour of aortic valves is the Maxwell model. Anssari-Benam and Screen (2011) used the Maxwell model to characterise the time-dependent behaviour of the AV at different strain and load increments [98]. **Fig.1- 21** shows the typical normalised stress-relaxation and creep curves from circumferential and radial samples in their study. Results show that the time dependent response of the tissue differed with the loading direction, and also with the level of applied load or strain, in both stress-relaxation and creep phenomena. Both phenomena were consistently more pronounced in the radial loading direction [98]. In fitting experimental data to a Maxwell model, this study highlighted that the time dependent modes required to model the data varied at different applied stress or strain increments, and additionally with the loading direction [98]. These results suggest that different micro-structural mechanisms may be activated in stress-relaxation and creep, determined by the microstructural organisation of the valve matrix in each loading direction, at each strain or load increment [98].

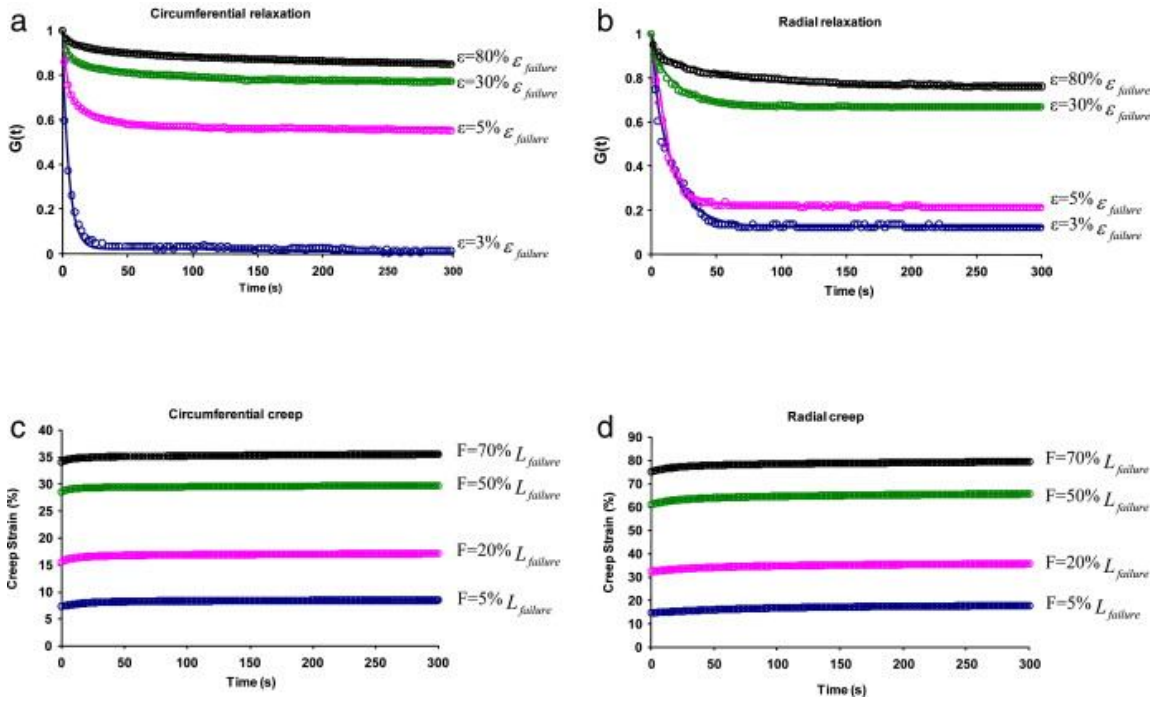

Fig.1- 21. Typical normalised stress-relaxation and creep curves from circumferential and radial samples (adapt from [98]). Experimental data are shown with circles (∘∘), and the model with a continuous line (—). Graphs show stress relaxation in the circumferential (a) and radial (b) directions; and creep strain in the circumferential (c) and radial (d) directions.

Studies regarding the biaxial time-dependant behaviour of heart valves are very rare in the literature. Stella et al. (2007) performed a biaxial stress-relaxation study on AV samples, loading the specimens up to 60 N/m of equibiaxial tension and monitoring relaxation over 3 hours (**Fig.1- 22**) [164]. These data indicate more apparent relaxation in the radial than circumferential direction, with values of 33.28% and 26.51% respectively [164].

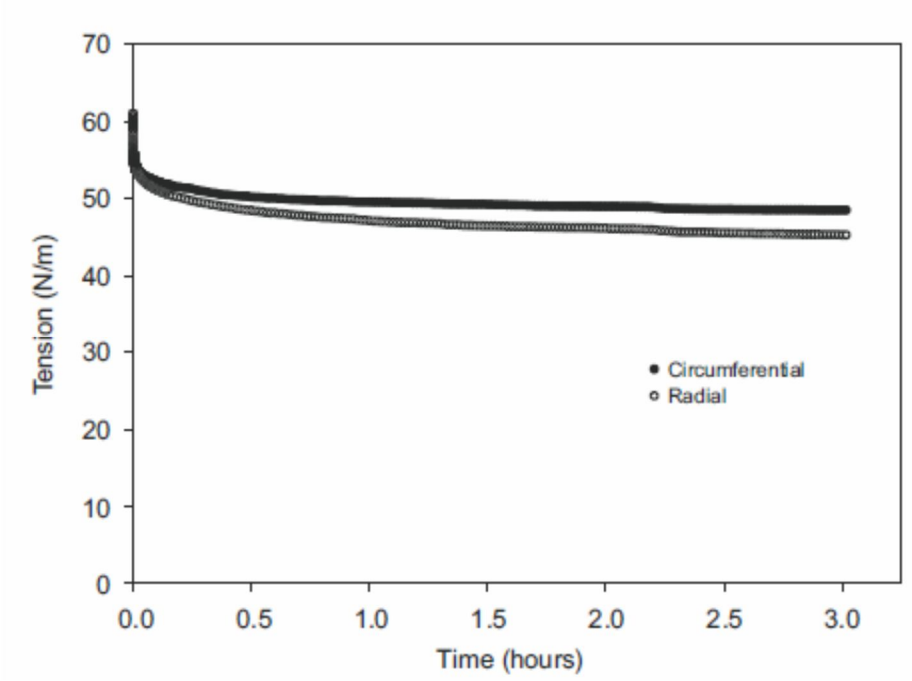

Fig.1- 22. Representative biaxial stress-relaxation curves of the AV (adapted from [164]).

Robinson and Tranquillo (2009) performed biaxial stress-relaxation tests, comparing equi- and non-equibiaxial loading regimes [193]. Their results indicated that as the ratio of radial to circumferential load increased, the amount of relaxation decreased in both directions [193]. Interestingly, they didn't find a significant difference between the relaxation values in each direction, even under equi-biaxial loading, in contrast to the previous study [164]. The reported relaxation values at different loading ratios are summarized in **Fig.1- 23**. Possible reasons for the differences between studies might be the geometry of the specimens and the gripping methods used, as Robinson and Tranquillo used cruciform test specimens and clamps as the grips, compared to the square shaped samples and the suture load-transfer mechanism employed in [164].

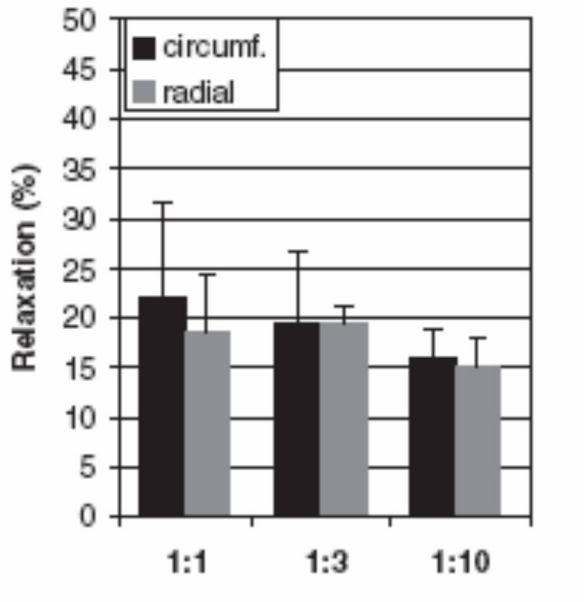

Fig.1- 23. The percentage of relaxation in AV specimens at different loading ratios, in each direction (Adapted from [193]).

1.5. Experimental structure-function analyses

There is increasing interest in the specific ECM components of the AV, and how they contribute to the AV mechanical behaviour [5, 6, 9, 88, 92, 155, 194]. However, the exact contribution of different component of ECM, especially the GAGs, to the mechanics of AV have not yet been adequately elucidated. Varied, even contradictory data concerning the effects of GAGs on mechanics of the AV have been reported by researchers [104, 108, 195].

Tseng et al (2013) studied the relationship between GAG concentration and the tensile and viscoelastic properties of aortic valve leaflets. GAGs were digested from aortic

valve leaflets by hyaluronidase, and then uniaxial tensile tests were used to explore the mechanical properties of the AV. It was found that modulus, maximum stress, and hysteresis all significantly increased with decreasing GAG concentration, but the extensibility and time-dependent properties did not change [195]. Borghi et al (2013) removal GAGs from aortic valve leaflet by a cocktail of enzymes, which included hyaluronidase, chondroitinase ABC, and keratinase, after which biaxial tests were used to investigated the viscoelastic properties of the valve leaflets [108]. In this study, it was found that removal of the GAGs from the AV lead to significantly slower relaxation, but had no effect on sample stiffness [108]. In another study conducted by Eckert et al (2013) [104], GAGs were digested from the AV by hyaluronidase and chondroitinase ABC prior to biaxial and flexion testing. The planar biaxial tension tests indicated that removal of GAGs had no effect on sample mechanical properties including peak stretch, hysteresis and time-dependent properties, but the results of three points bending tests showed that hysteresis was markedly reduced as a result of GAG removal [104].

These contradictory data indicated that the roles of GAGs on the mechanics of the AV are very complicated. Although GAGs are present throughout of the leaflet, they are mainly located in the central spongiosa, connecting the outside layers of the fibrosa and ventricularis. As described in chapter 1.4.2, manually separating the fibrosa and ventricularis in a leaflet leads to changes in the thickness and mechanical properties, suggesting that the spongiosa plays an important role in the mechanical properties of

the AV [9]. However, the regional distribution of GAGs and the effect of GAGs on local strain transfer across the aortic valve has not been fully investigated. Rigozzi et al (2009) studied the distribution of GAGs in the Achilles tendon, finding an inhomogeneous regional distribution. Furthermore, when they compared GAG digested samples with controls, no statistical change in ultimate tensile stress, failure strain, stiffness, or elastic modulus were evident, however, the local strain analysis revealed non-homogeneous distributions of strains in the tendon. Enzyme digestion of GAGs did not affect the strain distributions within the proximal and central midsubstance but significantly increased the tendon strains closer to the bone insertion. Digesting the GAGs caused local changes of elastic modulus in tendon in different regions and it seems likely that similar effect will be evident in other tissues. [196]. Therefore, it is critically important to understand and characterize the regional distribution of ECM in the AV, and establish how the microstructure responds to applied mechanical stimuli.

1.6. Aims and objectives

As in shown in **Fig.1- 24**, mechanical research involving aortic valves has been reviewed according the structure –function relationships from the organ and tissue to the molecular level: Firstly, AV's function and haemodynamic environment were reviewed in Section 1.1, and then the composition and structure of the aortic valve

and how this meets AV function were reviewed in section 1.2. Secondly, problems of dysfunction of the AV were introduced in Section 1.3. After which the mechanical environment of the AV in vivo was introduced, followed by some of the underlying mechanisms contributing to maintaining normal physiological function of the AV in vitro were reviewed; in section 1.4 and 1.5.

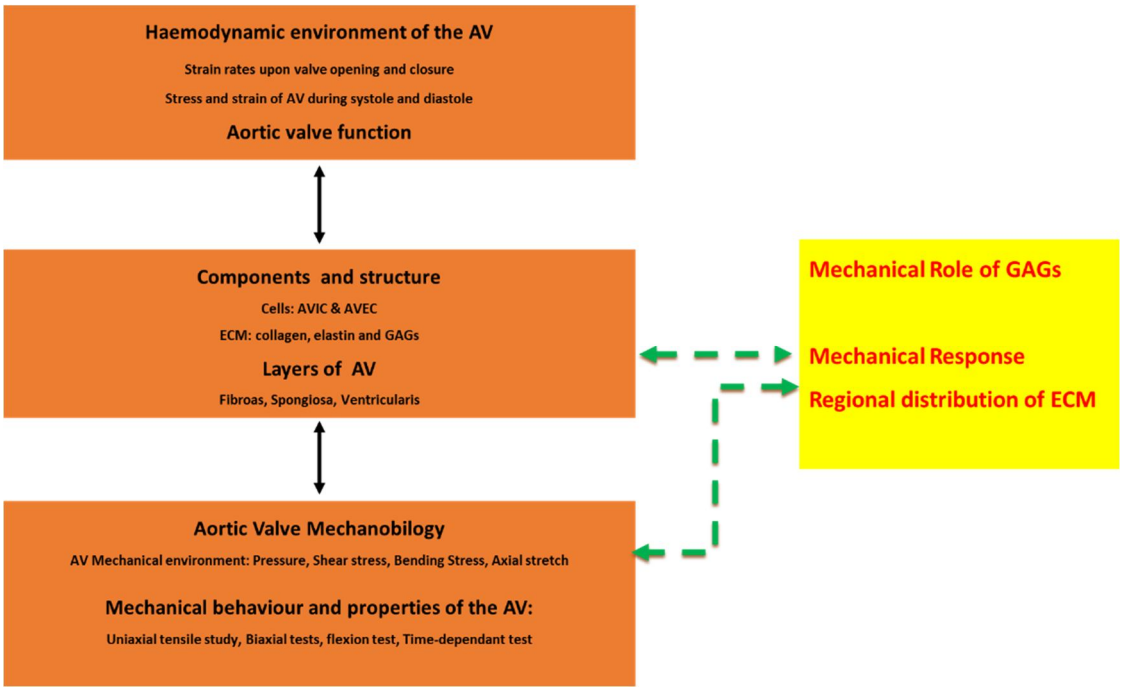

Fig.1- 24. Organization of the literature review in this study and identification of the area under investigation in this study.

This thesis aims to investigate the role of GAGs on the mechanical behaviour of the AV at both the tissue and microstructural levels. The objectives of this study are to:

1) Investigate the response of the tissue microstructure to applied loads, monitoring ECM reorganization and the response to applied strain.

2) Relate ECM micromechanics to the regional distribution of ECM through the AV leaflet.

3) Investigate how tissue micromechanics and gross mechanical behaviour are influenced by the enzymatic removal of GAGs

4) Relate the microstructural and micromechanical changes in AV behaviour before and after GAG removal.

Quasi-static uniaxial tensile tests were used to investigate the mechanical behaviour of AV, while AV micromechanics was studied using a custom designed rig, for straining samples as they are viewed under a confocal laser scanning microscope. ECM components were stained with fluorescence dyes, to monitor ECM reorganization. Histology was used to quantify the distribution of the ECM. Finally, initial biaxial studies of AV micromechanics were carried out. These data help to understanding the contribution of GAGs to the mechanical properties of the AV. Additionally, analytical information on AV micromechanics will help to design more efficient prosthetic and AV substitutes.

Chapter two

General Methodology

Aortic valves from porcine hearts were utilized to establish the objectives outlined in section 1.6. In this section, the general methodologies for sample preparation are described, alongside details of experimental equipment or techniques used throughout the study.

2.1 Sample preparation

Hearts were obtained from 18 -24 month old pigs, from a local abattoir (Cheale Meats Ltd, ESSEX, UK) and delivered to the laboratory on ice within two hours of slaughter. The three aortic valve leaflets were dissected from the heart, and first rinsed, then stored in Dulbecco's Modified Eagle's Medium (DMEM, Sigma–Aldrich, Poole, UK) for use within 30 minutes. As shown in **Fig.2- 1**, a 5mm wide strip was excised from each leaflet in either the circumferential or radial direction.

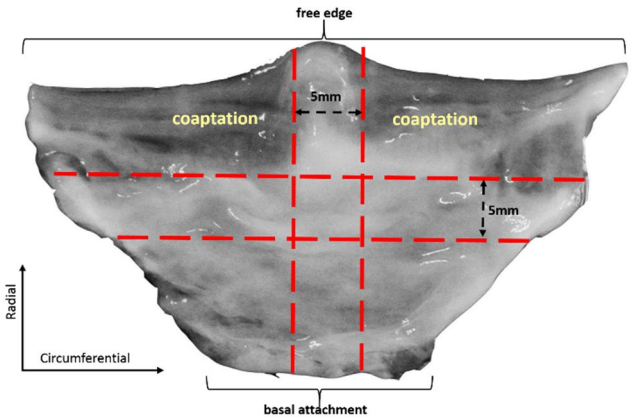

Fig.2- 1. Full length test strips were cut from the central region of each leaflet, in either the circumferential or radial direction.

2.2. Macro-mechanical tests

Mechanical testing of leaflets was performed on a material testing machine (ElectroPuls E1000, Instron, Bucks, UK) with a 250N load cell. The machine allowed for strain rates of over 1000%/min, and data acquisition frequencies of up to 100 Hz. Before loading the samples, an initial grip to grip distance of 10mm was set to maintain a consistent initial sample length. This length was selected for consistency with micro-mechanical tests, as it is the maximum length that can be analyzed in micro-mechanical tests. Samples were secured in one grip and hung so their own weight was used to keep them straight as they were secured in the second grip. Once secured,, the load cell was zeroed and then a tare load of 0.1 N was applied to the specimens, to establish a consistent zero position [98, 99, 155].The new distance between the grips was then used as the initial sample length to calculate the stretch ratios and strains [98, 99]. The force-elongation data was recorded at a frequency of 100 Hz. Throughout all tests, PBS was used to maintain hydration of samples.

2.3. Micro-mechanical tests

Micro- mechanics of the AV ECM were investigated using protocols based on a previously established method in the host lab [197, 198]. Tissue samples, after labelling with a fluorescence dye, were mounted in a custom made loading rig and imaged with confocal laser scanning microscopy. The samples were imaged before

and after the application of strain, and local strains in response to the application of mechanical stimuli. More details about fluorescing labelling agents, the imaging technique, and the loading rig are described in the following sections of this chapter.

2.4. Fluorescing labelling agent

Previously, 5-(4, 6-dichlorotriazinyl) aminofluorescein (DTAF) has been successful used to label the ECM of tendon [197, 198]. DTAF binds to proteins in the extracellular matrix through reactions between the chloro groups in the triazine ring and free amine groups found on lysine side-chains and protein N-termini at pH > 9 [199, 200], so it bind to almost all proteins which contain amine. The absorption and emission of DTAF is about 492 nm and 516 nm, respectively. Microscale deformations of labelled ECM can be measured by texture correlation [201-203] or by tracking the displacements of lines photobleached through the strain [197, 198, 200].

To find the optimal concentration of DTAF and the best incubation time for staining the AV in the present study, AV leaflets were incubated in a series of concentrations of DTAF for different incubation times from 5 to 60 minutes at 37℃. A buffer solution of 0.1 M sodium bicarbonate was made, and adjusted to a pH of 9.0. All staining conditions are shown in **Table 2- 1** (N=3 per condition). The resulting samples were viewed under a Perkin Elimer confocal laser scanning microscope.

Typical images are shown in **Fig.2- 2**, with data indicating that incubation for 10 minutes in 0.5 mg/mL DTAF at 37℃ was sufficient to successfully stain the collagen with the AV.

To image the cells of the AV leaflet, Hoechst 33258 and CellTrace™ Calcein red-Orange were selected to stain the nucleus and cytoplasm, respectively. The AV leaflets were incubated in a series of concentration of stains for different incubation times (**Table 2- 1**) at 37℃ to find the optimal conditions for both Hoechst and Calcein red-Orange. All staining was carried out in Dulbecco's Modified Eagle Medium (DMEM). Typical images are shown in **Fig.2- 3** and **Fig.2- 4**. Data indicated that incubation for 10 minutes in 1μg/mL Hoechst, and 30 minutes in 1μg/mL Calcein red-Orange, both at 37℃ was sufficient to successfully stain the cell nucleus and cytoplasm with the AV, respectively.

Table 2- 1 Conditions of dyes tested in present study

Dyes	Incubation times	Stain concentrations
DTAF	5, 10, 20, 40 and 60 minutes	0.5, 1, 2, and 4mg/ml
Hoechst 33258	10, 30 and 60 minutes	1 and 5μg/ml
Calcein red-Orange	10, 30 and 60 minutes	1, 5 and 10μg/ml

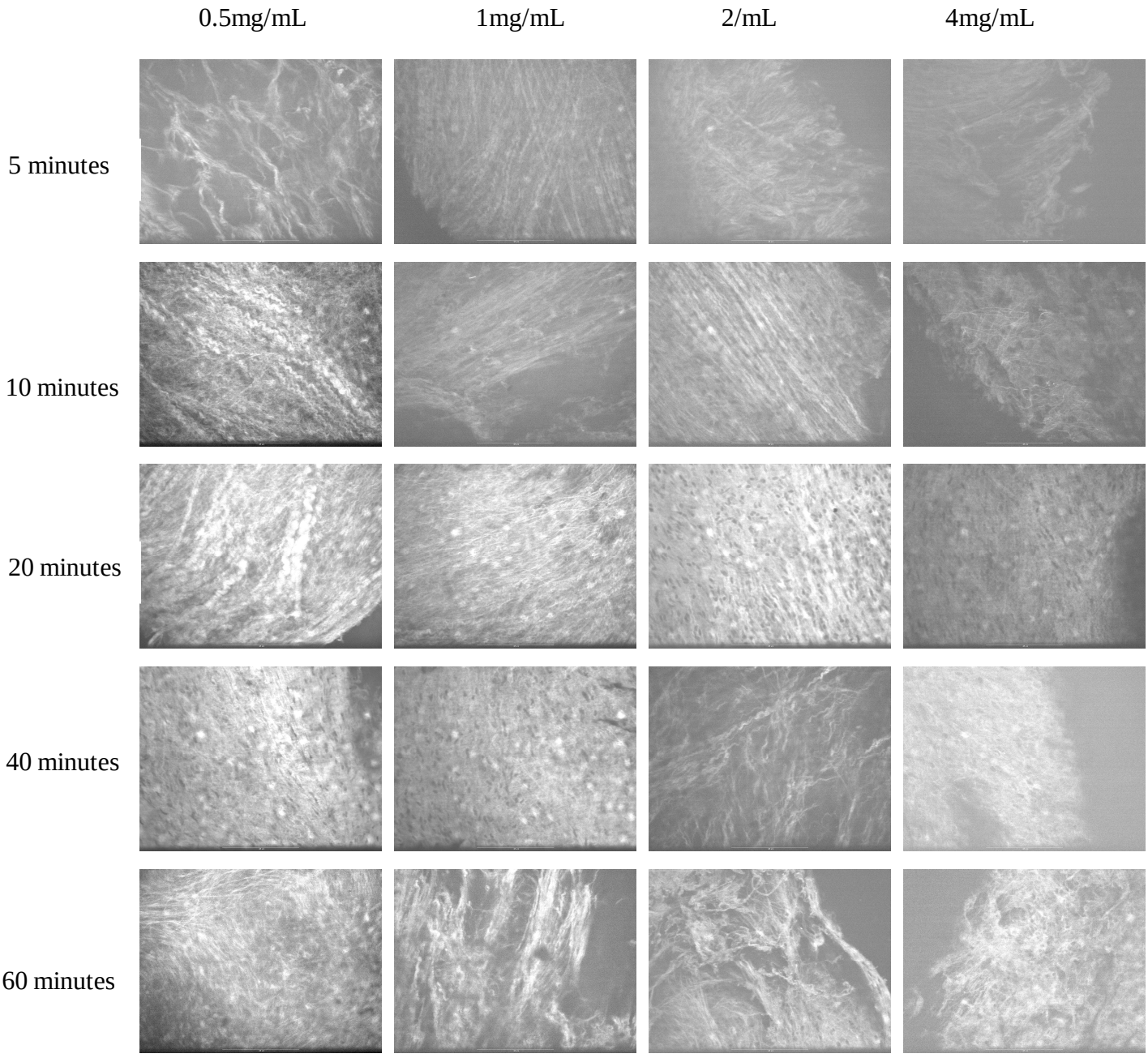

Fig.2- 2. Typical images of AV leaflets, stained with different concentrations of DTAF, for different incubation times.

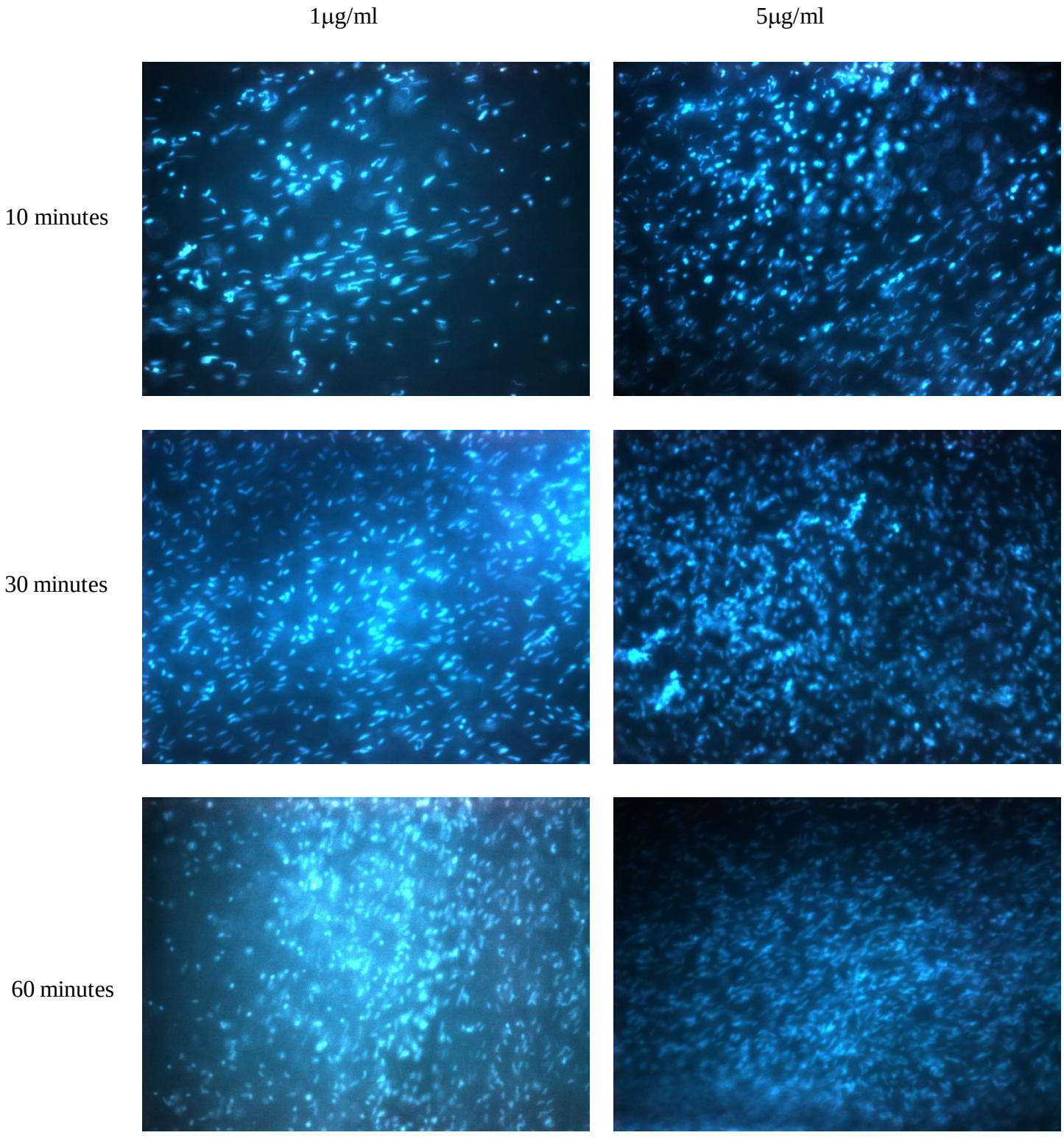

Fig.2- 3. Typical images of AV leaflets, stained with different concentrations of Hoechst 33258, for different incubation times.

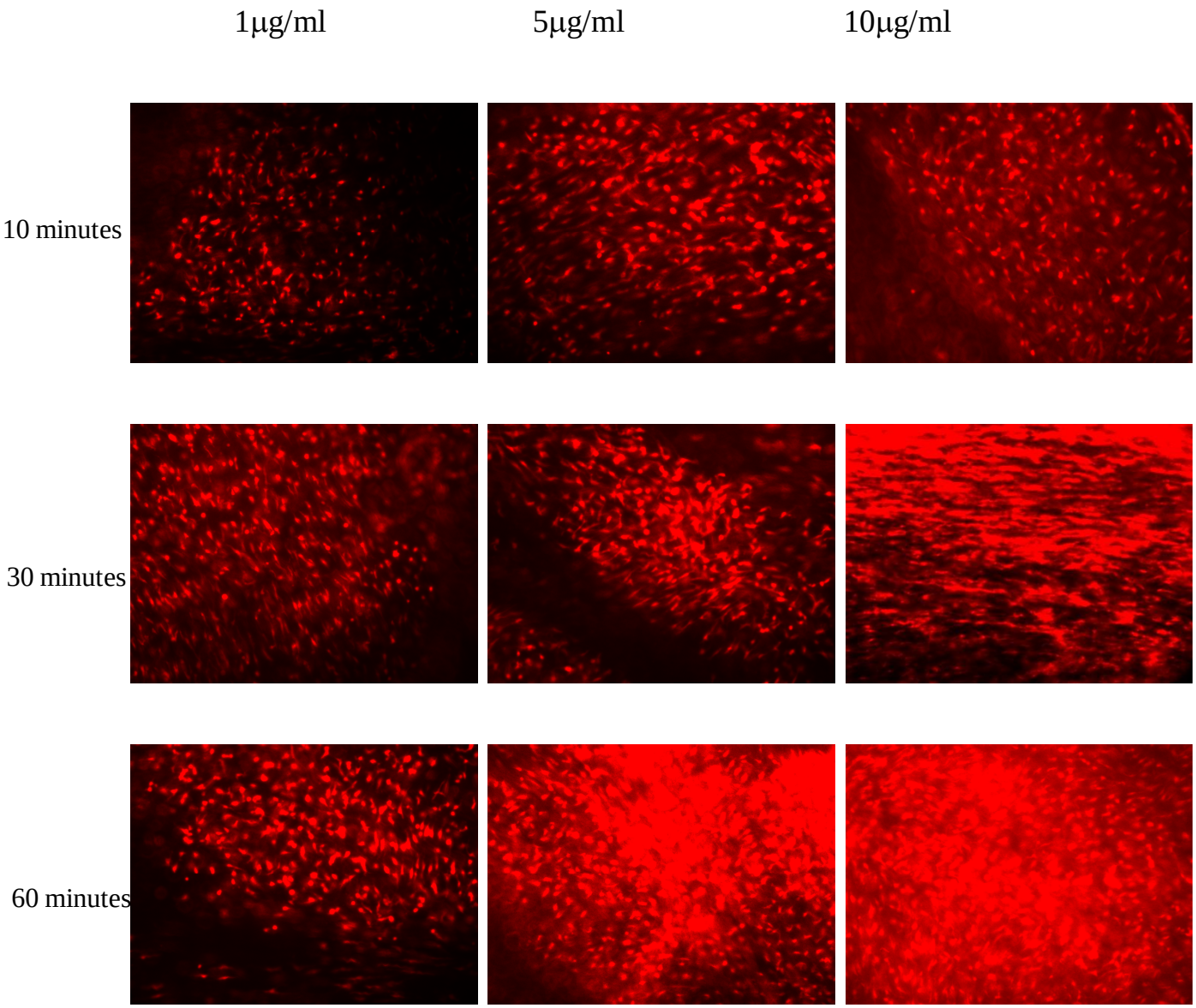

Fig.2- 4. Typical images of AV leaflets, stained with different concentrations of Calcein Red-Orange, for different incubation times.

The final condition selected for staining the aortic valve with each dye are summarized in **Table 2- 2**. Typical images are shown in **Fig.2- 5**.

Table 2- 2. The final conditions of dyes used in present study.

Dyes	Buffer	pH of buffer	concentration	Incubation time
DTAF	0.1 M sodium bicarbonate	9.0	0.5 mg/ml	10 minutes
Hoechst 33258	DMEM	7.4	1 µg/ml	10 minutes
Calcein red-Orange	DMEM	7.4	1 µg/ml	30 minutes

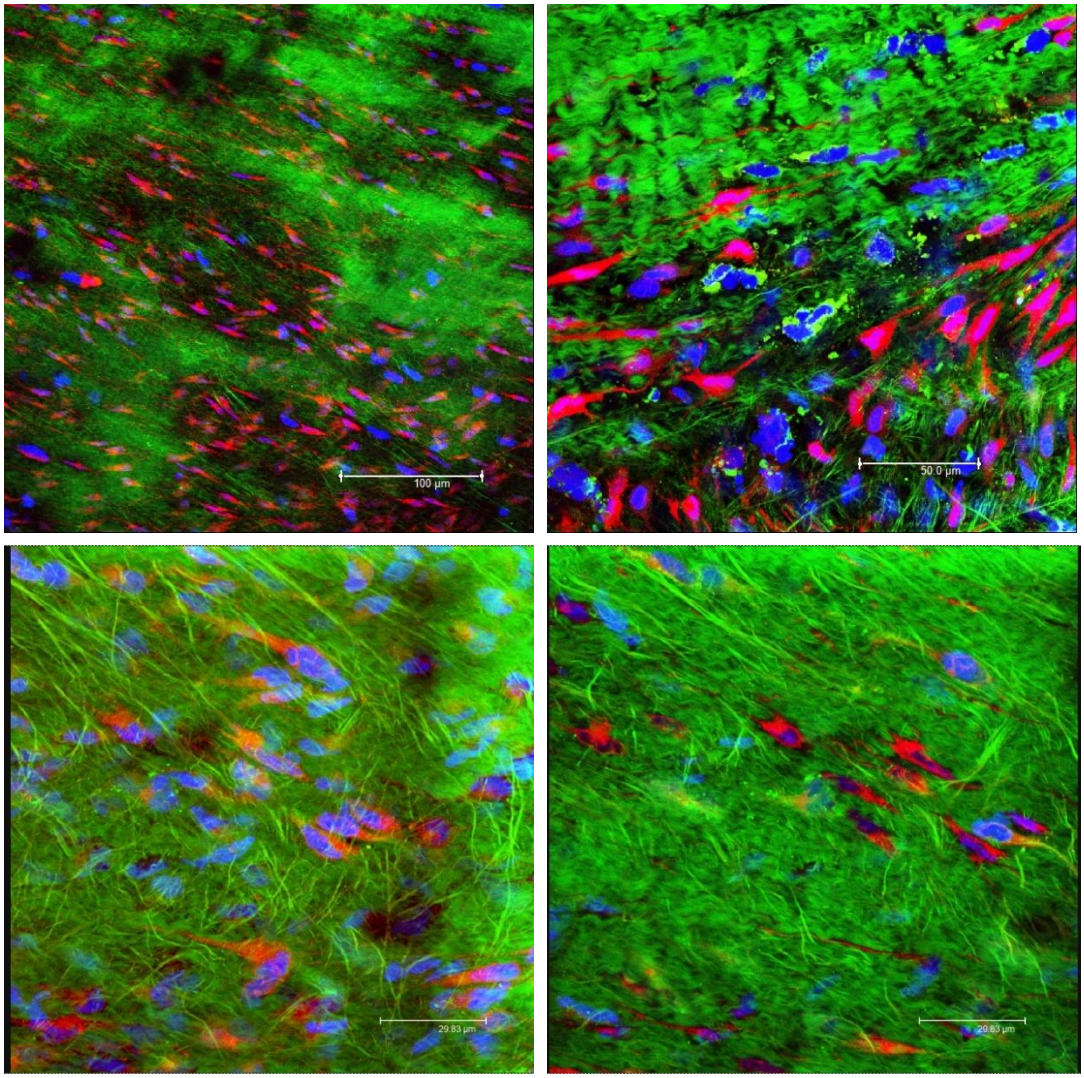

Fig.2- 5. Typical images of AV leaflets, stained with DTAF (green), Hoechst (blue) and Calcein Red-Orange (red).

2.5. Confocal laser scanning microscopy

A confocal laser scanning microscope (CLSM) uses a laser light source to excite a fluorescing contrasting agent within an imaged sample. The operational principal of a CLSM is shown schematically in **Fig.2- 6**. An illumination light is launched from a gas or solid-state laser of a specific wavelength or several wavelengths and then filtered to produce the specific wavelengths required [204]. Samples for analysis under the CLSM are dyed with fluorescent dyes, and the wavelength of the illuminating light, selected to excite the desired dye. When excited by a light source, the dye emits a longer wavelength that is then directed back along the same optical path as the illumination beam (**Fig.2- 6**). A beam splitter or dichroic mirror is used to divert the florescent emission towards a photodetector. Before the light hits the photodetector, it passes through set of filters (low pass and high pass) allowing only a narrow bandwidth of light to pass constituting the wavelength range of the peak of the emission wavelength curve. The confocal principle utilizes a pinhole (confocal aperture) to eliminate out-of-focus light from fluorescently labeled specimens (i.e., to provide “optical sectioning”). Lasers provide intense, point illumination that is scanned over the sample, and the fluorescence at each point is quantified and used to construct a representation of the object brightness (an image). This method provides high resolution for the x and y planes with the confocal optical sectioning also providing reasonable vertical (z plane) resolution.

The CLSM predominantly used in present study (TCS SP2, Leica Microsystems GmbH, Wetzlar, Germany) employs an argon laser as the illumination beam. Objective lenses were Nikon (HC PL Fluotar, Kingston-Upon-Thames, UK).

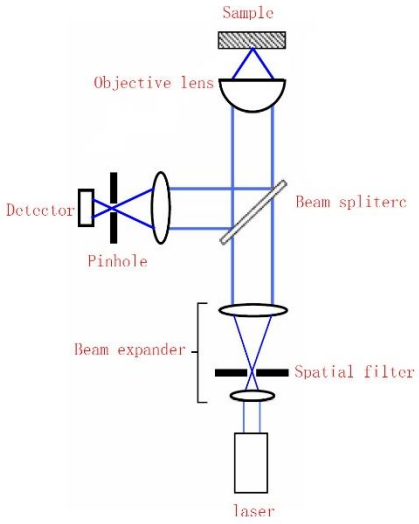

Fig.2- 6. Schematic of a confocal laser-scanning microscope (adapter from [204])

2.6. Loading rig

A uniaxial loading rig which was designed and developed in the host lab was used in this study [155, 194, 198]. It allows samples to be imaged whilst subjected to controlled applied deformation.

The samples were initially gripped at a length of 10 mm and were then given 0.1N preload, to provide a consistent zero-strain starting position for the tests. During imaging, sample were immersed in DMEM to maintain hydration. Under

displacement-control model, user-defined strains and strain rates were applied to samples via linear actuators. The force was measured by a 10N load cell with its upper limit set to 9.0 N to prevent potential overload during the experiments.

Chapter three

The Macro-mechanical Role of Glycosaminoglycans in the Aortic Valve

3.1. Introduction

Within the tri-layered AV, GAGs are the primary component of the central spongiosa layer, and it has been speculated that they provide resistance to compressive forces [5, 6, 205] and allow shearing between the layers of the cusp [5, 6, 205] due to their ability to bind water molecules [5, 6, 104, 108, 195]. However, the contribution of GAGs to AV, biomechanical properties has not been adequately studied. GAGs exist throughout the AV leaflet but are primarily located in the spongiosa, either in the form of HA or chondroitin (CS) and dermatan sulfates (DS) attached to the proteoglycan (PG) versican [101, 195, 206]. Chemically, GAGs are long, unbranched polysaccharides, which have been demonstrated to interacting with both collagen and elastic fibres [108, 206].

Several studies in the literature have analysed the effect of GAGs on the tensile properties of the AV and other GAGs-rich tissues. Viscoelasticity was found to be decreased in chordae tendinae and tendons, while no effect was found in cartilage and an increase in energy dissipation was found in lung tissue [108, 207-209]. Some studies have shown that GAGs do not play a direct role in modulating the time-dependent tensile properties of valvular tissues [104] and have no visible effect on stiffness [108] under biaxial mechanical testing. However, other uniaxial testing results show that the removal of GAGs from the spongiosa using hyaluronidase significantly increased sample stiffness [195]. The above studies are summarised in

Table 3- 1. These contradictory results indicated that the roles of GAGs on the mechanics of the AV may be very complicated. From these and other studies, it is hypothesized that under tensile loading, the biomechanical behavior of the AV is dominated by collagen and elastin, and removing the GAGs will have no significant effect on the macro tensile properties of the AV. Uniaxial tests were performed on samples pre- and post-GAG removal, using an enzymatic technique to remove the GAGs from the leaflet tissue.

Table 3- 1 Review of studies investigating the effects of different enzyme treatments to remove GAGs from porcine aortic valves.

Author	Methods	Enzyme	Incubated time	Mechanical properties
Tseng et al [195]	Cyclic preconditioning and uniaxial test to failure	0, 1, 2, 5, 10 U/mL of hyaluronidase, respectively	0, 8, 24 h, respectively	Elastic modulus, maximum stress and hysteresis significantly increased with decreasing GAG concentration. No effect on stress relaxation
Eckert et al [104]	Tensile test and Flexion test	30 U/mL Hyaluronidase and 0.6 U/mL chondroitinase-ABC	2 h	Hysteresis was reduced in low-force range with removal of GAGs. GAGs do not play a direct role in modulating the time-dependent tensile properties
Borghi et al [108]	Biaxial tensile test	5 U/mL hyaluronidase, 0.1 U/mL chondroitinase ABC, 0.15 U/mL keratanase	24 h	A slower relaxation with removal of GAGs, no effect on stiffness
Present study	Cyclic preconditioning and uniaxial test to failure	30 U/mL Hyaluronidase and 0.6 U/mL chondroitinase-ABC	24 h	No effect

3.2. Materials and methods

3.2.1. Tissue harvest

The aortic valve leaflets were prepared as described in chapter 2. Briefly, 28 porcine hearts were obtained from animals between 18 and 24 months, from a local abattoir (Cheale Meats Ltd, ESSEX, UK) within two hours of slaughter. The three Aortic valve leaflets were dissected from the heart, rinsed and stored in Dulbecco's Modified Eagle's Medium (DMEM, Sigma–Aldrich, Poole, UK) until use within 30 minites. The leaflets were then randomly divided into three groups: fresh control, buffer incubated control and digested group (N=28 in each group).

Leaflets in the fresh control group underwent mechanical testing immediately after harvesting. 100 mM, pH7.0 ammonium acetate buffer solution (AABS) buffer solution was made for the samples of the remaining 2 groups. To remove all of the GAGs from the digested groups samples, the specimens were placed in a conical tube with 2.4 ml of buffer solution per leaflet, adding 5 U ml^{-1} hyaluronidase (#H3631, Sigma–Aldrich) and 0.1 U ml^{-1} chondroitinase ABC (#C3667, Sigma–Aldrich). The protocol was adapted from Lovekamp et al [108, 206]. The buffer incubated samples were subjected to buffer, with no added enzymes. Samples in both the digested group and buffer incubated group were placed in their respective solutions and continuously

shaken for 24h at 37^{o}C. The buffer solution was then removed and the leaflets were washed with PBS three times, for 5 min each time. All samples were maintained in PBS to retain hydration until mechanically tested.

3.2.2. GAG content quantification

Quantification of GAG content was performed with the uronic acid assay using previously published methods [206, 210]. Briefly, the leaflets (N=5 in each group) were frozen and lyophilized overnight, then ground to a powder using a mortar and pestle. The dry weight (DW) of each ground leaflet was measured before 20 mL of 0.5M Sodium hydroxide (NaOH) was added to each sample, and samples shaken at 4°C overnight. Trichloroacetic acid was added to the suspension, to obtain a 10% final concentration and then the samples were shaken at 4°C overnight again. All samples were centrifuged and the supernatant was dialyzed (#PURG35015, Pur-A-Lyzer™ Mega Dialysis Kit 3500kD MW, Sigma–Aldrich) against water for 24 h, changing the water periodically. The GAGs in the supernatant were then precipitated with cetylpyridinium chloride for 24 h at 37 °C in glass centrifuge tubes, and collected by centrifugation (2000g, 10 min). The supernatant was removed, the sample resuspended in sodium acetate, and then re-precipitated with absolute ethanol for 48 h at -20 °C. The GAG pellet was then collected by centrifugation (2000g, 10 min).

GAG pellets were dissolved in 1 mL of benzoic acid saturated water in a glass tube. 5

mL of borax-sulfuric acid reagent (0.025M sodium tetraborate decahydrate solution in concentrated H_2SO_4) was layered on top, with constant cooling by dry ice. These samples were then heated for 10 min in a boiling water bath, and then allowed to return to room temperature. To each tube, 0.2 mL of 0.125% carbazole in absolute ethanol was added, and the tubes were again heated in boiling water for an additional 15 min. The samples were cooled to room temperature and then transfer into a 96 well plate. The optical absorbance at 540nm was measured using a microplate spectrophotometer. Glucurono-6,3-lactone standards were prepared at concentrations of 0, 30, 60, 90, 120,150,180 and 210 mg/mL in a solution of benzoic acid saturated water, and a standard curve obtained, to quantify the GAG concentration.

2.2.3 Histology

Alcian Blue/Penodic Acid Shift (PAS) staining was employed to investigate removal of the GAGs. AV leaflets (N=3 in each group) were fixed overnight in 4% paraformaldehyde, then dehydrated, embedded in paraffin, and sectioned according to standard procedures. Staining was then performed. Sections were deparaffinized in three changes of xylene, 3 minutes each, followed with hydration through two changes each, of first 100% and then 95% ethanol, performing 10 dips in each wash. Finally samples were washed well with distilled water. Sections were then stained in Alcian blue (1%, in 3% Acetic Acid) for 30 minutes and then washed for 2 minutes under tap water and several changes of ultrapure water. Sections were treat with 0.5%

periodic acid (#HC6405TCS, Bioscience) for 10 minutes then rinsed under running tap water for 5 minutes, followed by a distilled water rinse. Sections were treated with schifs reagent (#3952016，Sigma–Aldrich) for 15 minutes and then washed under running tap water for 5 minutes. Mayer's Haemalum (#51275, Sigma–Aldrich) was used to stain the nuclei within the section, and then the sections were washed in running tap water for 5 minutes. Sections were dehydrate in two changes each of 95% and 100% ethyl alcohol, and cleared in three changes of xylene, performing 10 dips each time, they were finally mounted with clarion mounting media.

3.2.3. Mechanical testing

For leaflets in each group, a 5 mm wide strip was cut in either the circumferential or the radial direction for uniaxial mechanical testing (N = 60: 3 test groups × 2 loading directions × 10 samples). The thickness of each sample was measured, using a non-contact laser micrometer (LSM-501, Mitotuyo, Japan; resolution = 0.5μm). Each sample was first place on a cover slip and then moved through the laser beam, and thickness measurements recorded at 5 places, from which the mean thickness was then used to determine the cross-sectional area of each sample. The samples were returned to PBS to maintain hydration before performing the experiments. All experimental tests were carried out within four hours of excision of the tissue strips.

Mechanical testing of leaflets was performed on a material testing machine (ElectroPuls E1000, Instron, Bucks, UK) with a 250N load cell and an initial grip to grip distance, L_i = 10mm. Samples were firstly gripped in the top grip to allow samples to hang under their own weight before gripping the other end. Prior to the start of each test, the load cell was zeroed, and then a tare load of 0.1 N was applied to the specimens, to establish a consistent zero position, and the adjusted distance L_0, used to as the initial sample length to calculate the strains. The force-elongation data was recorded at a frequency of 100 Hz. The sample was subjected to 15 preconditioning cycles at a strain rate of 1% per second, going to a maximum strain of 12% in the circumferential direction and 30% in the radial direction, equivalent to 40% of the failure strain of a freshly dissected sample for each direction [211]. After the preconditioning cycles, the sample was pulled to failure at the same rate. Throughout the test, hydration of the samples was maintained by spraying with PBS. **Fig.3- 1** show the strain profile of the mechanical test.

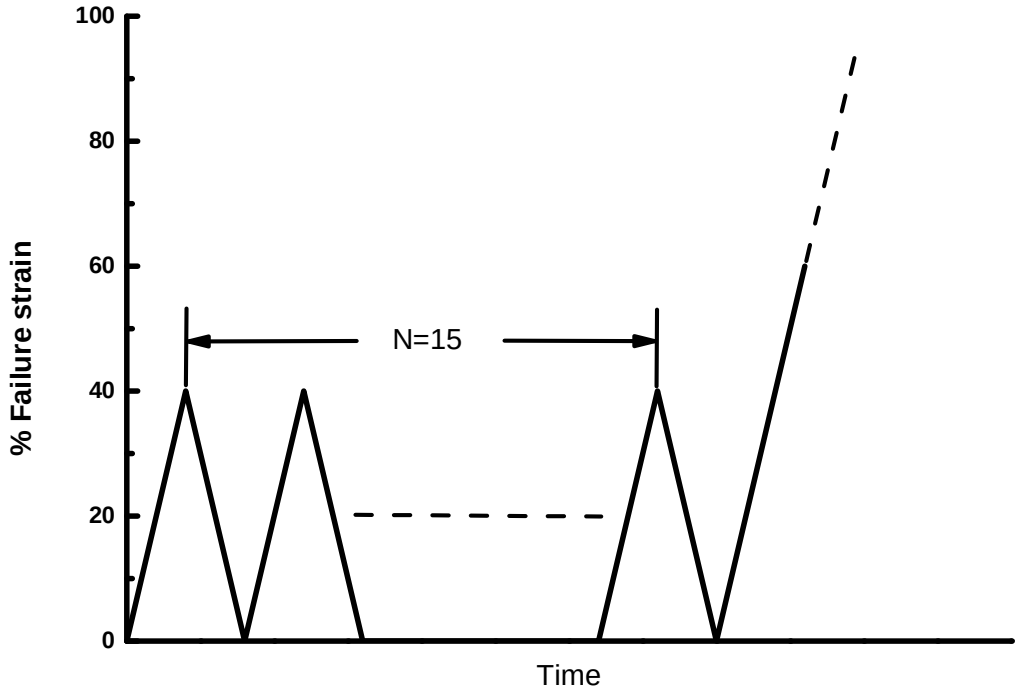

Fig.3- 1. The strain profile for mechanical testing. Leaflets were preconditioned by stretching to 12% in the circumferential direction or 30% in the radial direction, equivalent to 40% of the failure strain of a freshly dissected sample for each direction [211]. After 15 cycles of preconditioning, samples were pulled to failure.

3.2.4. Data analysis

The preconditioning cycles were analyzed to investigate the viscoelastic properties of the leaflets. To normalize data for easy comparison, all parameters, include load, hysteresis and modulus, were expressed as a percentage of the peak values in the first cycle.

All computed values were represented as mean ± standard error of the mean. Statistical analysis was performed using statistical analysis software (IBM SPSS®

Statistics 22, Chicago, USA), and a one-way ANOVA test was used for statistical analysis between the test groups. When significant, least-significant difference (LSD) multiple comparisons were performed to determine the significance between groups. Statistical significance was assumed at $p<0.05$.

3.3. Results

3.3.1. GAG content

Incubation in 5 U ml^{-1} hyaluronidase and 0.1 U ml^{-1} chondroitinase resulted in a significant reduction in GAG content in the digested group relative to the buffer incubated control and the fresh control group (**Fig.3- 2**). There was also a significant reduction in GAG in the buffer control group relative to the fresh control group (6.14μg GAG/mg tissue vs. 8.77 μg GAG/mg tissue, in the buffer control and fresh control group respectively, $p<0.05$). However, this was not as significant as the reduction in the digested group, where 96% of GAG was removed (0.35 GAG/mg tissue in digested group, $p<0.01$).

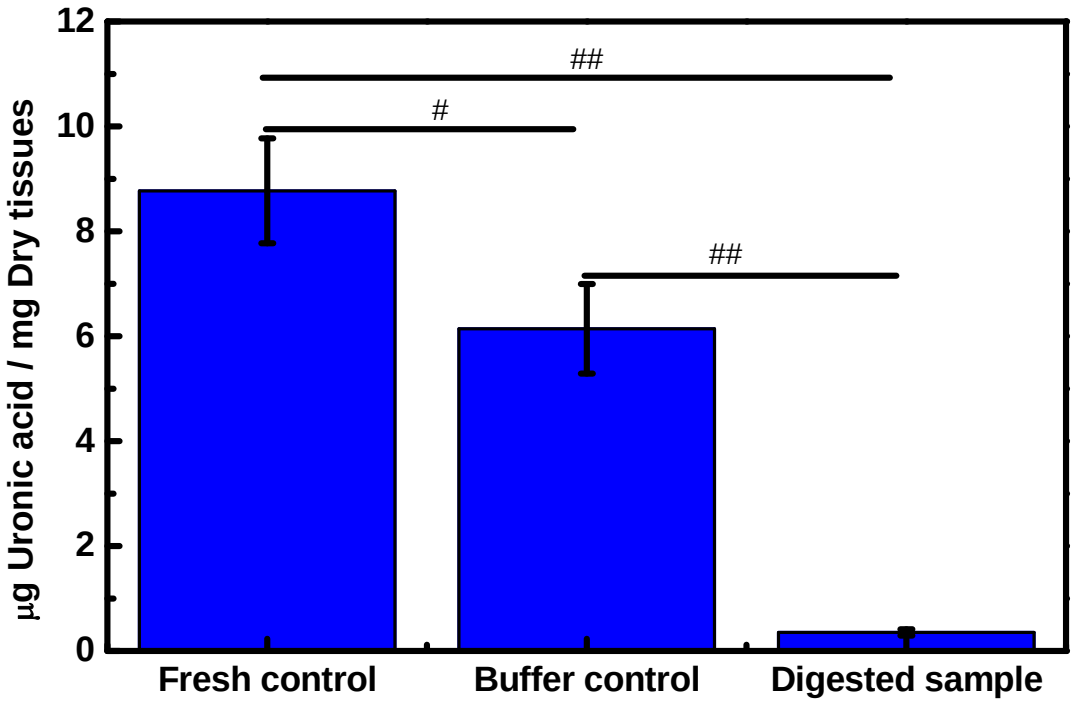

Fig.3- 2. GAG quantification by uronic acid assay. The digested sample group showed a significant decrease in GAG relatively to both the fresh dissected and buffer incubated groups. However, the GAG content was also significantly different between the fresh control and buffer control groups ($p<0.05$) (#: $p<0.05$; ##: $p<0.01$).

3.3.1. Histology

The removal of GAGs from the spongiosa was additionally confirmed by histology. **Fig.3- 3** shows cross sections of the valves in the three different groups, in which GAGs are stained in blue. From **Fig.3- 3**, it can be seen that GAGs were presented throughout the tissue in fresh control and buffer control samples, while no GAGs could be seen in the digested group.

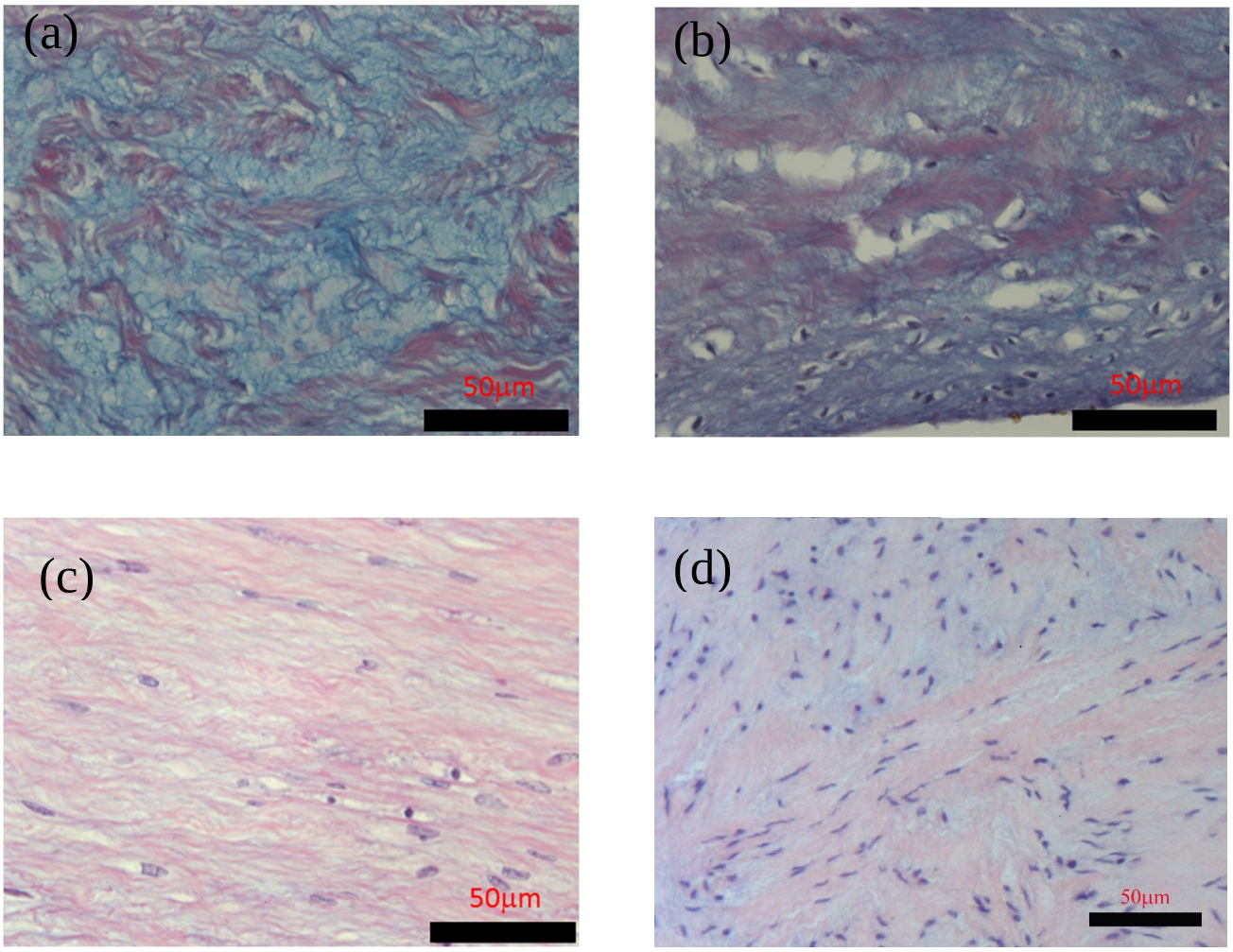

Fig.3- 3. Alcian Blue /PAS staining of AG leaflets, comparing (a) fresh control, (b) buffer incubated control, and (c) GAG digested samples (blue staining is positive for GAGs), (d) H & E staining showing the cell population (blue) of a fresh control leaflet.

3.3.2. Mechanical testing

Initially, the degree of extension required to apply the tare load, and load the samples to 0.1 N was assessed. Caution must be exercised when analysing these data, owing to the potential variation in the initial laxity of the samples. However, all samples were loaded into grips in an identical manner, and the relatively small error bars concerning

sample extension to reach the tare load, indicate consistency in the approach. It was notable that in the circumferential direction, ΔL was significant larger in the buffer control and digested groups relative to the fresh control (**Fig.3- 4** a). However, data also indicated that the extension required to reach the tare load was reduced in the digested group (**Fig.3- 4** a). Comparing the ΔL for the two different loading directions, unsurprisingly ΔL was larger in the radial direction than the circumferential direction in all samples group (**Fig.3- 4** b).

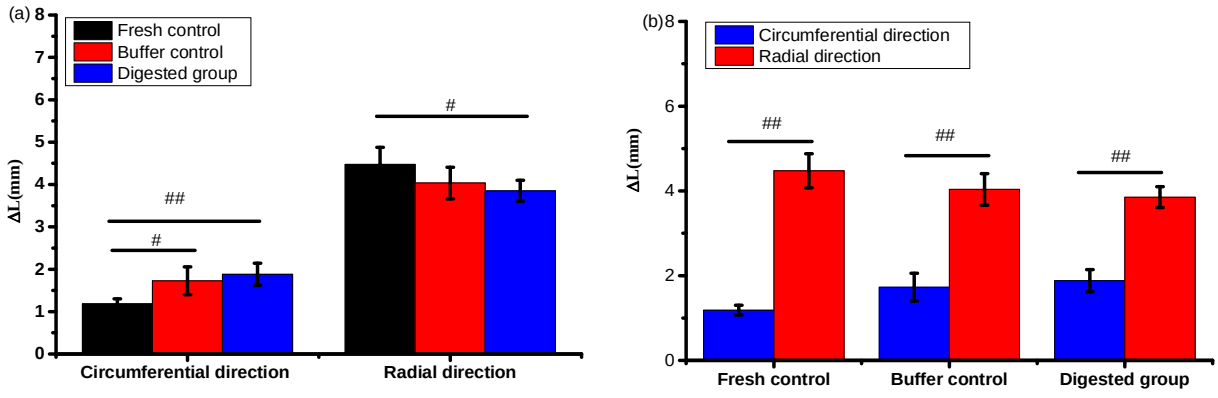

Fig.3- 4. Companion of the initial extension required to reach the 0.1N tare load in each test group and strain direction

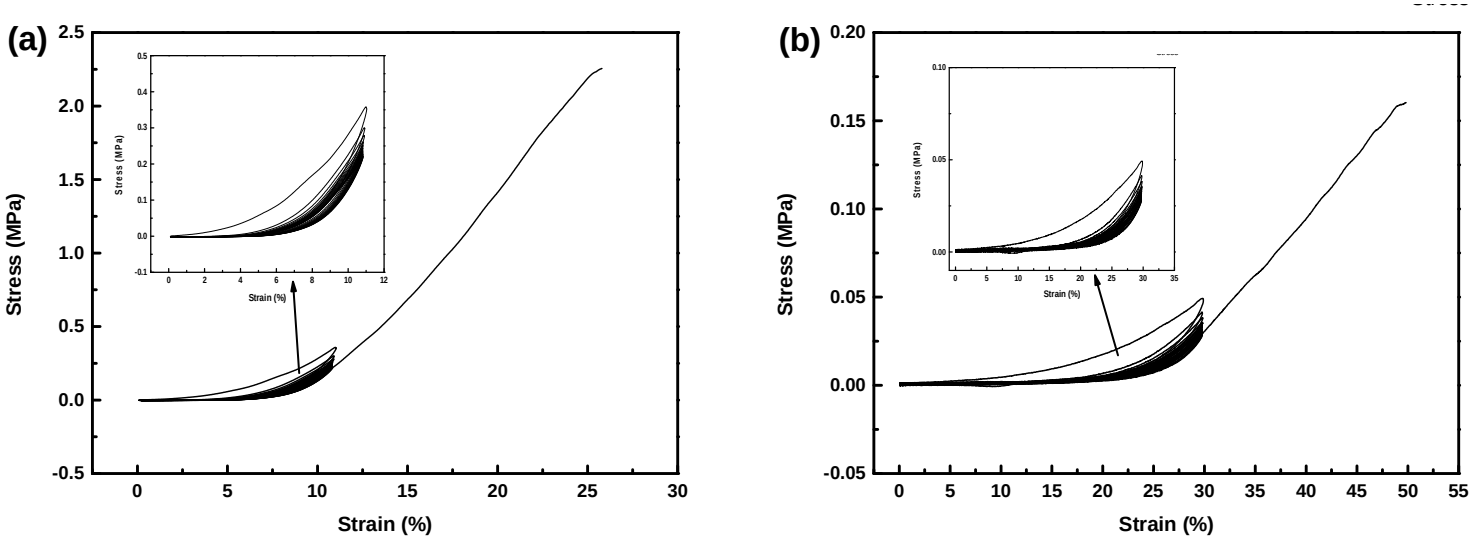

Fig.3- 5. Typical strain−stress curves for the fresh AV strips (a) circumferential specimens, and (b) radial specimens. Insert pictures show the preconditioning cycles. Note that due to the highly anisotropic behaviour of the AV, the scale of the axes in the two graphs are not the same

Typical strain-stress curves for the AV samples were shown in **Fig.3- 5**. The hysteresis loss, peak load, and maximum loading modulus for each loading cycle were determined over the preconditioning cycles, and the % drop in peak load calculated under both circumferential (**Fig.3- 6** a-d) and radial (**Fig.3- 6** d-h) loading. There were no significant differences between treatment groups in hysteresis loss (**Fig.3- 6** a & **Fig.3- 6** e), peak load (**Fig.3- 6** b & **Fig.3- 6** f), % drop in peak load (**Fig.3- 6** c & **Fig.3- 6** g) or maximum modulus (**Fig.3- 6** d and **Fig.3- 6** h) in either the circumferential or radial direction. Hysteresis drop was greatest in the first cycle, then constant for further cycles, with no significant differences between groups.

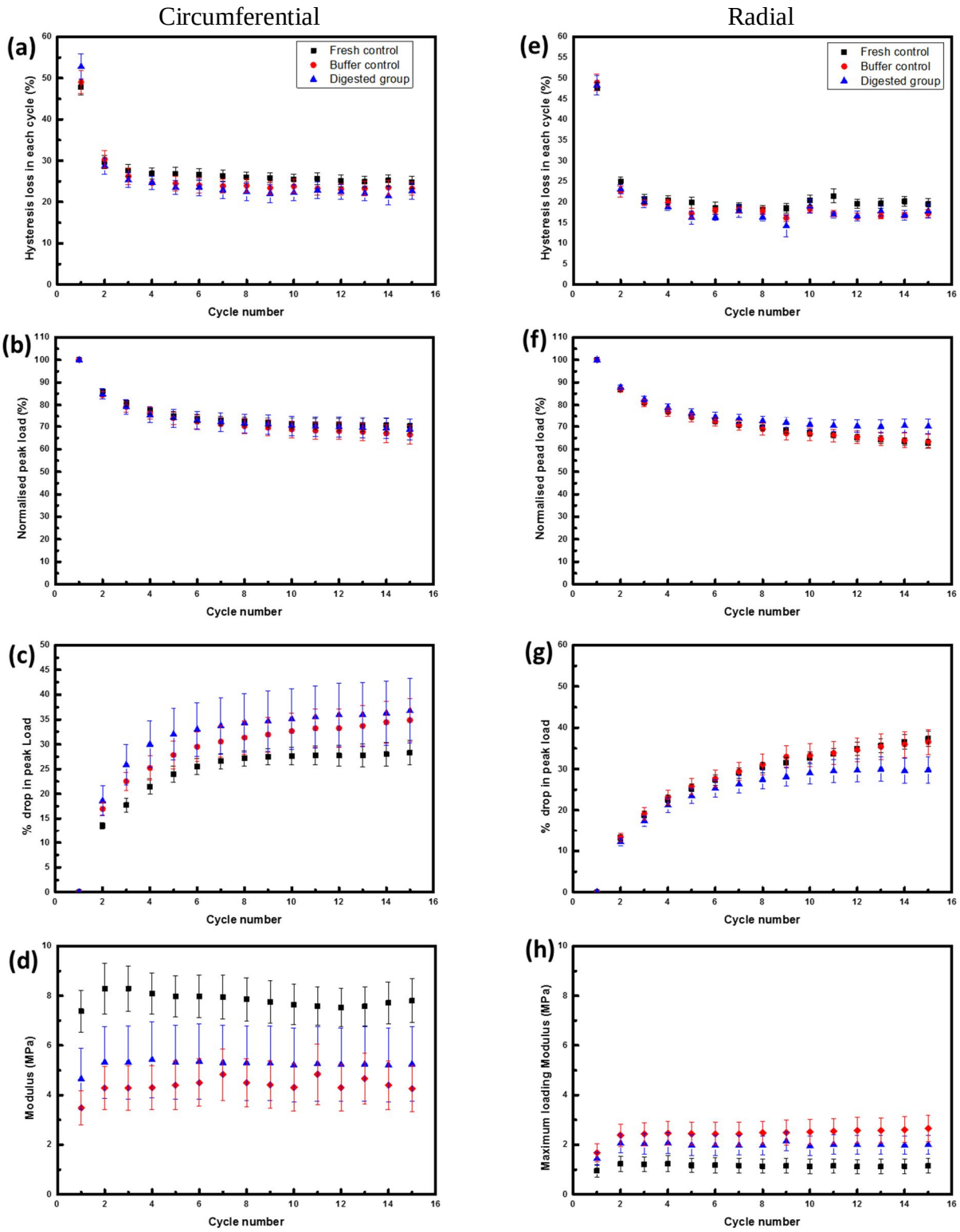

Fig.3- 6. Hysteresis (a, e), peak load (b, f), % drop in peak load (c, g) and loading modulus (d, h) of leaflets in each group, in both the circumferential (a–d) and radial directions (e–h) in each cycle. No significant differences were seen between groups in any of the parameters. Hysteresis was large in the first cycle, but then dropped rapidly. The module was calculated over every eight data points at 0.01 % increments along the stress–strain curves and smoothed with a five-point moving average filter. Maximum loading modulus is given.

The strain at peak modulus in each cycle was also investigated. There were no measureable changes between groups for either loading direction (**Fig.3- 7**).

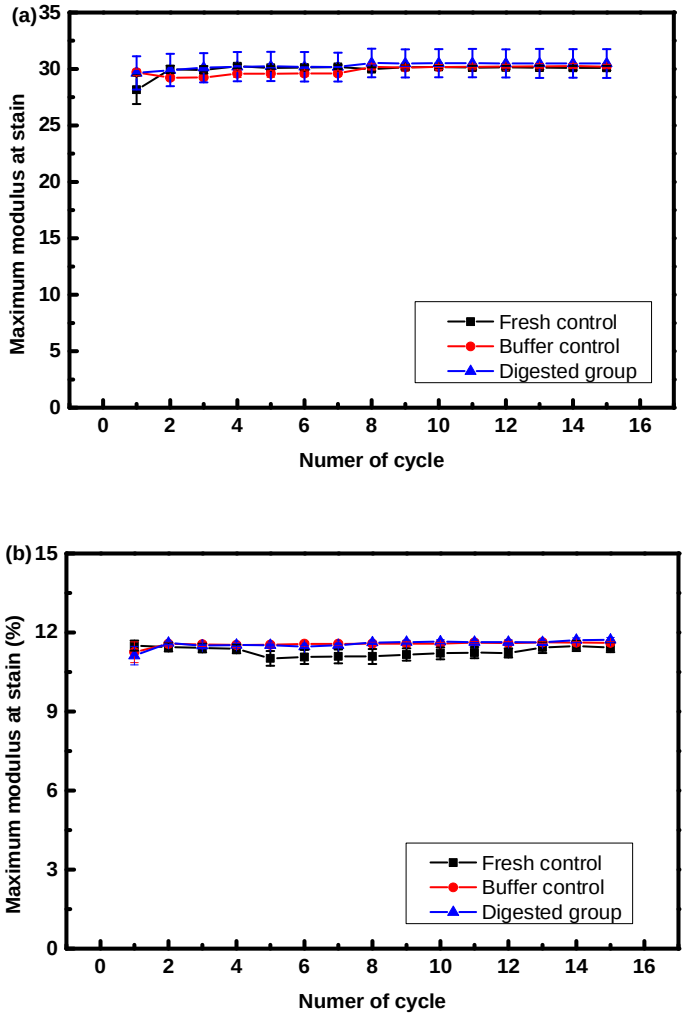

Fig.3- 7. Strain at the maximum modulus in each cycle for samples in each group strained in the radial (a) and circumferential (b) directions.

3.3.3. Tensile Testing

After 15 cycles of preconditioning, the samples were stretched to failure at the same loading rate. The failure strain, ultimate tensile strength (UTS) and maximum modulus were established for each sample. The removal of GAGs did not affect any

loading parameter in either loading direction. However, similar to previous studies [98, 99, 155], all groups shown anisotropy properties, with significant differences seen between the circumferential and radial loading directions (**Fig.3- 8**).

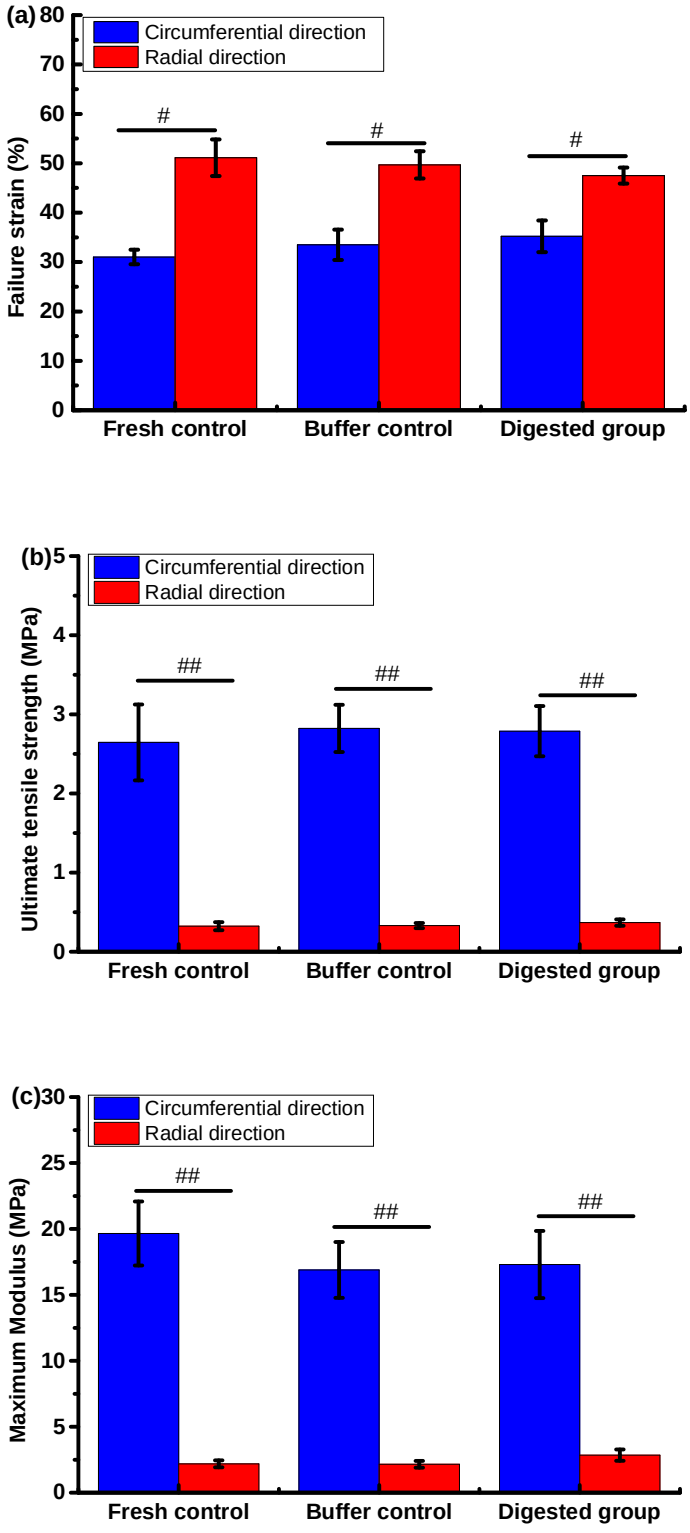

Fig.3- 8. Results of the quasi-static tensile test to failure in each group. No significant differences in failure strain (a), ultimate tensile strength (UTS) (b) or maximum modulus(c) were seen between test groups. However, all parameters were significantly different when straining in the circumferential and radial directions (#: $p<0.05$; ##: $p<0.01$).

3.4. Discussion

For investigating the mechanical role of GAGs in the aortic valve, GAGs were successfully removed from the AV leaflet by Hyaluronidase and chondroitinase-ABC, with removal confirmed by biochemical assay and histology.

Uniaxial tests were performed on specimens pre- and post-GAG removal. Interestingly, in the present study, we observed that removal of the GAGs from the aortic valve had no significant effects on the gross mechanical properties of AV leaflet tissue.

During preconditioning, large levels of hysteresis and a big drop in peak force were seen during the first loading cycle, but both parameters then stabilized.

Such a response it quite typical of soft connective tissues [212] but there were no significant differences with GAG digestion. The quasi-static test to failure also showed no direct role of GAG in the mechanical properties of aortic valves (**Fig.3- 8**), with no differences between treatment groups. However, samples did show marked anisotropy in the mechanical behaviour of the tissue. In agreement with previous studies [98, 99, 173, 174], valves were much stiffer in the circumferential than radial direction.

Previous studies have suggested that GAGs play an important role in aortic valves. It is hypothesised that GAGs absorb shear between layers of the valve, to cushion shock

between the ventricularis and fibrosa during cyclical valve motion [94, 109]. Research in the field of bioprosthetic heart valves (BHVs) has demonstrated that there is a correlation between the loss of GAGs and early BHV failure [206, 213], with the resulting dehydrated leaflets being stiffer in planar shear and experiencing increased hysteresis [214]. A further study showed that the 4-sulfated/6-sulfated GAG ratio correlated with tensile and compressive loading parameters, and increased levels of sulfated GAGs were consistent with an altered matrix microstructure, capable of increasing the hydration of these pathological tissues, and resulting in a reduction in mechanical strength [215].

Eckert et al [104] measured the effects of GAGs on the biaxial mechanical properties of the aortic valve. In this study, GAGs were removed from leaflets using 30 U/mL Hyaluronidase and 0.6 U/mL chondroitinase-ABC, and no significant changes were found in AV tensile behaviour, suggesting that the GAGs do not play a direct role in modulating the tensile biomechanics of AVs [104]. Interestingly, hysteresis was also calculated from a flexion test in this study, and no significant differences were seen in the hysteresis of digested leaflets at peak physiological tension (90 N/m), while significantly lower hysteresis was found at low tension (10 N/m). Comparing this study to the present study, different concentrations of enzymes and different enzyme incubation times were used. In the study by Eckert and coworkers, only about 55% of the GAGs were removed, and the hysteresis was calculated from a flexion testing technique, while the present study used a uniaxial tensile test. Another study

conducted by Borghi et al also found that removal of GAGs from aortic valves had no effect on stiffness, but they did show a significant effect on the time-dependent properties, with GAG digested samples showing a significant slower relaxation rate [108]. A recent study in porcine aortic valve leaflets used hyaluronidase in concentrations ranging from 0 to 5 U/mL for 0 –24 h to digest GAGs prior to uniaxial tensile testing or stress relaxation testing [195]. In this study, the elastic modulus, maximum stress, and hysteresis of samples all significantly increased with decreasing GAG concentration, which strongly contrasts the results of present study, as it suggest that GAGs influence both elastic and viscoelastic properties of aortic valves leaflets [104, 108, 195]. Studies investigating the effects of enzyme treatments to remove GAGs from porcine aortic valves are summarized in

Table 3- 1.

The contradictory results of the mechanical role of GAGs are not only found in studies of aortic valves, but also in other GAG-rich tissues. There is some evidence that sulfated GAGs play a role in quasi-static tendon mechanics [216-218], while other studies indicate that this may not be true [196, 219, 220]. Marturano et al [221] found that there was no correlation between glycosaminoglycan content and modulus in embryonic tendon, but statistically significant correlations with between modulus and collagen content. Iinhibiting lysyl oxidase-mediated collagen cross-linking significantly reduced tendon modulus. In vitro experiments by Lujan et al [219] in human knee ligaments depleted dermatan sulfate through chondroitinase B digestion and showed no differences from controls in elastic modulus, hysteresis, or failure behaviour. Experimental evidence yields a convoluted picture on the role of GAGs in modulating viscoelastic properties [220]. One study has shown that removing GAGs from ligaments with chondroitinase ABC has no statistically significant effects on viscoelasticity [222]. By contrast, Chondroitinase ABC treatment has been shown to reduce viscoelastic effects in tendon and palmer aponeuroses [223], but also to increase the stress-relaxation response of tendon fascicles [224].

Considering all the data presented in **Table 3- 1**, it could be hypothesized that GAGs play a different role at low and high strains. The tensile stress–strain curve of the AV can be split into a number of regions or phases (**Fig.1- 13**), whose characteristics are

thought to be associated with specific physiological functions [172]. The main phases of the curve are: (i) the low stress–low strain pre-transition phase, which can be linked to the straightening of the crimped collagen fibers and elongation of the elastin fibers; (ii) the highly non-linear transition phase that might be related to the transfer of force from the elastin to the collagen fibers; and (iii) a post-transition linear elastic region, linked with the elongation of elastic and collagen fibers [172].

The viscoelastic response of the AV under tensile deformation was investigated and quantified in this chapter, using quasi-static mechanical tests. These tests have confirmed the previously reported nonlinear and anisotropic behaviour of the AV, with a stiffer response in the circumferential direction (**Fig.3- 5**). Further, data from the current study suggests very few changes in gross AV mechanics in response to GAG depletion, not only on non-linear transition phase but also post-transition linear elastic phase. However, there is some indication that the amount of sample extension required to reach the tare load at the start of tests may vary with GAG removal. Care must be taken when interpreting these data, as small variations in the initial laxity of the sample will potentially affect this parameter, making it hard to draw any conclusive conclusions. However, with practise, it was possible to secure all samples in the grips in a consistent manner, with minimal laxity prior to the application of the tare load, and the small error bars evident when investigating the extension required to reach the tare load within any group highlights the consistency in the gripping approach, and lends confidence to attempts to carry out a tentative comparison of

treatment groups.

The strain required to reach the tare load increased in the circumferential direction, but decreased in the radial direction with GAG digestion (**Fig.3- 4**), indicating that the initial low stiffness behaviour of the valve may have been altered with GAG digestion, to provide greater extensibility in the circumferential direction, but slightly stiffer behaviour radially. If these data are considered in light of the studies by Vesely and coworkers, in which samples were pulled apart through the spongiosa, showing the fibrosa to elongate and the ventricularis to contract, findings indicate that GAGs may play an important role in maintaining the initial preloads in the AV and managing the very low stiffness behaviour of the tissue.

It is possible that different types of GAGs have different mechanical contributions, or even contradictory effects on tissue mechanics, and the widely varying choices of enzymes and digestion protocols between studies can make comparisons difficult [104, 108, 195, 196, 217, 219, 220, 223, 224] (

Table 3- 1). Even when combined enzymes were used [104, 108], none of the above-mentioned studies successfully digested all of the GAGs from tissues, and those remaining GAGs could still contribute to the mechanical properties of tissues. The spongiosa is believed to dampen valve vibrations during closing, confering flexibility to the leaflets and lubricating shear between the outer layers of the structure, all functions which are derived from the ability of GAGs to retain water [195]. It has been shown that if only hyaluronan is removed from a leaflet, there is no effect on tissue water content [195], whilst chondroitinase ABC digestion does significantly reduce water content [222]. Digesting the GAGs with different enzymes may cause the tissues to swell differently when they are incubated [225], and may subsequently cause different water content in tissues, which may lead to different mechanical properties.

3.5. Conclusion

In the present study, leaflets treated with combined enzymes which removed 96% of GAGs showed no influence of GAG removal on any elastic or viscoelastic mechanical property of the values. However, removal of the GAGs may have affected the preloading extensibility of the tissue, increasing radial stiffness and reducing circumferential stiffness. Data from other studies shows a mixed response to removing GAGs from the AV. The complex organization of GAGs within the AV, and

their inhomogeneous abilities in absorbing the water suggests that future studies may benefit from investigating more specific GAGs effect on mechanics in the AV and how GAGs may influence these.

Chapter four

Variations in Local Valve Mechanical Properties are related to Glycosaminoglycan Content

4.1. Introduction.

The complex mechanical environment, incorporating tension, flexion, pressure, and shear stress [5, 6, 9, 34, 155, 184, 226, 227], required the aortic valve (AV) to have special structure to meet its function. The three morphologically distinct layers of the AV each possess different extracellular matrix (ECM) compositions [9, 184]. The effects of each matrix component on valve structure-function relationships has received some attention [6, 88, 89, 104, 184, 226]. However, it remains unclear how the externally applied deformations at the tissue level are transmitted through the layers of the valve microstructure. There are side-specific variations in the flow and shear experienced by the leaflet, where the ventricularis/inflow side experiences high magnitude laminar flow (64-71 dyn/cm^2), while the fibrosa/outflow side experiences low magnitude disturbed flow (20 dyn/cm^2) [31-36]. This side-dependent flow pattern correlates with CAVD, as the outflow side preferentially calcifies, suggesting that the low magnitude shear and the disturbed flow patterns are positively correlated with CAVD [18, 30, 34, 158]. The different flow pattern caused different shear stress between ventricular and aortic side, it have reported that the shear stress on the aortic and ventricular sides of the aortic valve leaflet differ greatly, which was 20 dyn/cm2 in aortic side while 64–71 dyn/cm2 in ventricular side.

Collagen fibrils are relatively short and arranged as a discontinuous fibril network

implying that collagen fibrils and their surrounding matrix must transfer forces between neighboring fibrils for the valve to be mechanically viable [196]. In other tissues, some studies have hypothesized that GAGs act like cross- linking elements between collagen fibris to transfer forces [196, 217, 228], and GAG digestion has been shown to affect the tensile and viscoelastic properties of aortic valves [108, 195] and other collagenous tissues [196, 216, 217, 228]. However, this theory is disputed, with other studies showing evidence against GAG mediated collagen interactions [104, 219, 220].

The current study attempts to examine the functional role, if any, of GAGs on strain transfer through the aortic valve. The hypotheses are that the local strains across a native aortic valve leaflet are inhomogeneous and that the local strains across a GAG depleted aortic valve will differ from those in the native tissue.

Most biological tissues display a non-linear stress strain relationship, which can be described by a non-liner theory, e.g. viscoelastic theory or, better still, poro-elastic theory [244]. The non-linear behavior of the tissue arises largely from the interaction between the interstitial fluid and the solid components, e.g. fibrils of the tissue. This is most significant during the transit phases of the on- and off- set of stresses. Although one may argue that the non-linear properties of the tissue still exist in quasi steady state, they are far less significant, as the relative movement of the solid and fluid, hence the drag force between the two components of the tissue is weak. In the

following study in this chapter, all observations were obtained after the tissue samples were strained and hold for approximately 2 minutes. This is limited by the experimental setup using the laser scanning confocal microscopy. At this time, tissue samples were in quasi steady state, exhibiting little non-linear behavior.

4.2. Materials and methods

4.2.1. AV leaflets dissection and preparation

The aortic valve leaflets were harvested as described in chapter 2. Briefly, 16 porcine hearts were obtained from animals between 18 and 24 months, from a local abattoir (Cheale Meats Ltd, ESSEX, UK) within two hours of slaughter. The three aortic valve leaflets were dissected from each heart, then rinsed and maintained in Dulbecco's Modified Eagle's Medium (DMEM, Sigma–Aldrich, Poole, UK) for up to 30 minutes until used. The leaflets were then randomly divided into two groups: “buffer control” and “digested” (N=24 in each group). Both groups were incubated in buffer overnight, one containing hyaluronidase and chondroitinase ABC to digest the GAGs, as described in chapter 3.

4.2.2. Local strain analysis

The AV leaflets in both the buffer control and digested groups were incubated for 10 minutes in 0.1 M sodium bicarbonate buffer at pH 9 containing 0.5 mg/ml 5-([4, 6-dichlorotriazin-2-yl] amino) fluorescein hydrochloride (DTAF) at 37 °C. DTAF reacts with the amino groups and N-terminal amino acids of proteins non-selectively, to stain the collagen and elastin within each leaflet. Following staining, the leaflets were washed in two changes of DMEM for 20 minutes. A 5-mm-wide strip was excised from the central region of each leaflet in either the radial (**Fig.4- 1** (a)) or circumferential (**Fig.4- 1** (b)) direction and secured in the grips of a custom-made tensile testing rig (**Fig.4- 1** (c-d)) [155, 194, 198], allowing samples to be incrementally strained at a user-defined rate and imaged during straining. Leaflets were maintained in DMEM for the duration of the experiment.

Local strains were measured from the fibrosa side or the ventricularis sides of a sample, by carefully ensuring, the desired region was held closest to the objective lens for analysis. There were 6 samples imaged from each side in both the radial and cirumferential directions, leading to a total of 48 leaflets (2 test groups × 2 loading directions × 2 AV layers × 6 samples).

Each leaflet was viewed under a laser scanning confocal microscope (TCS SP2, Leica Microsystems GmbH, Wetzlar, Germany) using a ×10 objective lens (HC PL Fluotar,

Nikon, Kingston-Upon-Thames, UK). Leaflet alignment and orientation were checked under brightfield settings to ensure that samples were aligned with the loading direction and no gross twisting of the sample had occurred. The samples were initially gripped at a length of 10 mm and then were taken to a 0.1N preload, to provide a consistent zero-strain starting position for the tests. Sample length was recalculated, and this starting length used to compute the applied strains. In order to investigate the distribution of local strains across each specimen strip, samples were divided into three hypothetical equidistance regions. For the radial direction, as shown in Fig.4-1(a): M denotes the middle (central) region, while F and B are closer to the free edge and basal attachment, respectively. For the circumferential direction, shown in Fig.4-1(b), M once again donates the central region, while L and F denote the areas to the left and right of central region. The central area of each of these regions was selected for imaging.

For each sample, once held at the tare load (the zero strain condition), a grid was photobleached into the DTAF stained matrix at a depth of approximately 20–40 μm within the leaflet in either the fibrosa or ventricularis layer, using a 488 nm krypton–argon laser at full power. The grid consisted of four identical squares, each 300 × 300 μm^2, with grid lines 8 μm thick (**Fig.4- 2** (a)). The laser intensity was then reduced to the imaging range, and the sample imaged with the same objective lens at a resolution of 1024 × 1024 pixels. The size of the imaged region was 1.5mm×1.5mm, and each pixel was 1.465 μm^2. Samples were incrementally strained in 2% increments from 0%

to 12% strain, and the grid imaged at each strain increment, with a hold period of approximately 3 minutes at each strain increment, whilst the focal plane was located and the images captured. The samples were imaged in each of the 3 regions along the sample strip in a varied random order at each strain increment.

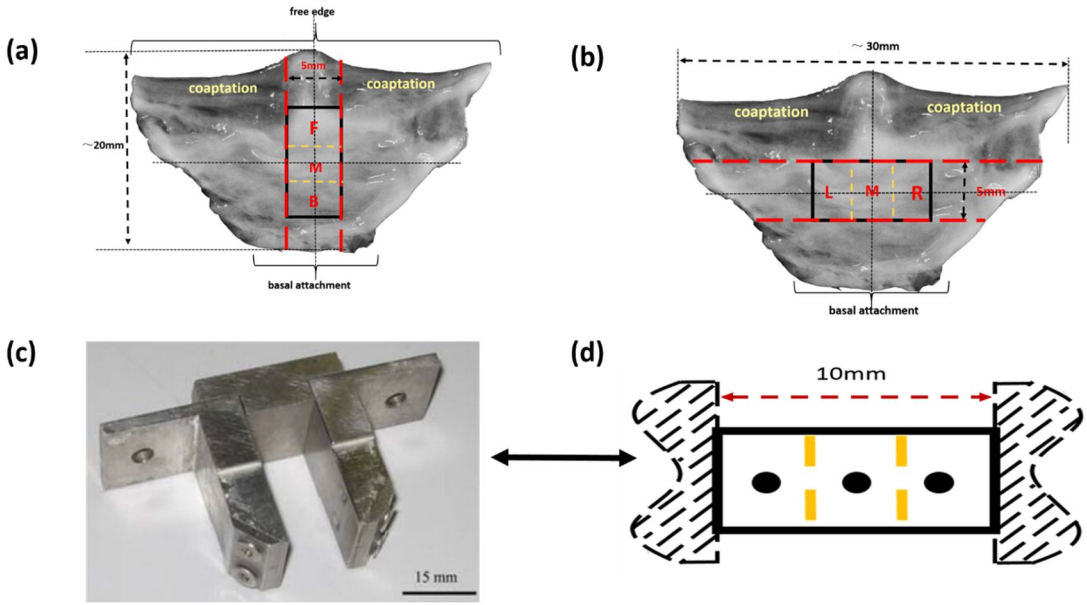

Fig.4- 1. 5mm strip samples were cut from the central region of the AV leaflet in (a) the radial or (b) the circumferential direction. Sample were secured within the grips (c), and the 10 mm sample length divided into 3 imaging regions (d).

Images from the confocal experiments were processed using the analysis software ImageJ (1.48V, National Institute of Health, USA) [198]. A typical confocal image of a photobleached grid before (**Fig.4- 2** (a)) and after (**Fig.4- 2** (b)) 12% applied strain is shown in **Fig.4- 2**. In order to calculate the local strain in the loading direction (S_L) and the strain transverse to loading direction (S_T) , the 9 points where lines in the x- and y-planes crossed were marked, and the image thresholded and skeletonized, so the resulting image consisting of just nine pixels representing the grid corners. The

coordinates of these pixels were exported to Microsoft Excel for data analysis. For S_L, the points at either end of each horizontal line were used to calculate the loading strain (**Fig.4- 2** c), so 3 values were acquired for each strained grid, and averaged to find S_L. S_T were calculated as the same manner using the vertical lines.

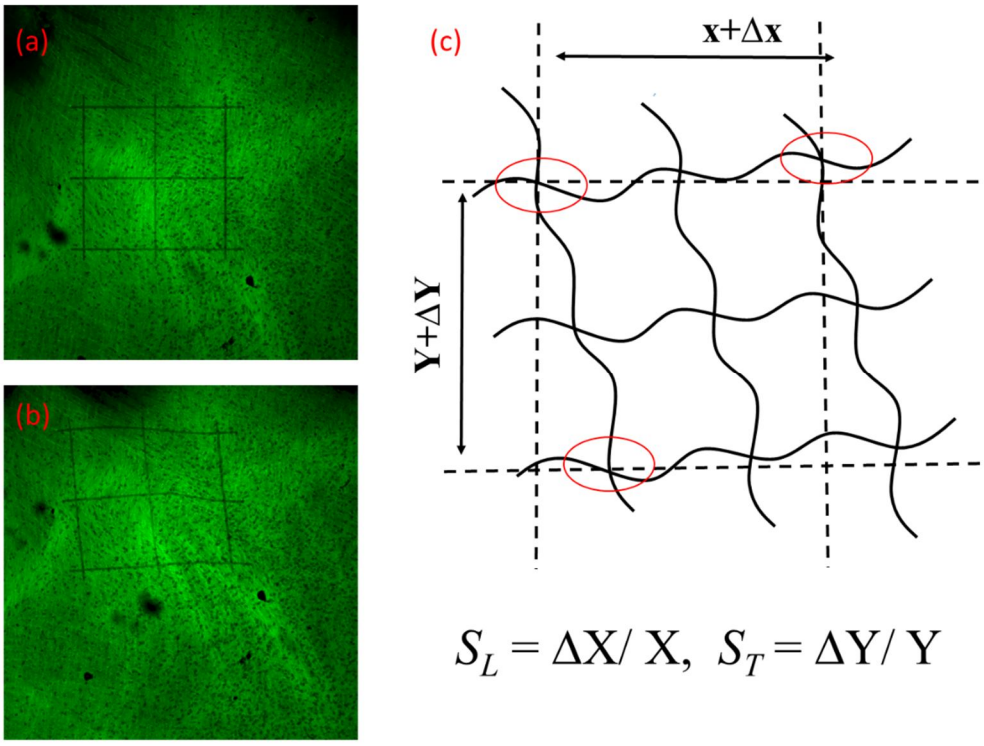

Fig.4- 2. Typical confocal image of a photobleached grid before (a) and after (b) applied 12% strain. (c) Schematic of the grid after deformation, showing the 2 deformation measurements. S_L: Percentage strain in the x direction (with axis of loading). S_T: Percentage strain in the y direction (transverse to loading axis).

4.2.4. Statistics

For analyzing the effect of GAG removal on the local strain parameters, statistical comparisons of the grid deformation parameters for digested and control samples

were performed using student t-tests. For analysis of the regional differences across the sample, comparisons of the grid deformation parameters within test groups were performed with one-way or two-way ANOVA. Statistical significance was set at $p < 0.05$. Data in the figures are presented as the mean and standard error (n=6), Statistical significance: # $p \leq 0.05$; ## $p \leq 0.01$.

4.3. Results

4.3.1. Local strain measurement

Images of the grids highlighted that the local strains at each strain increment varied notably in different strain directions and between different valve layers. **Fig.4- 3** shows the local strain results in the loading direction ($\boldsymbol{S_L}$) for radial strips. Concerning the buffer control group, $\boldsymbol{S_L}$ increased with applied strain in a predominantly linear manner, but the local strains in different regions ranged from roughly 30% to 100% of the applied strain (**Fig.4- 3** (a-f)). Whilst local strains across the ventricularis were reasonably homogenous, gradually decreasing in magnitude from the basal attachment region to the free edge, local strains across the fibrosa were much more varied. Strains in the middle region matched those applied to the tissue, but at both edges, local strains were markedly lower than applied values, particularly in the free edge region, where local strains were only 30% of those applied at a tissue level (**Fig.4- 3** (c)).

After removal of the GAGs, inhomogeneity in strain distribution across the leaflets was reduced. These changes are more clearly seen in **Fig.4- 4**, in which the strains across the three regions of the sample in each group are compared directly. Strains within the middle region of the fibrosa were significantly reduced (**Fig.4- 3** (b)), whilst those in the free edge region showed a trend towards increasing, leading to a homogenous strain profile across the value. GAGs digestion had no clear effect on strain distributions across the ventricularis (**Fig.4- 4** (b & d)), where strain fields were notably more uniform in the control group also.

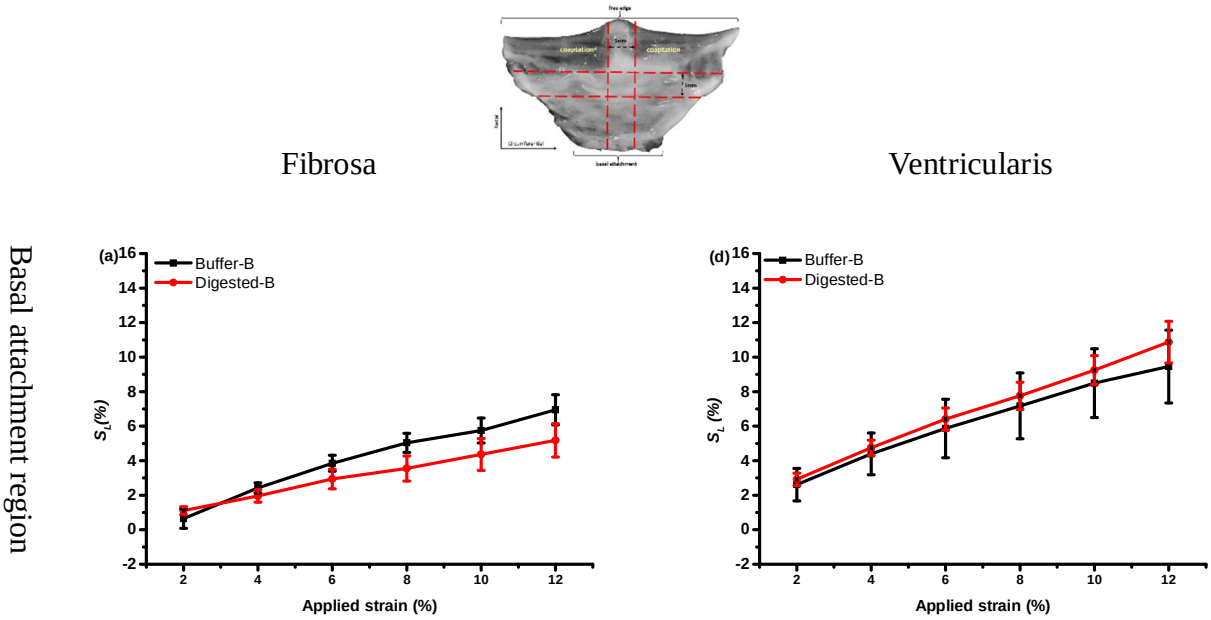

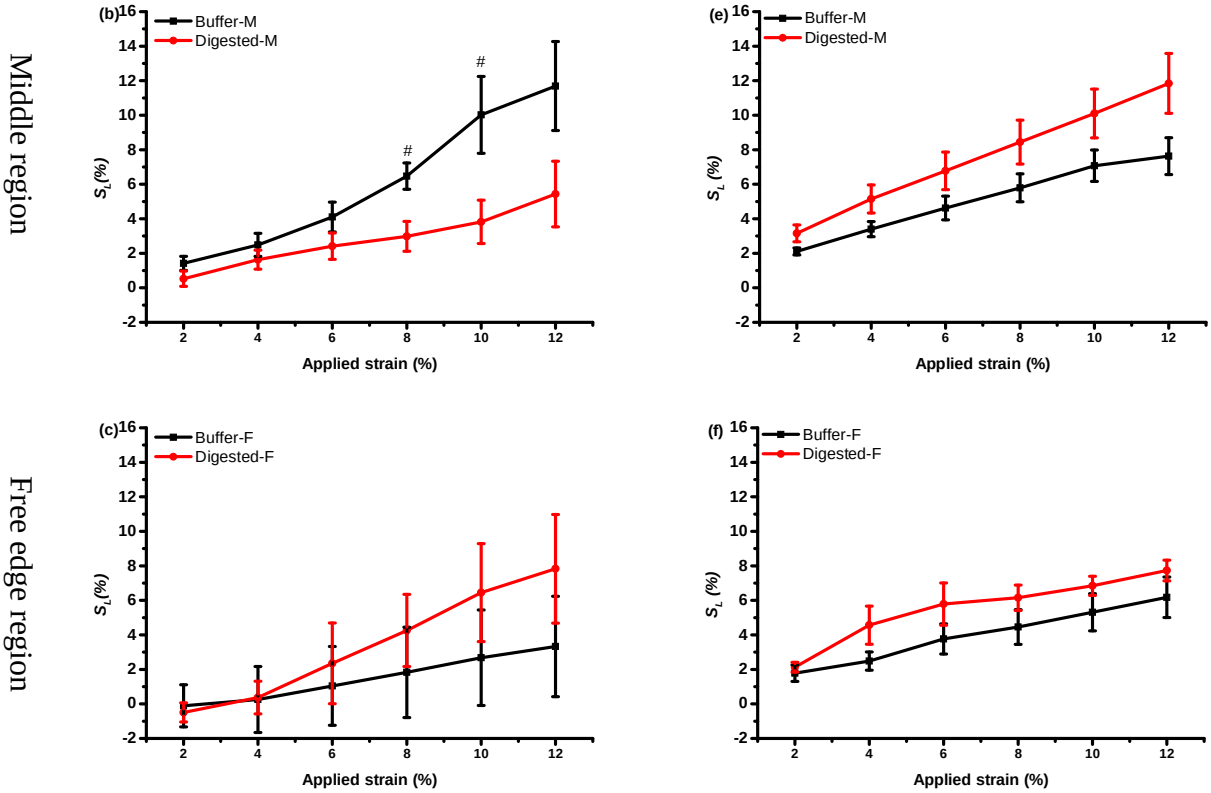

Fig.4- 3. Local strain in the loading direction (S_L) at different applied strains, for radial samples viewed from the fibrosa layer (a-c) and the ventricularis layer (d-f), as measured in the region closest to the basal attachment (B), the middle (central) region (M) and the region closest to free edge (F).

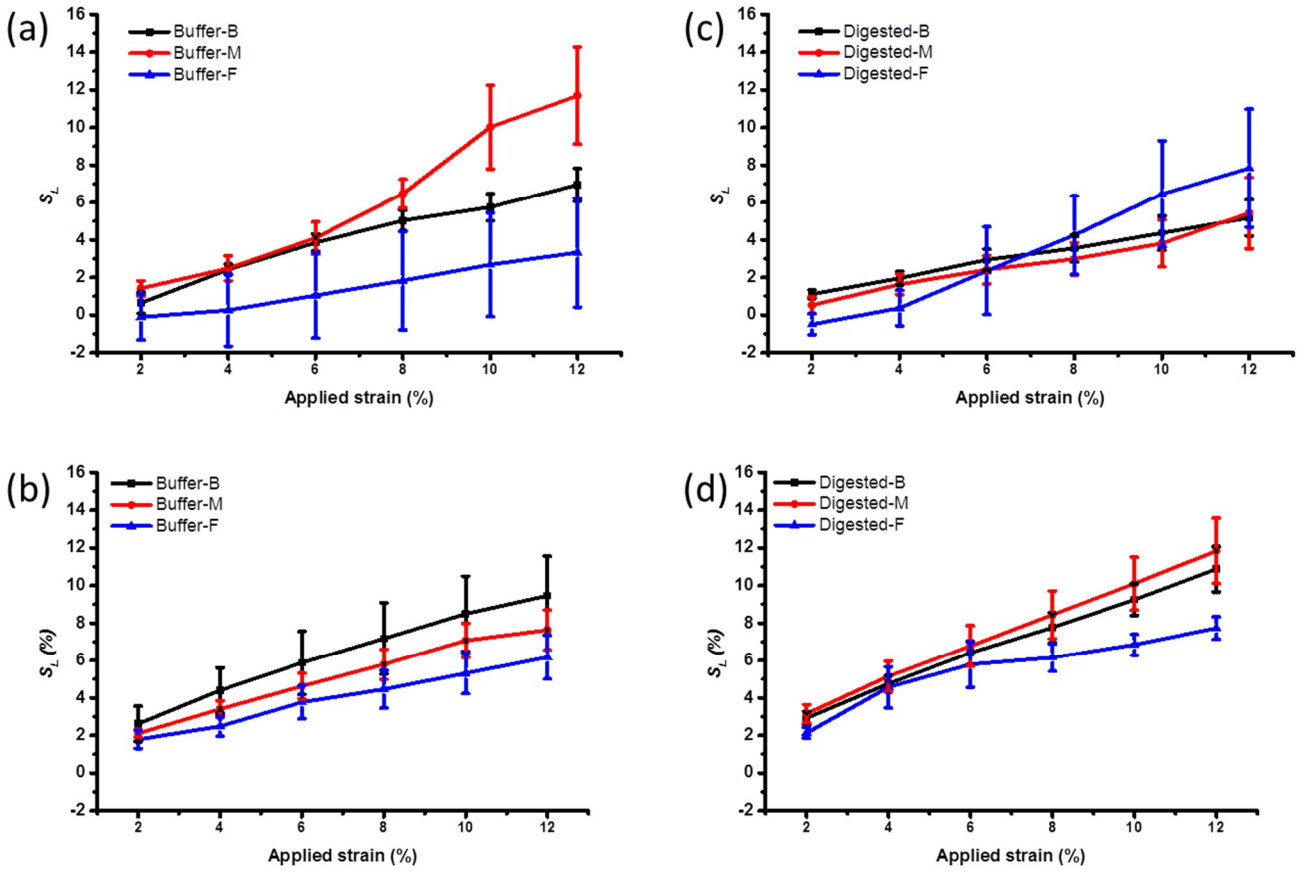

Fig.4- 4. A direct comparison of S_L across the three regions of each sample group, comparing buffer group (a, b) and digested samples (c, d) in fibrosa layer (a, c) and ventricularis (b, d) for **radial strips**. Buffer incubated samples show notable inhomogeneity in stiffness across the fibrosa, with lower stiffness in the middle of the leaflet when strained in the radial direction. Removing the GAGs eliminate this variation in regional stiffness, and the valve extends more homogeneously.

Considering strains transverse to the loading direction, strain distributions across the ventricularis in buffer controlled samples were again homogenous, but large transverse strains were evident, with Poisson's ratios[ii] of between 0.6 and 0.8 recorded across the sample (**Fig.4- 5** and **Fig.4- 6**). Whilst no significant changes were noted with GAG digestion, the strain distribution across the ventricularis did

[ii] **Poisson's ratio** is the ratio of the relative contraction strain (or transverse strain) normal to the applied load to the relative extension strain (or axial strain) in the direction of the applied load：

become somewhat more varied, with Poisson's ratios ranging from 0.4 in the free edge region, to 1.1 in the middle of the sample (**Fig.4- 5** and **Fig.4- 6**).

By contrast, as most seen easily shown in **Fig.4- 6**, strains transverse to the loading direction across the fibrosa varied significantly between regions in buffer controlled samples. In both the middle and basal attachment regions, typical Poisson's ratios of around 0.7-0.8 were seen. However the free edge showed a Poisson's ratio of 0, indicating no reduction in sample thickness in this region during loading. It was notable that removing the GAGs once again eliminated the inhomogeneity's in strain and led to a more consistent Poisson's ratio across the fibrosa.

.

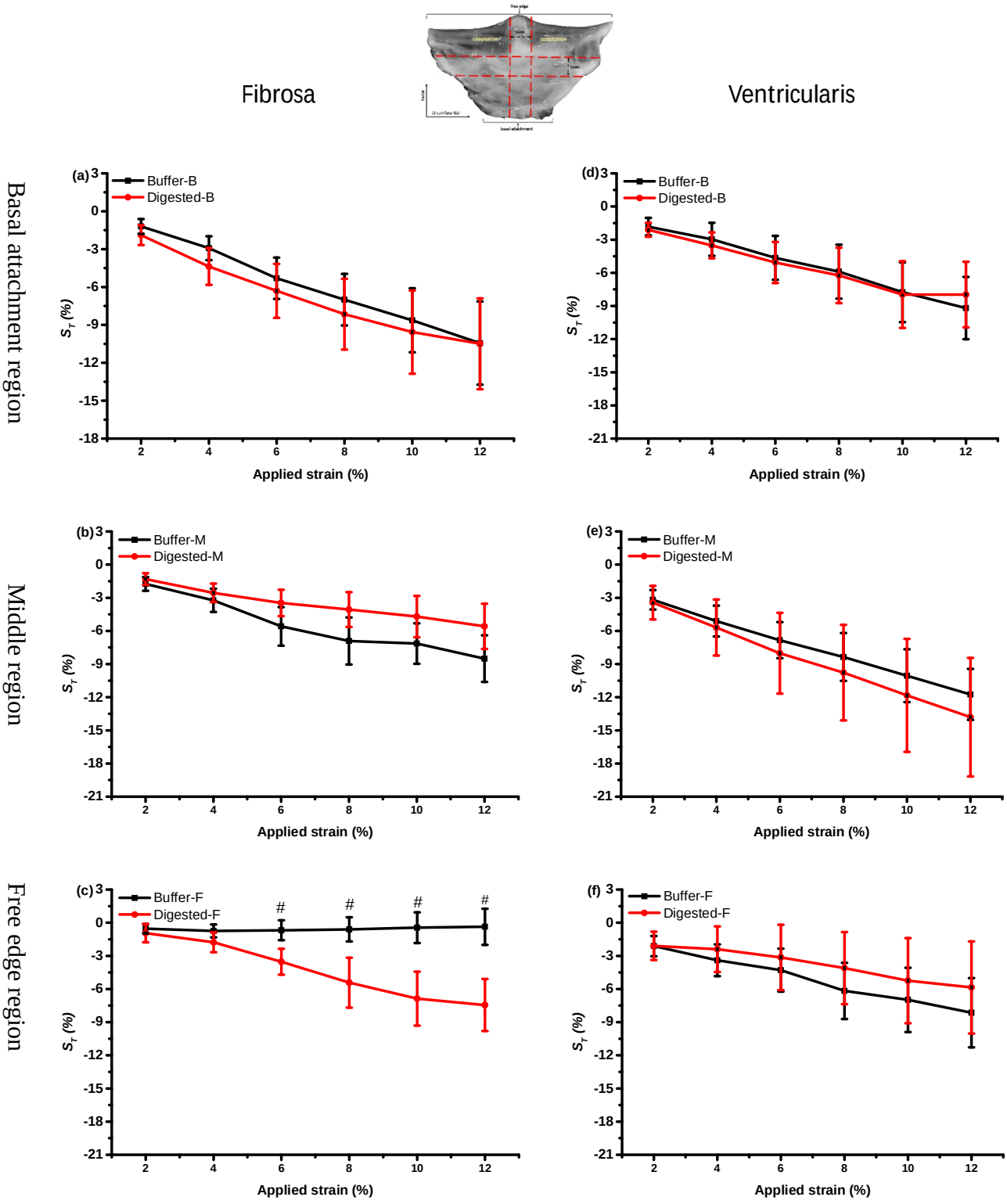

Fig.4- 5 Local strains transverse to the loading direction (S_T) at each applied strain increment, for **radial strip** samples viewed from (a-c) the fibrosa layer and (d-f) ventricularis layer, as measured within the basal attachment (B) (a, d), the middle (central) region (M) (b, d), and the region closest to free edge (F) (c, f) regions of the sample as previous described.

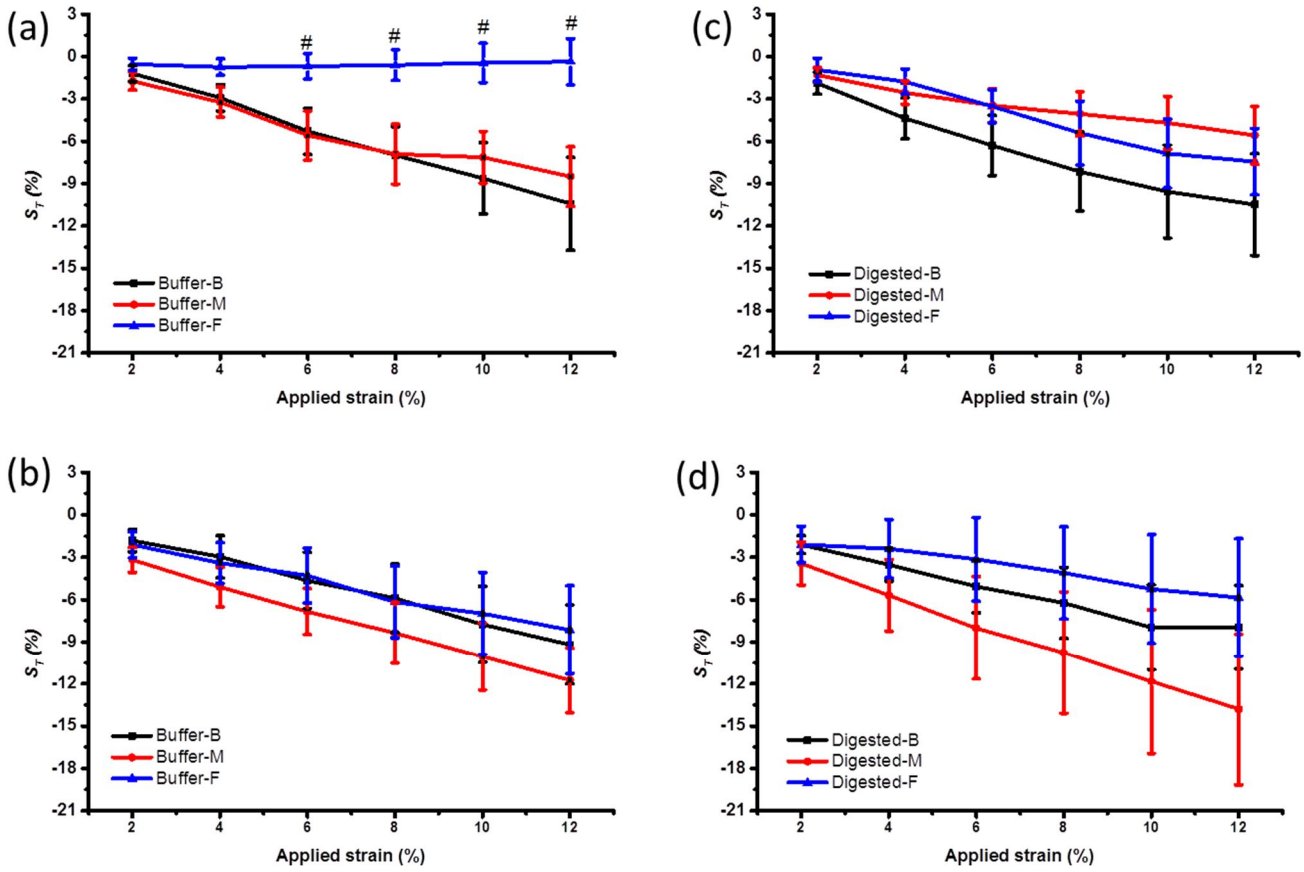

Fig.4- 6. A direct comparison of S_T in the three different regions of each sample group, comparing buffer control (a, b) and digested samples (c, d) in fibrosa layer (a, c) and ventricularis (b, d) for radial strips. Buffer incubated samples show notable inhomogeneity in stiffness across the fibrosa, with higher stiffness in the region closest to the free edge region of the leaflet when strained in the radial direction. Removing the GAGs eliminate this variation in regional stiffness, and the valve extends more homogeneously.

Fig.4- 7 shows the local strains in the loading direction (S_L) across strips cut in the circumferential direction. It was notable that in the fibrosa direction, all local strains were smaller than applied strains, across all sample regions in both the buffer control and digested samples. Strains across the ventricularis were once again more homogenous than strains across the fibrosa in buffer controlled samples (**Fig.4- 8**), with GAG digestion making little difference to any of these strains. Considering the fibrosa side of the leaflet, in buffer control samples, local strains to the right of the

strips were somewhat smaller than strains in either the M or L regions (**Fig.4- 7** (a-c) and **Fig.4- 8** (a)). However, digesting the GAGs removed this non-uniformity in strain distribution, and lead to homogenous strain distributions across the radial strip (**Fig.4- 8** (b)). Inhomogeneities across the circumferential strips were less pronounced than seen in radial strip.

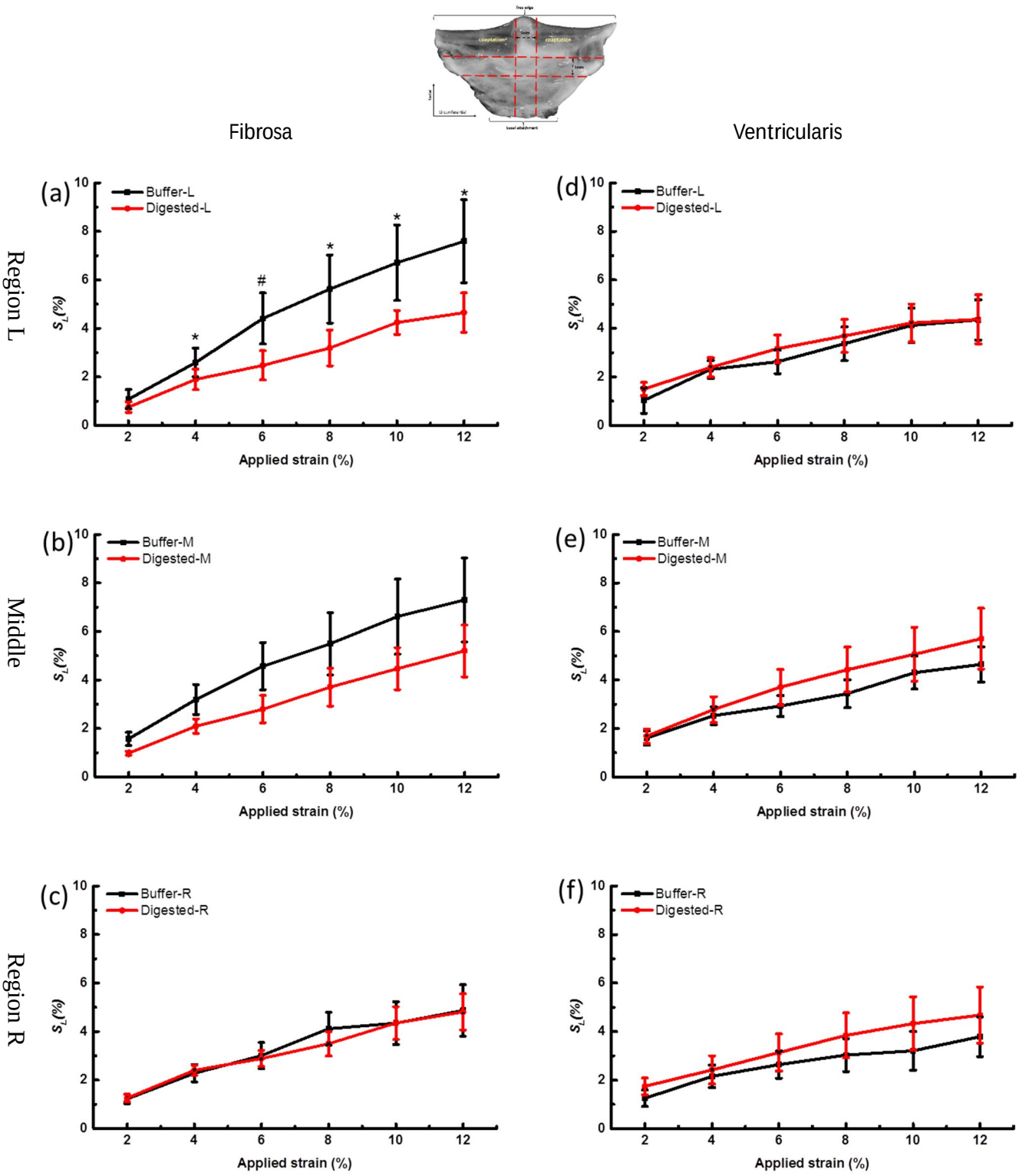

Fig.4- 7. Local strains in the loading direction (S_L), for **circumferential samples** viewed from the fibrosa layer (a-c) and the ventricularis layer (d-f), as measured in the region closest to the left (L), middle (M), and right (R) of the strip.

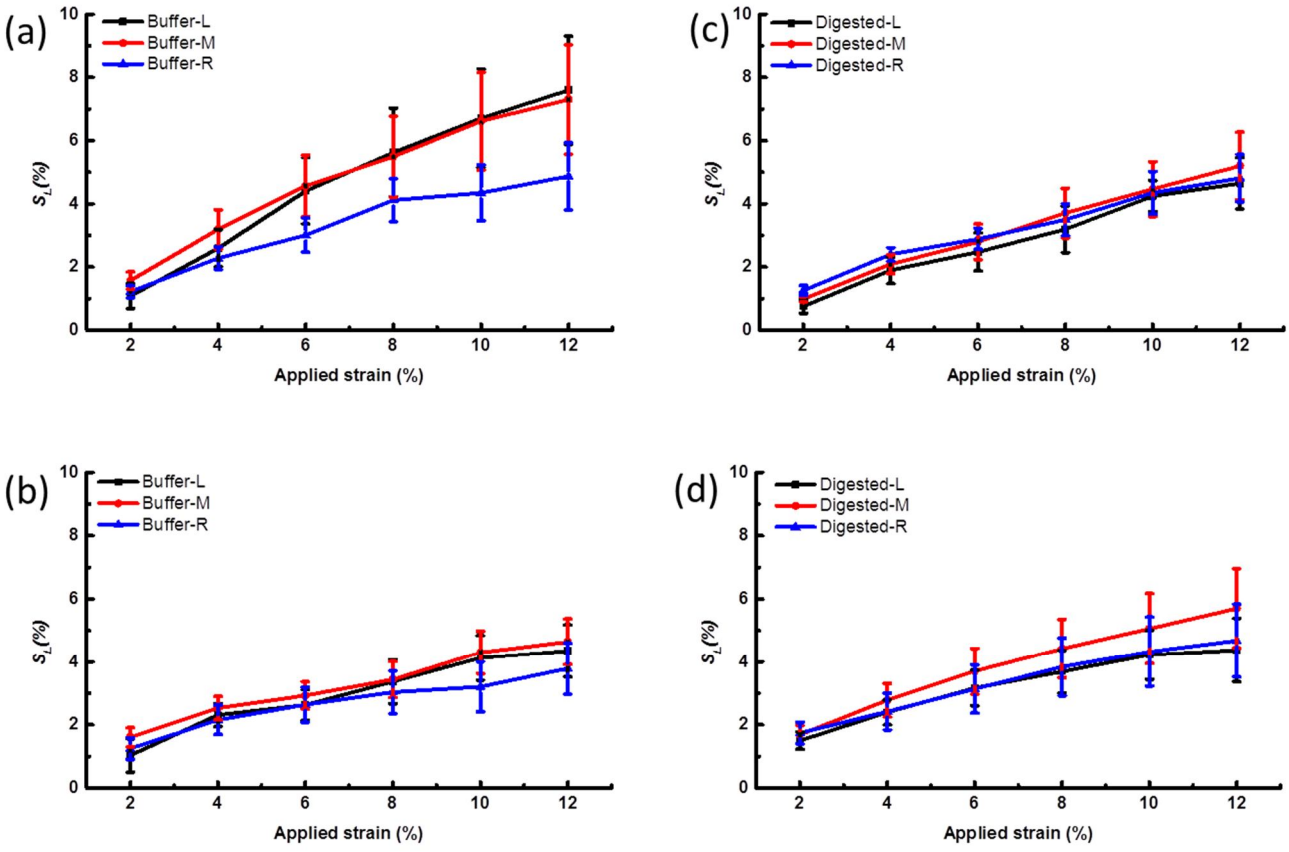

Fig.4- 8. A direct comparison of S_L across the three regions of each sample group, comparing buffer control (a, b) and digested samples (c, d) in fibrosa layer (a, c) and ventricularis (b, d) for circumferential strips.

Considering strains transverse to the loading direction in circumferential strips, Poisson's ratio values were generally far smaller than seen in radial strips and even negative in some regions. In buffer control samples, the Poisson's ratio across the ventricularis side of the valve was consistently negative (Fig.4- 9 and Fig.4- 10), indicating an expansion of the sample width upon the application of strain. The Poisson's ratio of approximately -0.5 was highly consistent across regions of the circumferential strip, and unaltered by GAG digestion.

By contrast, Poisson's ratios across the fibrosa side of circumferential strips were all positive in the buffer control samples (Fig.4- 10), but far less homogenous across the strip. Large Poisson's ratios, greater than 1, were seen in the middle of the fibrosa, with values of around 0.3-0.5 at either side (Fig.4- 9). However, upon removing the GAG from these samples, all Poisson's ratios across the fibrosa side increase to negative values, more closely matching those seen across the ventricularis side (Fig.4- 9 and Fig.4- 10).

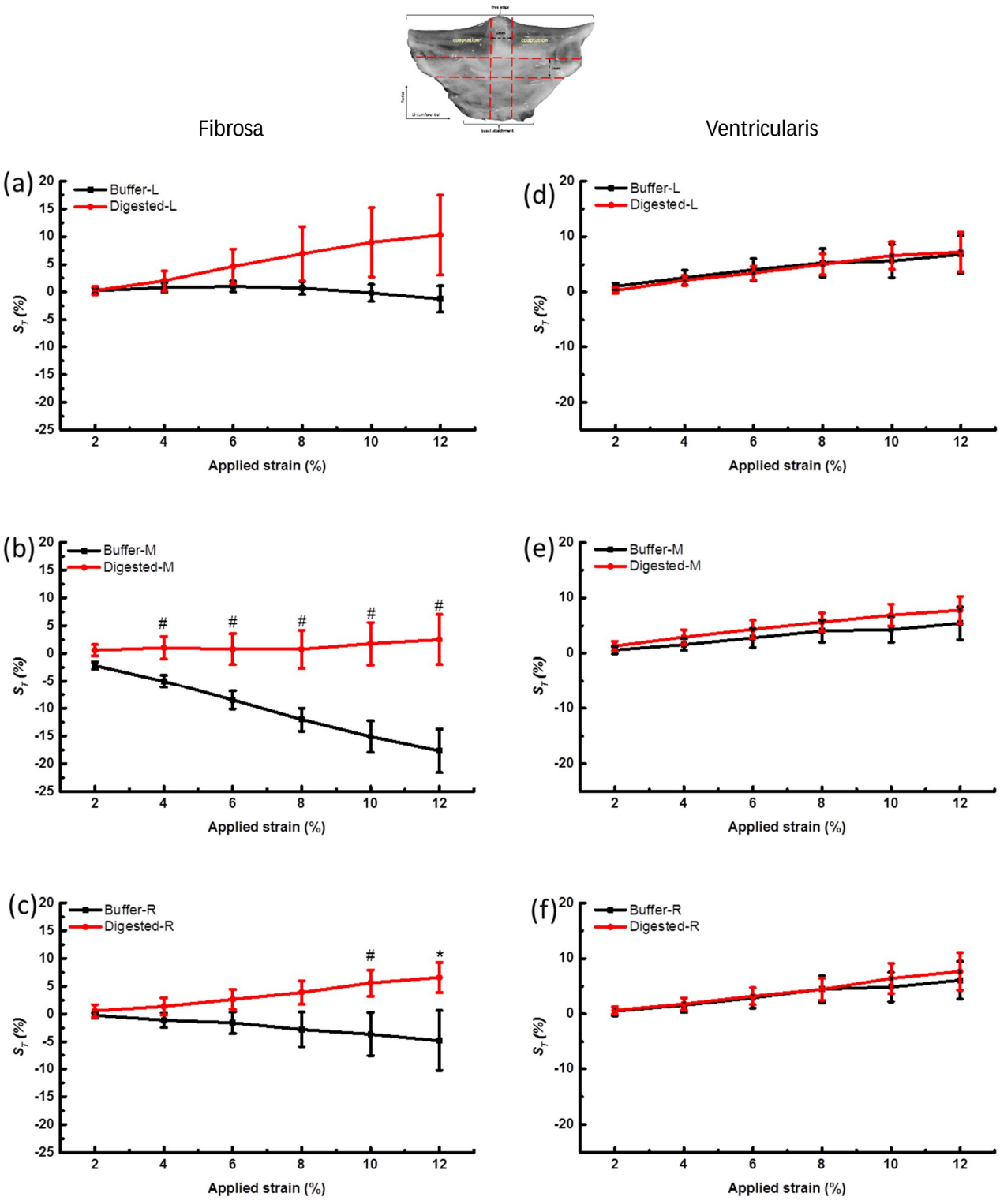

Fig.4- 9. Local strains transverse to the loading direction (S_T) at each applied strain increment for **circumferential strip** samples viewed from (a-c) the fibrosa layer and (d-f) ventricularis layer, as measured in the region closest to the left (L), middle (M), and right (R) of the strip.

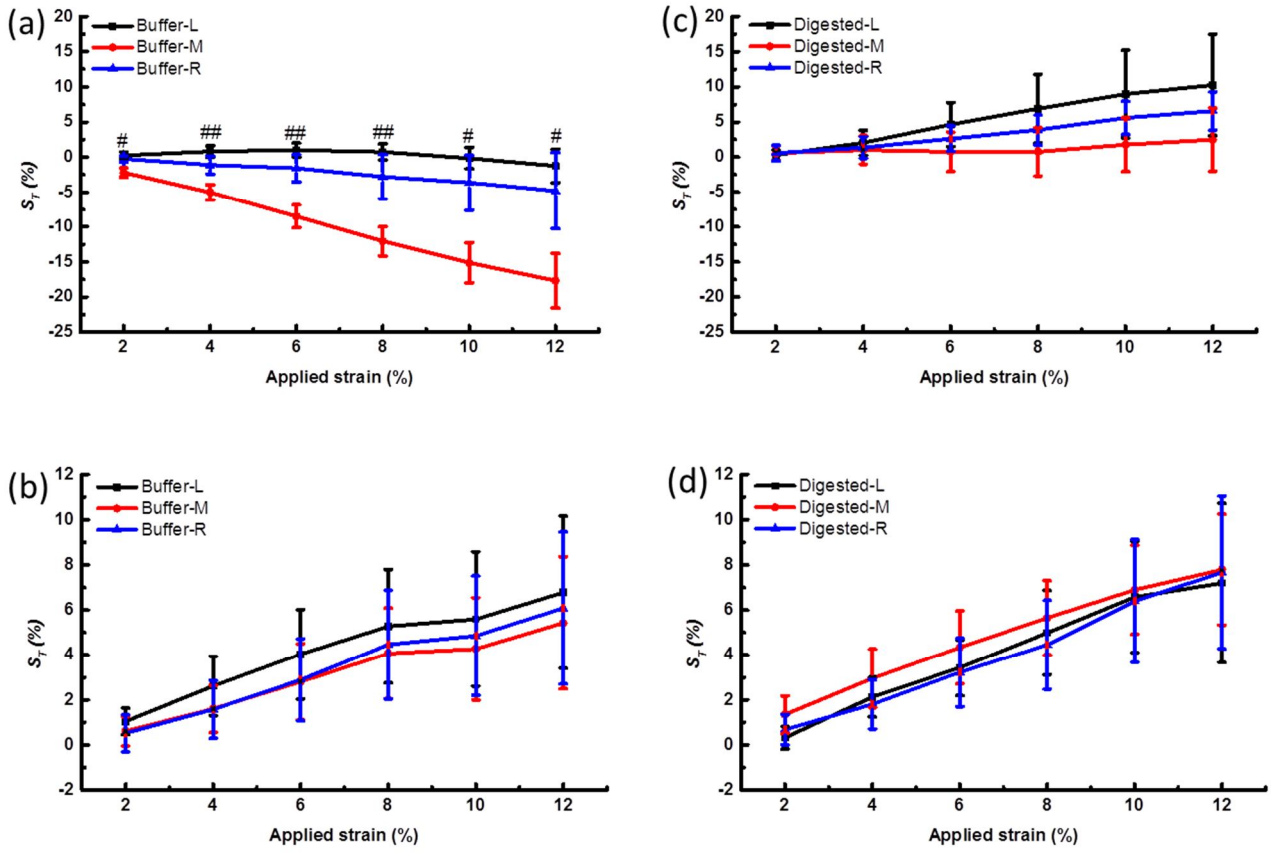

Fig.4- 10 A direct comparison of S_T at the three different regions of each sample group, comparing buffer control (a, b) and digested samples (c, d) in fibrosa layer (a, c) and ventricularis (b, d) for circumferential strips. Buffer incubated samples show notable inhomogeneity in stiffness across the fibrosa, with lower stiffness in the middle region of the leaflet when strained in the circumferential direction. Removing the GAGs eliminate this variation in regional stiffness, and the valve extends more homogeneously.

The local strains at 12% applied strain across both the fibrosa and ventricularis are summarized in **Table 4- 1** and **Table 4- 2** for radial strips and circumferential strips, respectively.

Table 4- 1 Summary of local strain magnitudes at 12% applied strain across the sample in radial strips, comparing control and digested samples.

		Fibrosa			Ventricularis		
		B	**M**	**F**	**B**	**M**	**F**
S_L	**Control**	6.95 ± 0.87	11.69 ± 2.58	3.33 ± 2.91	9.46 ± 2.11	7.63 ± 1.07	6.18 ± 1.17
	Digested	5.18 ± 0.96	5.44 ± 1.90	7.83 ± 3.15	10.87 ± 1.20	11.85 ± 1.73	7.73 ± 0.6
S_T	**Control**	-10.44 ± 3.29	-8.51 ± 2.10	-0.37 ± 1.64	-9.19 ± 2.82	-11.75 ± 2.31	-8.14 ± 3.13
	Digested	-10.49 ± 3.60	-5.59 ± 2.05	-7.45 ± 2.35	-7.97 ± 2.97	-13.81 ± 5.37	-5.86 ± 4.17

Table 4- 2 Summary of local strain magnitudes at 12% applied strain across the sample in circumferential strips, comparing control and digested samples.

		Fibrosa			Ventricularis		
		L	**M**	**R**	**L**	**M**	**R**
S_L	**Control**	7.60 ± 1.71	7.30 ± 1.73	4.87 ± 1.06	4.35 ± 0.83	4.64 ± 0.73	3.79 ± 0.82
	Digested	4.65 ± 0.81	5.20 ± 1.07	4.81 ± 0.75	4.38 ± 1.01	5.70 ± 1.25	4.68 ± 1.16
S_T	**Control**	-1.24 ± 2.37	-17.68 ± 3.91	-4.81 ± 1.64	6.78 ± 3.38	5.43 ± 2.94	6.08 ± 3.37
	Digested	10.26 ± 7.20	2.49 ± 4.50	6.58 ± 2.73	7.19 ± 3.54	7.79 ± 2.45	7.67 ± 3.38

4.4. Discussion

Using the fluorescent dye, DTAF, it was possible to completely stain samples and then

photobleach a grid within different layers of the valves which can be viewed under a confocal microscopy. Our custom designed rigs enable us to incrementally load aortic valve samples in a controlled manner, whilst visualizing grid deformation, in order to understand the in situ micromechanical environment of the samples. Similar methods have proved very useful in studying local strains throughout different types of tissue [197, 198, 229-232].

This study hypothesised that the local strains across an aortic valve leaflet would be inhomogenous, and that GAG digestion would alter the strain distributions relative to the native tissue. To investigate these hypotheses, local strains were measured at incrementally increasing applied strains, in both the loading direction and transverse to this, in strip samples cut either radially or circumferentially from an aortic valve leaflet. Strains across both the fibrosa and vetricualris surfaces were compared.

Data is summarized in **Table 4- 1** and **Table 4- 2**, showing the local strains at 12% applied strain across the sample regions. This is also shown schematically in **Fig.4- 11** and **Fig.4- 12**. The data supports our hypothesis that local strains (both S_L and S_T) were inhomogenous across the native valve. However, it was also notable that the inhomogeneity was largely confined to the fibrosa side of the leaflets, and strains across the ventricularis were generally homogenous across regions and in both loading directions.

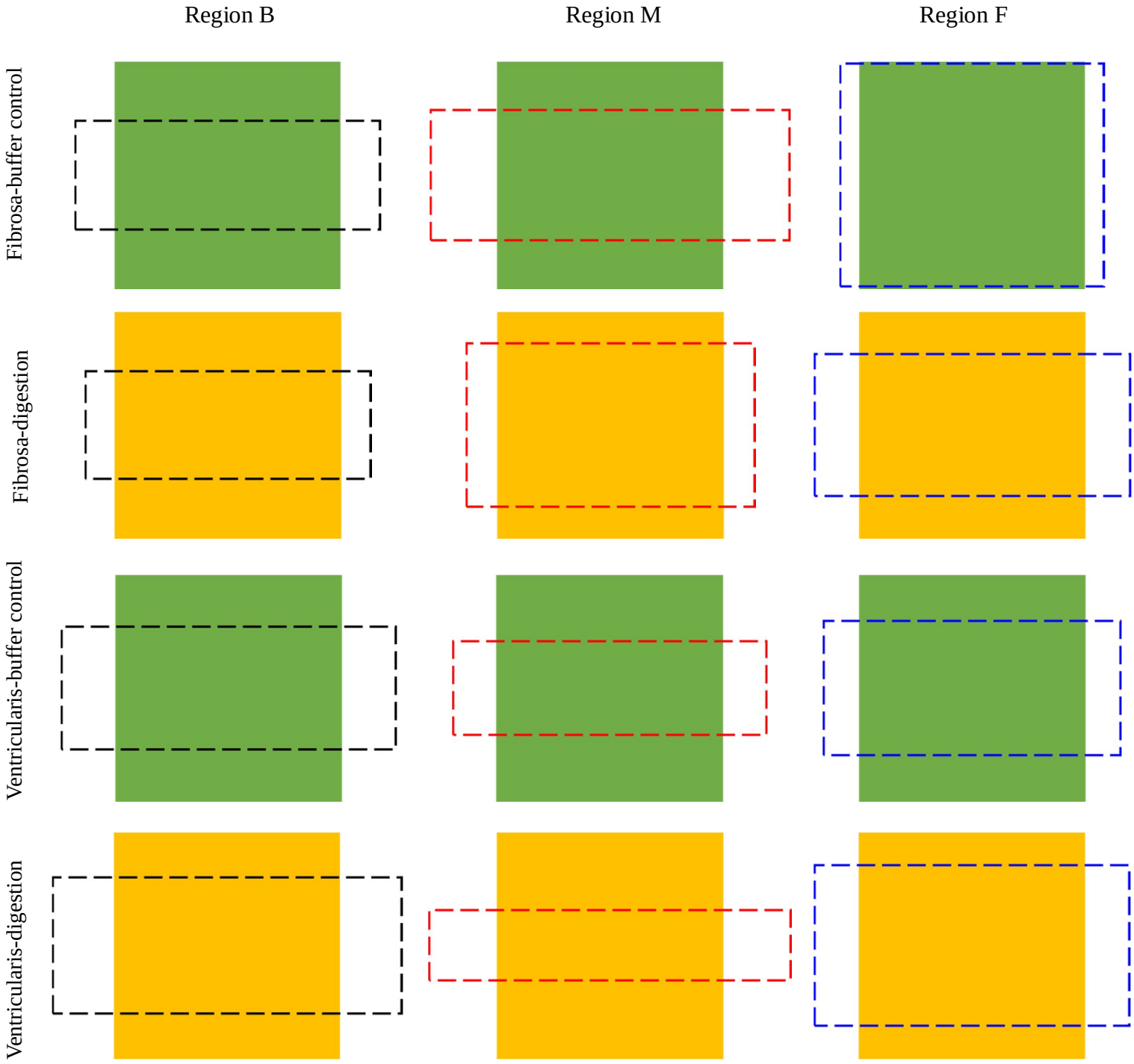

Fig.4- 11. Schematic depicting the mean deformation (local strain) in each region of the sample at 12% applied strain. The response of both fibrosa and ventricularis in radial strips are compared before and after GAG digestion. Deformation magnitudes are exaggerated for ease of viewing but all to relative scale (green and yellow square is the size of the bleaching square in buffer control and digested group, respectively, dotted square is the deformation of the bleaching square at three different regions).

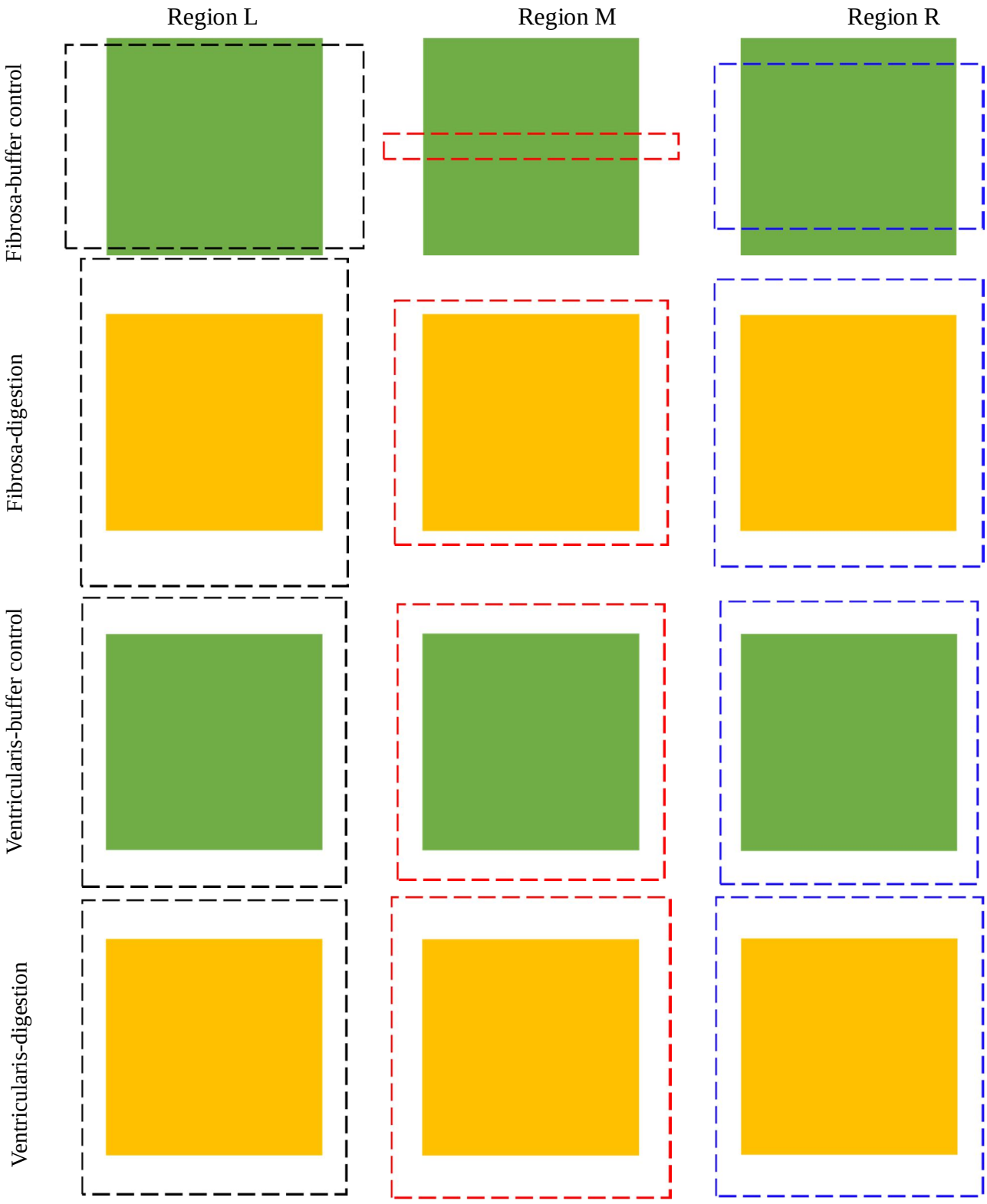

Fig.4- 12. Schematic depicting the mean deformation (local strain) in each region of the sample at 12% applied strain. The response of both fibrosa and ventricularis in circumferential strips are compared before and after GAG digestion. Deformation magnitudes are exaggerated for ease of viewing but all to relative scale.

The microstrain distribution across the two layers was inhomogeneous and non-uniform. The observed distribution has also been previously reported in some of the finite element modelling studies on the microstructure of the AV [194, 233]. These studies have suggested that this behaviour is a result of the local preferred direction of the collagen fibres within the valve ECM. In the regions close to the commissures the preferred direction of fibres is more uniformly towards the circumferential principal axes, while the fibres in the centre region are more randomly oriented [233, 234].

The fibrosa is the main load bearing layer of the valve, and when straining samples radially, the region nearest the free edge was stiffer than the other regions in the buffer control samples, leading to small strains in this region in both the loading direction and transverse to this. When straining the fibrosa circumferentially, the central region deformed the most both in the loading direction and transverse to this, indicating the lowest circumferential stiffness was seen in the centre of the sample.

It could be hypothesized that the lower stiffness in the middle of a circumferential strip was a result of collagen organization; fibres, running from the left and right edges of the leaflet meet in the middle, so there are fewer collagen fibres directly spanning this middle region to resist tensile load. By contrast, the stiffer edge region in radial strips could help the valve to withstand pressure during diastole to keep it closed, whilst lower stiffness nearer the basal attachment could help minimise damage from bending during valve closing and opening.

Results show that the local strain field is inhomogeneous in the two layers, under both circumferential and radial loading. Microstrain distribution was also anisotropic, reporting a more pronounced non-linear correlation with the applied strains in circumferential direction, in both layers. Internal shear strain also could be an explanation for the current finding. Local strains in the ventricularis layer were higher in radial specimen, compared to the equivalent regions in the fibrosa layer, especially at the free edge region (**Fig.4- 5**). These differences in local strains will subsequently lead to a non-uniform elongation of the two layers, and thus induce shear strain within leaflets. Previous studies shown that even under simple tensile strain, shear stresses are also induced within the AV and GAGs were may play important role in this behaviour [194].

However, after removal of GAGs, it was notable that the strain fields across the fibrosa, in both the radial and circumferential directions were far more uniform, much more closely matching the behaviour seen in the ventricularis. The GAGs are the primary component of the central spongiosa layer [104] with a role in regulating spongiosa water content [205, 206]. The spongiosa acts as a damper, to reduce the impact created by sudden changes in pressure gradient at systole. It also allows for relative movement of the outer two layers of the valve as it opens or closes through internal shearing [6, 99, 109]. The current data highlights how important the spongiosa is for enabling the fibrosa and ventricularis to act independently and modulate their strain patterns to manage the valve load environment.

A previous study has suggested that regional differences in local strain may have a relationship with GAG content in tendon [196]. Such a hypothesis might also be relevant to the aortic valve, as it is known that the thickness of the spongiosa, and thus valve GAG content, varies across a leaflet [88], perhaps matching the stiffness variations seen in micromechanics in the current study. In present study, we found that along the radial strip, the distribution of the GAGs was regional. As shown qualitatively in **Fig.4- 13**, more GAG appears to be present in the basal attachment region, with levels gradually decreasing across the strip to be lowest near the free edge. At the free edge region, the fibrosa accounts for over 70% of total leaflet thickness, while at the basal at basal attachment region, 60% of leaflet thickness is the spongiosa. As mentation in chapter one, the fibrosa is predominantly composed of circumferentially aligned, macroscopically crimped and densely packed type I collagen fibres, making it the strongest and stiffest layer of the valve. The spongiosa primarily contains glycosaminoglycans(GAGs), with a loosely arranged collagen fibre structure coupling the two outer layers. So it is easy to understand that, the free edge region is stiffer than the basal attachment region. Correlating the mechanical data with the data showing the distribution of the GAGs shows that there are more GAGs in the basal attachment region, where larger local strains were measured, however, there are less GAGs in the free edge region, where less strains were measured. These data suggest that the valve is stiffer in the regions with less GAGs , so presence of GAG lead to reduce in stiffness of the AV. A quantitative study of distribution of the GAGs

across the aortic valve should be carried out in the future, to see if GAG content can be correlated with sample stiffness.

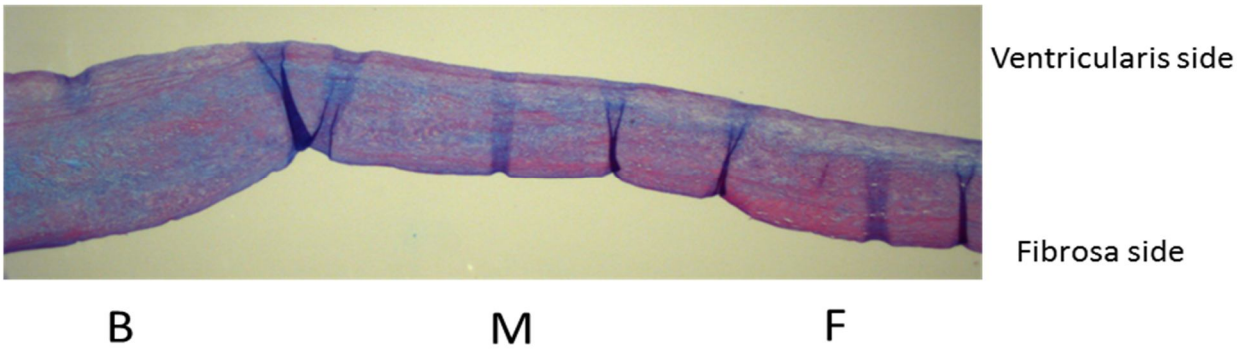

Fig.4- 13 A typical picture of a radial strip sample stained by Alcian Blue /PAS to view the GAGs.

A study by Anssari-Benham et al [194] investigated local strains across the aortic valve, using the aortic valve interstitial cells (AVICs) as fiducial strain markers. This study also characterised longitudinal strains across both the fibrosa and ventricularis in the radial and circumferential directions, but did not look at the Poisson's ratio of the leaflets, or at collagen strains directly. This study did not highlight the more detailed inhomogeneites in strain across the fibrosa seen here, perhaps due to the limited resolution available when tracking cells. However, it did highlight that the fibrosa as a whole was stiffer than the ventricularis when the valve was strained circumferentially. The current study confirmed this result, but was additionally able to show that this stiffness differential was largely a result of higher stiffness regions near the edges of the leaflet.

One particularly interesting result from the current study was the highly variable

Poisson's ratio values seen between regions and sides of the leaflets. While, a more typical positive Poisson's ratio was measured when straining radial strips, negative Poisson's ratios were evident when straining circumferential strips. These negative values were only seen in the ventricularis of buffer control samples and likely related to the organisation of elastin in the leaflet. One possible reason could be that, the samples were strained at the low stress–low strain pre-transition phase, which can be linked to the straightening of the crimped fibers of collagen and the elongation of the elastin fibers and the highly non-linear transition phase that might be related to the transfer of force from the elastin to the collagen fibers [172]. The ventricularis contains a dense network of elastin fibres, generally aligned along the radial direction [87, 89] and interconnecting the collagen fibres to help the leaflet recoil to its original unloaded configuration [9, 87, 89-92]. The current data suggest that the elastin in the ventricularis holds the valve in a pre-stressed state. When a circumferential strip is removed from the leaflet, the elastin is immediately able to contract the strip. However, once the strip is strained in the circumferential direction, the movement of collagen resists that contraction, and the strip will return to its original width. In this scenario particularly, the buffering effect of the spongiosa between the ventricularis and fibrosa is very evident. In the intact valve, it is only the ventricularis that shows the contraction and subsequent expansion of leaflet strips upon loading. However, once the GAGs have been digested, this effect propagates through all layers of the valve, and the same strain behaviour can be seen in the fibrosa.

In conclusion, results indicate that GAGs may play a direct role in strain transfer through aortic valves within the fibrosa, modulating stiffness of the free edge. They do not appear to play such a direct role in modulating mechanics in the ventricularis layer. However, data strongly supports the importance of the spongiosa as a buffer layer between the ventricularis and fibrosa, enabling these different valve layers to strain independently. Removal of the spongiosa led to homogeous strains across the valve leaflet, and enabled the contraction of elastin to influence mechanics across the leaflet, as opposed to confining its effects to the ventricularis.

Further studies of benefit may be to investigate more complex mechanical behaviours in the valve (such as stress relaxation, creep, fatigue resistance, shock dissipation) as these time dependent properties may be regulated by GAGs content.

Chapter Five

Biaxial Studies of the Aortic Valve

5.1. Introduction

In the present thesis, uniaxial studies of the aortic valve (AV) have shown that local strains vary across the valve, and the variations in local valve mechanical properties are related to glycosaminoglycan content. Uniaxial testing provides a simple manner in which AV mechanics can be investigated in a controlled manner. However, it does not reflect the complex multi-axial physiological loading conditions of the native functioning AV [5, 34, 54]. Biaxial testing more closely replicated AV physiological conditions, so biaxial testing protocols, using a previously developed rig, were developed during the course of this study. This chapter, covers the development and optimisation of the biaxial rig, alongside initial validation studies, using digital image correlation (DIC), cell tracking and fluorescence photobleaching to characterise AV strains.

5.2. Design of the loading system

The rig developed by Screen and Anssari-Benam, has four linear stepper motors, one on each side to applied forces or strains to the tissue samples, which are measured with load cells (**Fig.5- 1**). The rig allows the application of quasi-static or cyclic tensile loading on tissue samples, under either load or displacement control. The loading modes are controlled using the graphical computer language LabVIEW™ in

conjunction with counter-timers and logic. The two motors located on opposite side of the rig can move simultaneously, ensuring that the sample remains stationary in the centre of the rig during straining.

To grip the samples within the biaxial rig with minimal the end effects [179, 180], it was necessary to develop a gripping system. Trial and error of varying mechanisms during this project led to the development of a suturing protocol, outlined in **Fig.5-1**.Square samples 15mm × 15 mm were cut from the centre of the aortic valve leaflet, and then held in place in the rig with a continuous strand of 2-0 silk suture material, with four attachment points per side of the sample. Sutures were linked around three pulleys on each side of the rig to evenly distribute loading, and a needle used to help thread the sutures.

The rig is a sealed unit, and can be filled with Phosphate Buffered Saline (PBS) to keep the sample hydrated during the application of strain. The rig has been designed to fit on the stage of a confocal microscope, facilitating imaging of AV cells and ECM upon deformation of the sample in real time (**Fig.5- 1**).

(a)

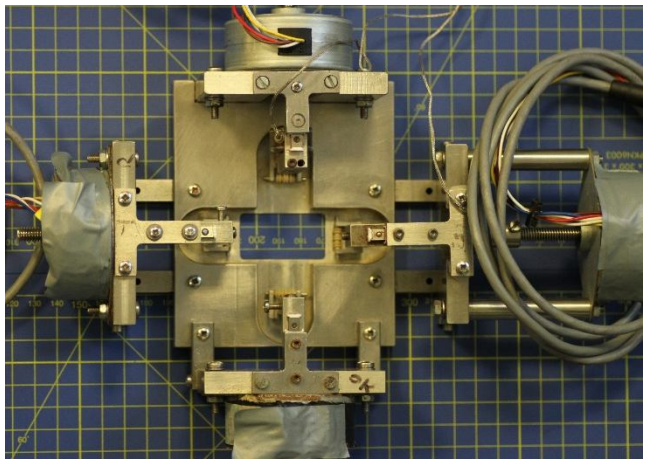

(b)

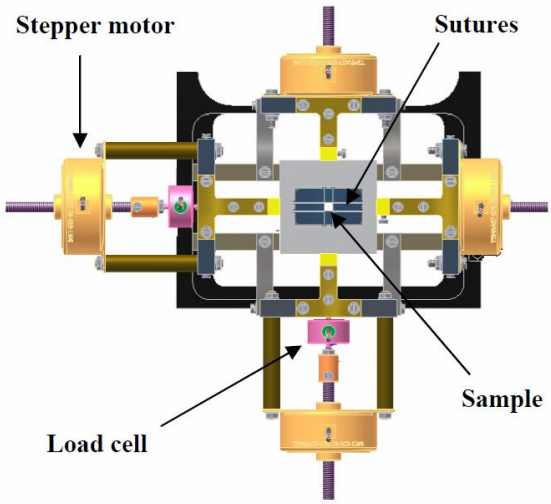

(c)

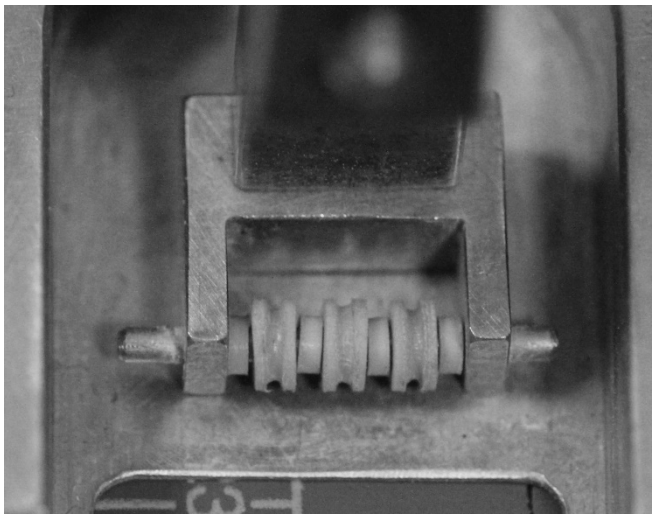

(d)

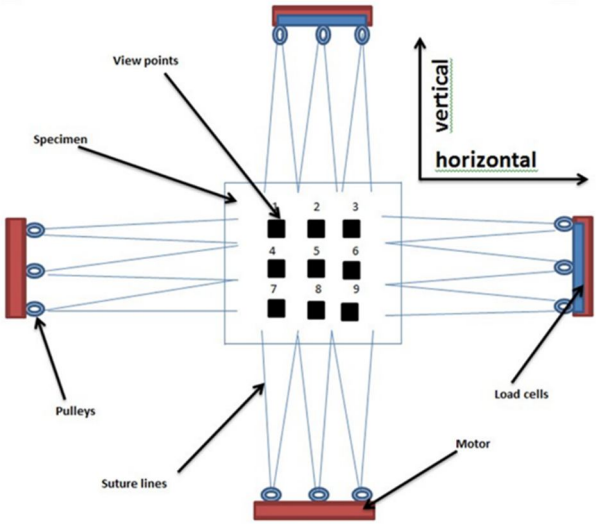

(e)

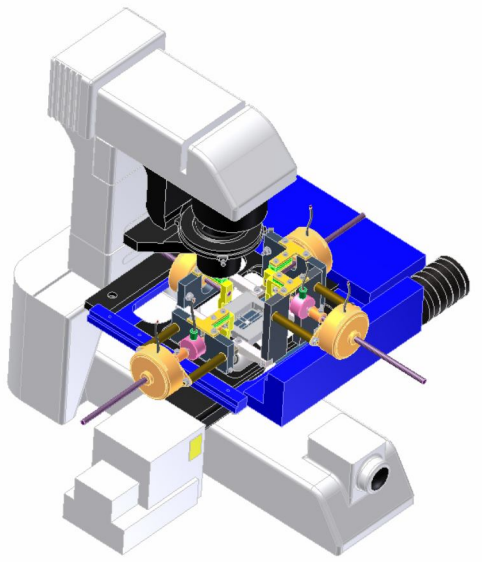

Fig.5- 1. (a) a picture of the biaxial rig; (b) Schematics drawing of the rig, showing its different parts; (c) a picture of the pulley system developed for securing samples; (d) schematic of a sample sutured into the rig; and (e) schematic of the rig on a confocal microscope stage.

5.3. Rig validation.

To ensure samples were loaded accurately and evenly within the rig, a series of validation tests were conducted. 6 aortic valve leaflets were used for these tests. As shown in **Fig.5- 2**, after the samples were loaded into the rig, nine separate point marks were made on the samples with a permanent marker pen. These marks were used to track macro strains across the samples. The samples were subjected to equibiaxial strain, straining in 5% increments up to 25% strain. Images were taken at each strain increment with a Canon EOS 7D camera (Cannon Inc. Japan) and the images processed using the analysis software ImageJ (1.48V, National Institute of Health, USA).

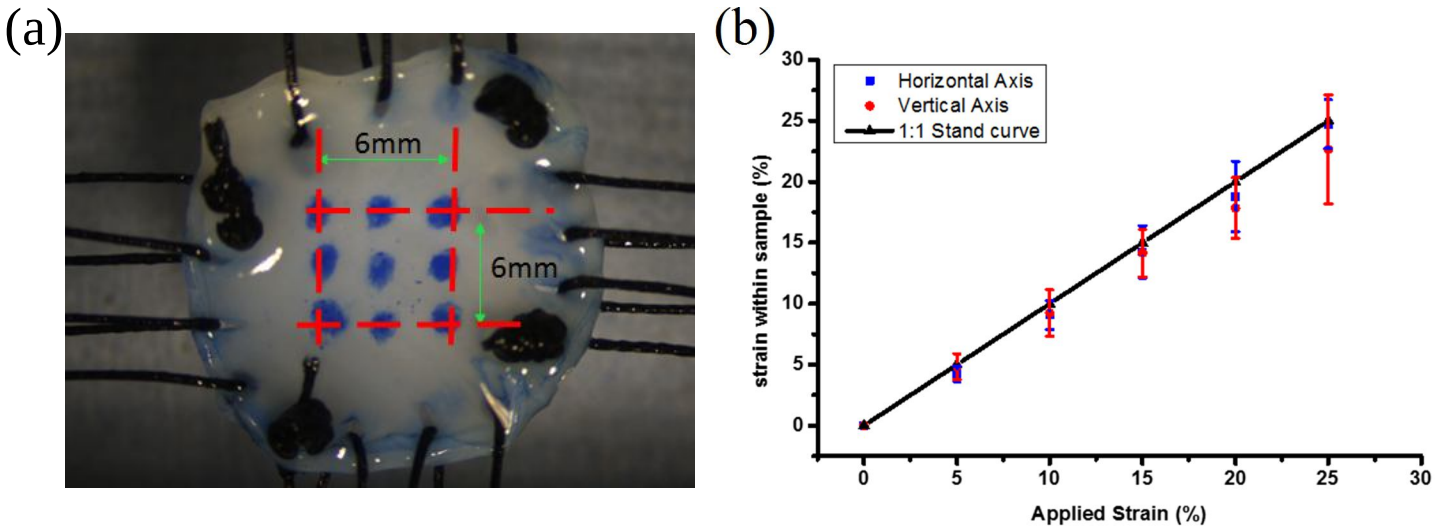

Fig.5- 2. (a) Image of an AV sample sutured into the rig, showing the macro strain markers; (b) summary of data comparing applied strains with sample macro strain in both then horizontal and vertical loading axes.

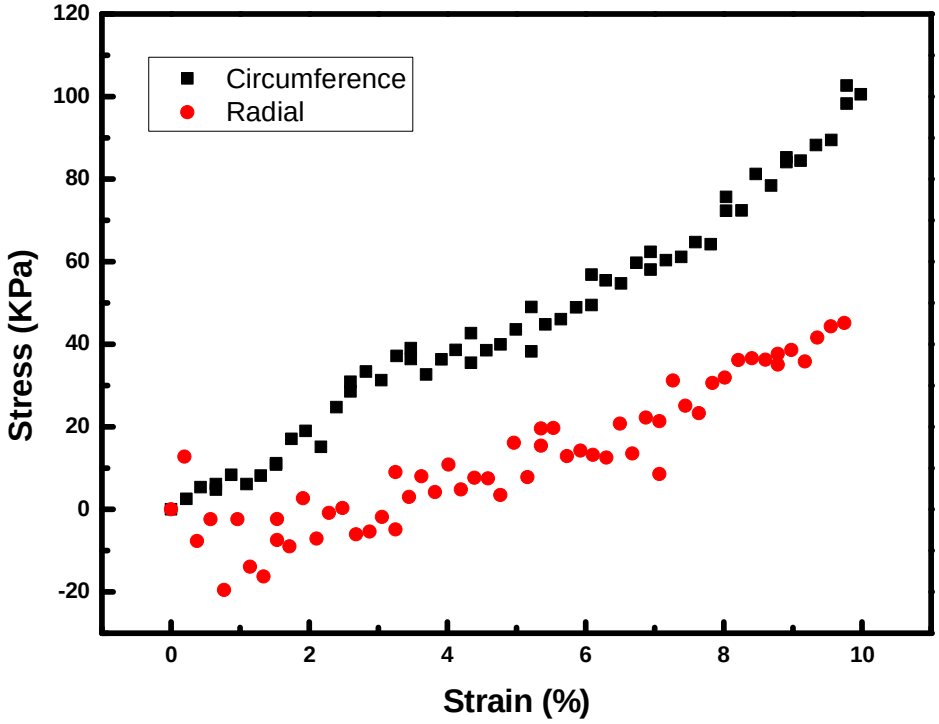

Fig.5- 3. Typical plot of strain-stress curve in biaxial loading test.

The results indicated homogenous local strains across the samples, which closely match the applied strains particularly at lower strains. Although local strains were generally smaller than applied values when large applied strains were adopted (25%-30%), data provides confidence in using the rig to investigate matrix mechanics up to 20% applied strain. A typical plot of a strain-stress curve from a biaxial loading test from 0% to 10% strain is shown in **Fig.5- 3**.

5.4. Strain measurement based on digital image correlation techniques

There are three methods for surveying strains developed in an object subject to

external forces. One method is to measure the relative displacement between two specific points on the surface of an object, and then estimate the strain between these two points. However, the global strain distribution of the object cannot be determined directly. The second method is to map meshes on the surface of an object before deformation occurs, and then survey the displacement of nodes surrounding these meshes after deformation. Further, the strain distribution of an object is derived from the displacement field. This technique is a complex and time-consuming process [235]. The third method is digital image correlation (DIC), which is widely used to measure displacement fields on the surface of a sample by comparing pictures acquired at different states of strain [236]. It is often used to measure deformation, displacement, strain, and optical flow. DIC is a non-contact optical correlation method used to measure full-field displacements on the surface of an object, based on the concept of using a search algorithm to execute image identification by tracking a random pattern on the sample surface. The analysis image is divided into several sub-images. The grayscale distribution of the image is used to identify the relative positions of the same point on the specimen surface in two images. Correlation analyses of images are carried out to search for the point that has the highest grayscale correlation with the initial position displacement vector, so that the displacement field of a specimen can be derived, and strain fields can be calculated [235].

5.4.1 Two-dimensional digital image correlation method

Based on the discretization operation of the finite element method (FEM), the undeformed image is meshed into several sub-images for image analyses. A random point prior to deformation is set as point **P**; which is shifted to point **P*** after deformation. The functional relationship is expressed as [235]:

$$x_{p*} = x_p + u(x, y) \qquad (1)$$

$$y_{p*} = y_p + v(x, y) \qquad (2)$$

where (x_p, y_p) and (x_{p*}, y_{p*}) are the coordinates of point **P** before and after deformation and **u (x, y)** and **v (x, y)** are the separate displacement functions in x- and y-direction respectively. Calculating the grayscale correlation coefficient will lead to finding the corresponding relationship between deformed and undeformed sub-images for establishing the deformation of sub-image. The correlation coefficient is defined as

$$\mathbf{COF} = \frac{\sum m_{ij}\widetilde{m}_{\bar{i}\bar{j}}}{\sqrt{\sum m_{ij}^2 \sum \widetilde{m}_{\bar{i}\bar{j}}^2}} \qquad (3)$$

Where m_{ij} and $\widetilde{m}_{\bar{i}\bar{j}}$ are the grayscale of the undeformed sub-image on coordinates (i, j) and the deformed sub-image corresponds on coordinate ($\bar{\imath}$, $\bar{\jmath}$) respectively. When the deformed sub-image corresponds exactly to the undeformed sub-image, the correlation coefficient between both sub-images equals 1. Accordingly, the optimal parameters of Equation (1) and (2) are determined based on the results of correlation

analyses, and the displacement and strain field can be computed individually.

5.4.2 Sample preparation and methods of DIC

Aortic valve leaflets were prepared described in chapter 2. 12 leaflets were harvested from four porcine AVs, and a 15mm×15mm square cut from the central part of each leaflet. The samples were maintained in Dulbecco's Modified Eagle's Medium (DMEM, Sigma–Aldrich, Poole, UK) and used within 2 hours. Samples were secured within the biaxial rig with a continuous strand of 2-0 silk suture.

Once the samples were secured, the sample surface was sprayed with a thin layer of bright red face paint (Snazaroo, Somerset) to give it an artificial granular appearance that is similar to optical speckle (

Fig.5- 4). A Cannon 7D (Cannon Inn. Japan) camera was secured above the specimen in a tripod, with the optical axis kept perpendicular to the surface of the sample. The samples were initially secured at a length of ～10 mm in each direction, after which an equibiaxial force of 0.1N was applied, to provide a consistent zero-strain starting position for the tests. Sample lengths were recalculated, and the starting lengths used to compute the applied strains. Samples were strained equibiaxially from 0% to 12% strain in increments of 2%, taking images at each increment.

The DIC software was kindly supplied from Professor K. Genovese, University of Della Basilicata, Italy. The tracking matrix was defined in the software as 7×7 (

Fig.5- 4), resulting in 6 measurement regions in the circumferential or radial direction. These were named as FI, FII, FIII, BI, BII and BIII in radial direction and LI, LII, LIII, RI, RII and RIII in circumferential direction (

Fig.5- 4). 6 samples were imaged from the fibrosa side, and the other 6 samples from the ventricularis, to compare local strains across the AV layers.

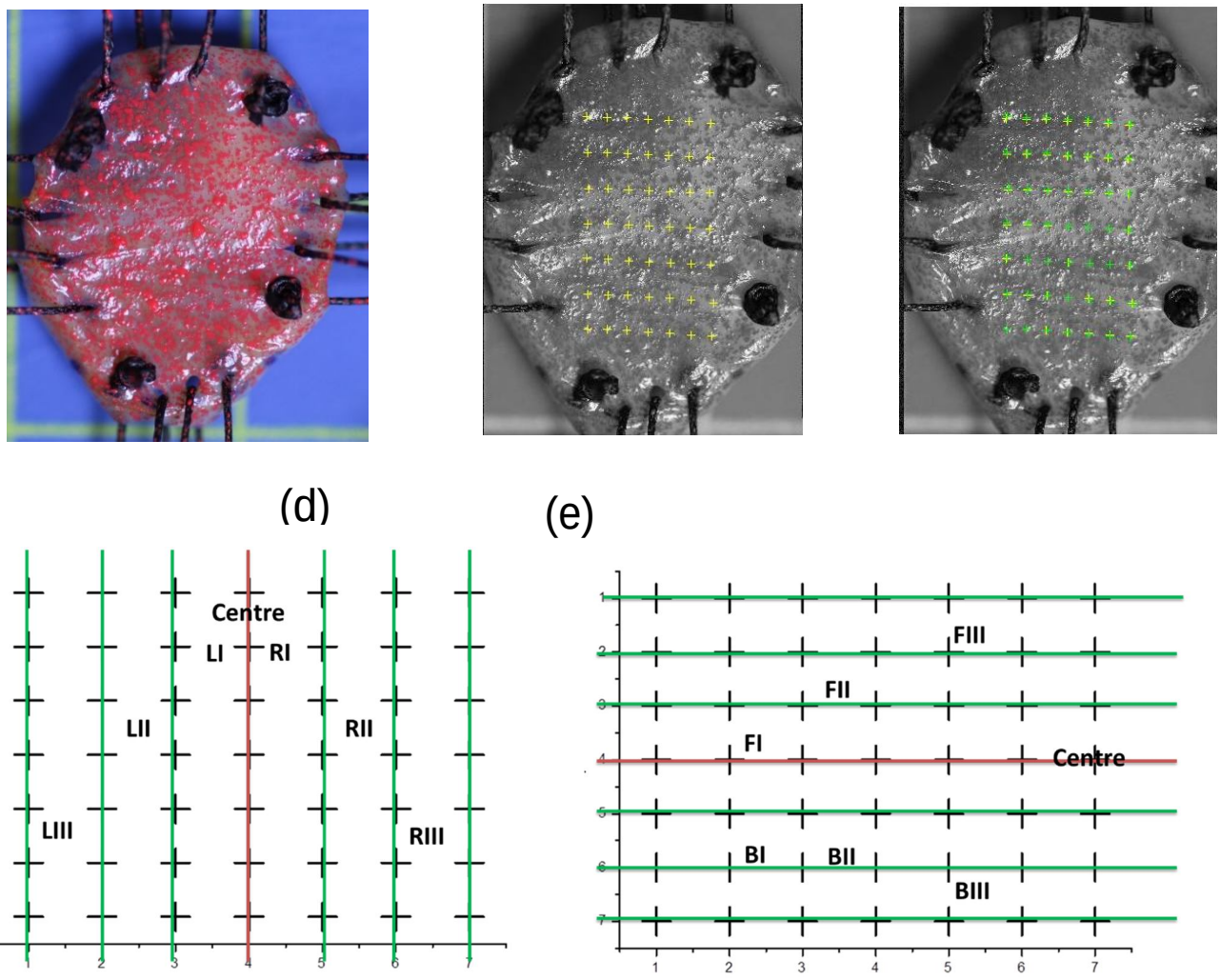

Fig.5- 4. (a) Photograph of a sample secured in the rig, after spraying with are paint. The software places the tracking matrix over the sample, and matrix marker locations identified (b) before and (c) after the application of strain. Schematics identifying the tracked regions in (d) circumferential and (e) radial direction.

5.4.3. Results of DIC

Fig.5- 5 depicts how local strains vary across both the ventricularis and fibrosa in both the radial and circumferential directions. In the circumferential direction, the local strains were less than the applied strains in all measurement regions, in both the ventricularis layer and the fibrosa layer. It was also notable that strains values appeared smaller in the fibrosa than the ventricularis. By contrast, strains were larger and more varied across the radial direction. In the region closest to the free edge (FI, FII and FII) local strains were less than the applied strain, but the local strains nearer to the base attachment region (BI, BII and BIII) were close to or higher than the applied strain, especially in the fibrosa layer (**Fig.5- 5** d). These data indicate that the AV leaflets were stiffer in the circumferential direction than the radial direction, but also showed inhomogeneity across the radial direction, where the leaflets were stiffest close to the free edge.

Ventricularis layer **Fibrosa layer**

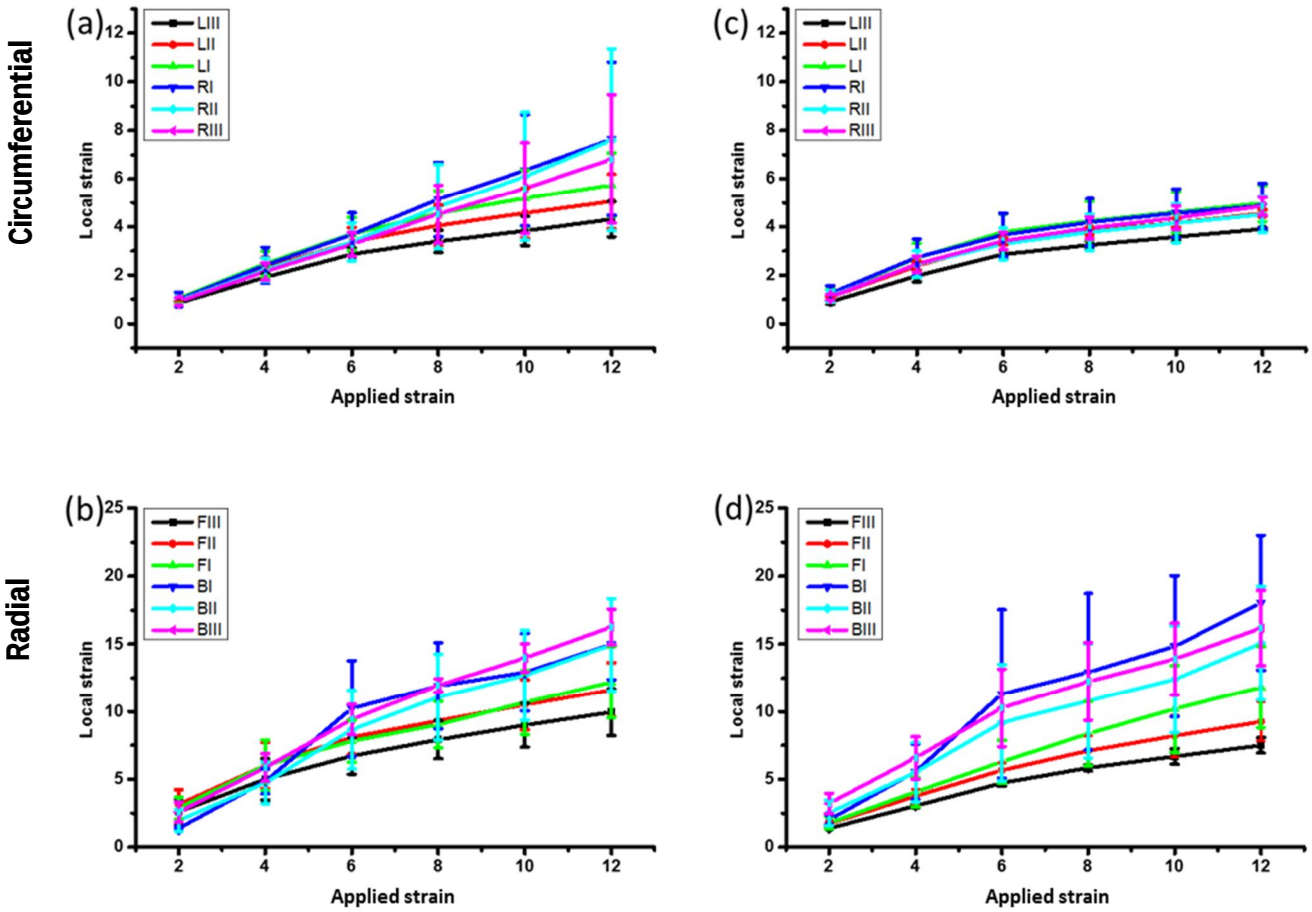

Fig.5- 5. Local strains under applied strains in ventriularis (a, b) and fibrosa (c, d) side in circumferential (a, c) and radial (b, d) direction at different regions.

5.5. Micro strain analysis methods

The DIC results suggest that on a meso scale, the strains across the aortic valve are heterogeneous and the AV leaflet has different stiffness properties in different regions to meet its complex hemodynamic environment. In order to study the how the aortic valve responses to the strain at the micro scale and the role of GAGs on the micro mechanical properties of aortic valves, it is necessary to develop protocols to investigate micro strains across the leaflet using confocal microscopy. In this thesis,

cell tracking and photobleaching methods were developed for these propose.

5.5.1. Strain measurement based on cell tracking

In order to investigate the distribution of local micro strains across the aortic valve in response to applied strain, the cell nuclei can be used as micro-markers of the strain distribution, as cells are known to be attached to the extracellular matrix (ECM) [194, 237]. In present thesis, cell tracking for biaxial testing methods were developed and tested, based upon previous studies in the host lab [155, 194, 238].

5.5.1.1. Sample preparation for cell tracking

Aortic valve leaflets (n=6) were prepared following the protocols outlined in chapter 2. The AV leaflets were cut from porcine heart and stained with 1μg/ml Hoechst 33258 at 37℃ for 10 minutes. After staining, the samples were cut into a 15mm×15mm square and then secured into the biaxial rig with a continuous strand of 2-0 silk suture. Loosely approximating the areas highlight with point markers in macro testing, 9 areas were selected in each sample for micro strain imaging, with a Leica confocal miscopy and a ×10 objective lens (HC PL Fluotar, Nikon, Kingston-Upon-Thames, UK). The samples were initially gripped at a length of ～10 mm at each direction, and then an equibiaxial tare load of 0.1N was applied, to provide a consistent zero-strain starting position for the tests. Sample length was recalculated, and this

starting length used to compute the applied strains.

The rig was placed onto the microscope stage, and cells within the first imaging region identified, imaging at a depth approximately 50-80 μm into the sample. 3 leaflets were randomly selected to image in the fibrosa layers and the other three leaflets were viewed from the ventricularis layer.

5.5.1.2. Cell tracking

An identifiable marker cell within the field of view was selected, to aid tracking of the cells during straining. The specimen was subjected to equibiaxial tensile strain, applied in increments of 2 %, up to 12 % strain in each direction. At each increment, the marker cell was identified, and an image of the same group of cells was captured. After 12% strain, the sample were returned to its original starting strain (0%), the second imaging region selected. This procedure was repeated until all 9 imaging regions had been tracked, ensuring a different order for capturing the regions in every sample. The resultant series of images were analysed using specialized object tracking image software (Imaris, Bitplane AG) to track the movement of the cell nuclei at each strain increment;the software tracked the coordinates of the centroid of every cell nucleus in each image. In each two-dimensional (2D) slice, nuclei were tracked at each applied strain increment, and then strain triads used to calculate the local strains, following previously described methods (

Fig.5- 6) [155]. To briefly review, displacement vectors were determined for each cell, and strain in the circumferential direction calculated by $\varepsilon_c = \Delta x/a$, where "a" is the original distance between any two tracked cells in the circumferential direction, and Δx is the relative movement after applied strain. ε_c was reported as a mean value encompassing all the values calculated from all tracked cells within a single image. Similarly, ε_r was calculated in the same manner.

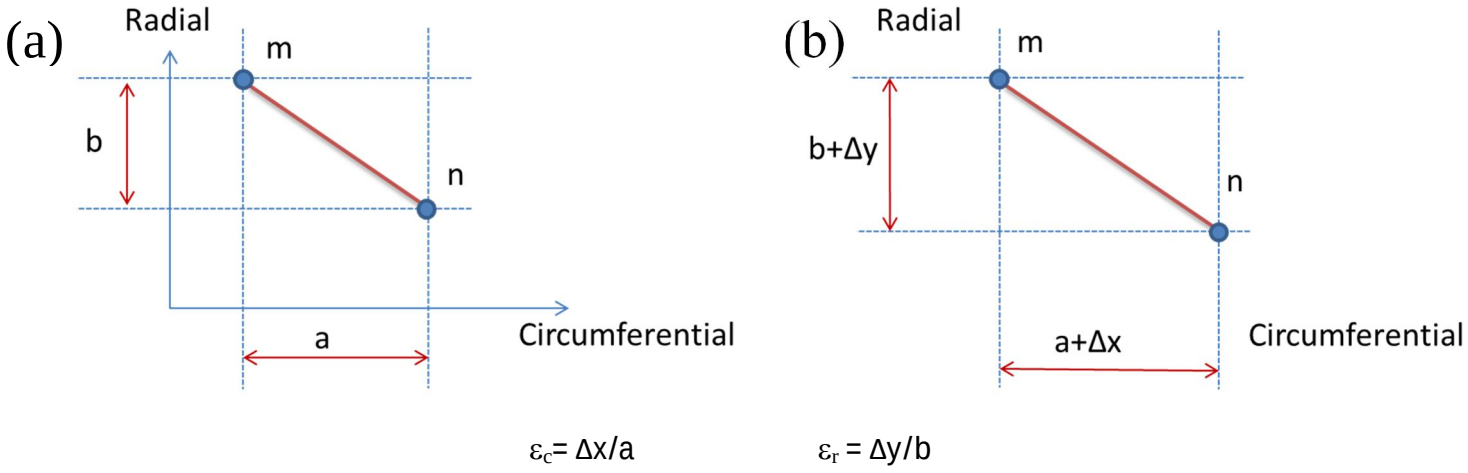

Fig.5- 6. Schematics depicting two cells before (a) and after (b) straining, to show the method for calculating local strain in the circumferential and radial directions across the valves

5.5.1.3. Results of cell tracking

Hoechst 33258 brightly stained the nuclei of the valve interstitial cells (ICs), with little background fluorescence from the collagen. A typical sequence of images of a group of cells tracked at each applied strain increment are shown in **Fig.5- 7** and a

colour map showing the local strains in each region of the AV at an applied strain of 8% is shown in **Fig.5- 8**. These data highlight the variability in strains across the samples.

However, a number of limitations were identified when trying to implement this micro strain analysis method: 1) firstly, although care was taken to refocus the confocal microscope during straining the sample, cells were often lost and could not be easily tracked after the application of strain. 2) When cells were close together within an image region, substantial errors in local strain measurements occurred, owing to the limited resolution of the microscopy and error in identifying the centroid coordinates of a deforming cell. 3) As the cell nuclei are small strain markers, a compromise between sufficient magnification to track the cells, and a large field of view for investigating micro strains was difficult to achieve. 4) The effects of repeatedly loading and unloading the sample to track all nine regions is unknown at a micro strain level, since AV leaflets are known to have different abilities of recovery in the circumferential and radial directions. Returning the sample to 0% strain during the process of imaging is likely to affect the local strains measured.

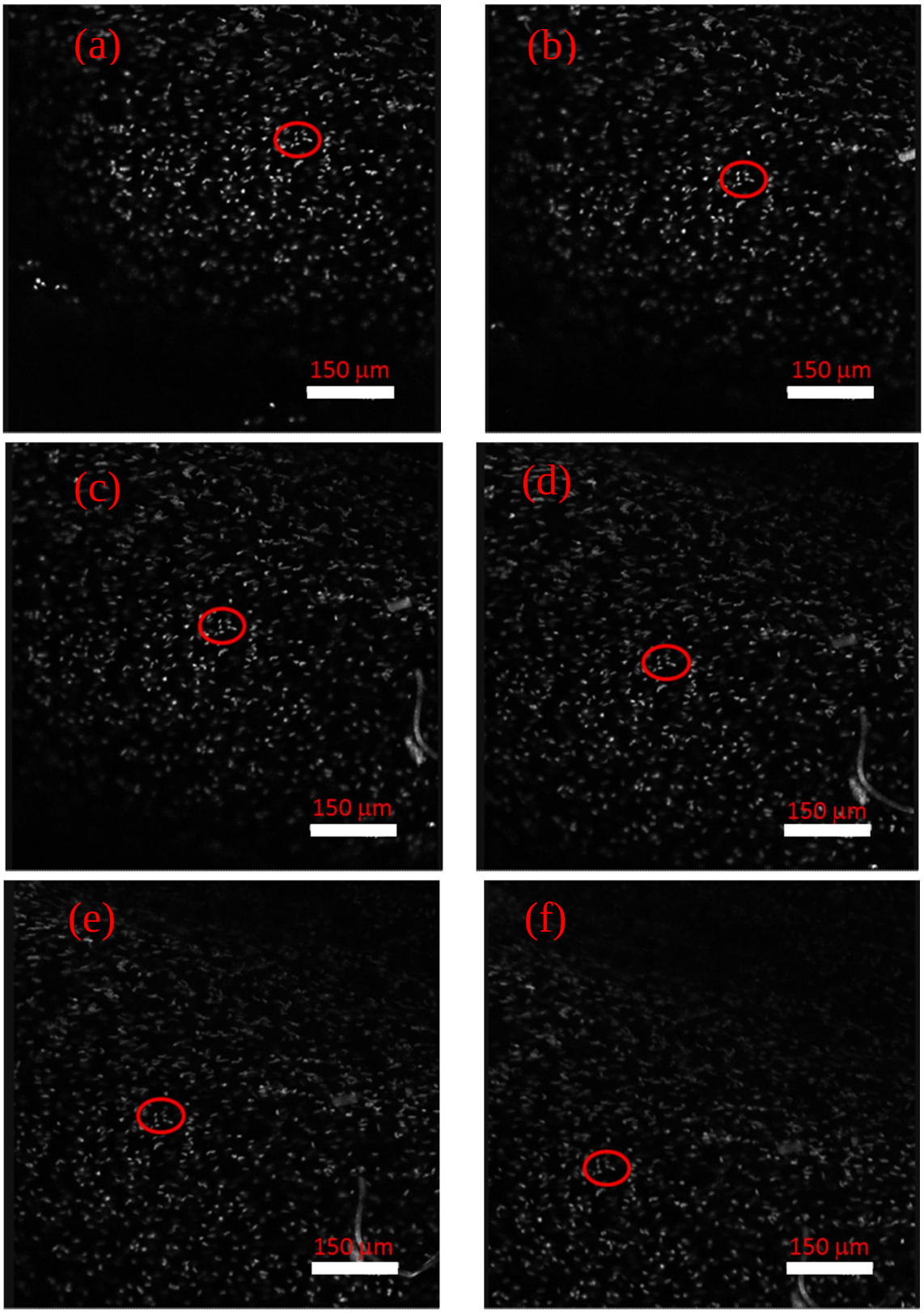

Fig.5- 7. A typical sequence of images of a group of cells tracked at each applied strain increment. The strain increases from (a) 0% to (f) 10% in increment of 2% strain. Red circles show the same group of cells, tracked through the applied strain increments.

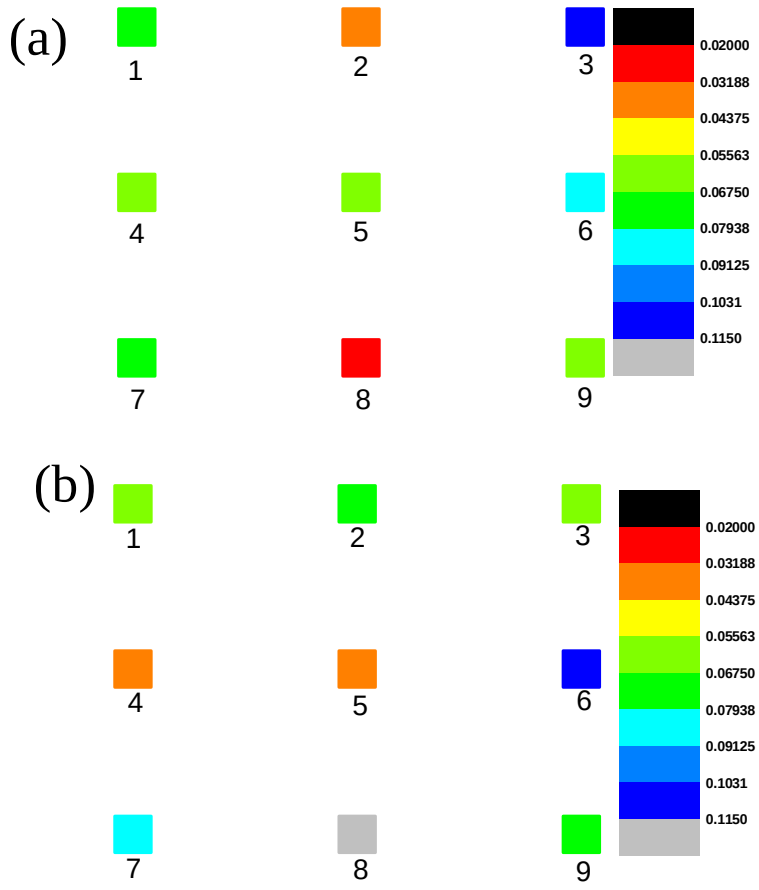

Fig.5- 8. Colour map for the local strains across the valve at an applied strain of 8%, in both the circumferential (a) and radial direction (b)

5.5.2. Strain measurement based on photobleaching

In chapter four, photobleaching methods were developed to investigate the strain distribution across the AV leaflet by uniaxial tensile tests. It has been proved that photobleaching method was good enough to quantitatively analyse the local strain under uniaxial straining. To investigate how AV leaflet response the applied strain under biaxial tensile test and the role of GAG on the mechanical properties of AV leaflet, photobleaching method were developed combine with the biaxial rig.

5.5.2.1. Sample preparation for photobleaching

Aortic valve leaflets were harvested as describe in chapter 2. Briefly, 9 porcine hearts were obtained from animals between 18 and 24 months, from a local abattoir (Cheale Meats Ltd, ESSEX,UK) within two hours of slaughter, and three aortic valve leaflets dissected from each heart, rinsed and maintained in Dulbecco's Modified Eagle's Medium (DMEM, Sigma–Aldrich, Poole, UK) for up to 30 minutes until used. The leaflets were then randomly divided into three groups: “fresh control”, “buffer control”and “digested” groups (N = 6 in each group), and prepared as describe in chapter 3.

After preparation, the AV leaflets of all three groups were incubated in 0.1 M sodium bicarbonate buffer at pH 9 containing 0.5 mg/ml 5-([4, 6-dichlorotriazin-2-yl] amino) fluorescein hydrochloride (DTAF) at 37 °C to stains the collagen an elastin as previously described in chapter two. Following staining, the leaflets were washed in two changes of DMEM for 20 min. After the washing, a square 15mm × 15 mm sample was cut from the centre of each leaflet, and secured within the biaxial rig with 2-0 silk sutures. The rig was filled with DMEM, so leaflets remained hydrated for the duration of the experiment.

5.5.2.2. Methods for photobleaching

Local strains were measured from the fibrosa side (N=6 in each group). Each leaflet was viewed under a laser scanning confocal microscope (TCS SP2, Leica Microsystems GmbH, Wetzlar, Germany) using a ×10 objective (HC PL Fluotar, Nikon, Kingston-Upon-Thames, UK). Leaflet alignment and orientation were checked under brightfield settings to ensure that samples were aligned with the two principle loading direction. The samples were initially secured at a length of ～10 mm at each direction, after which an equibiaxial tare load of 0.1N was applied, to provide a consistent zero-strain starting position for the tests. Sample length was recalculated, and this starting length used to compute the applied strains.

Four squares were bleached directly in the centre area of leaflet by the fluorescence photobleaching methods described in chapter 4. After bleaching, and sample was subjected to equibiaxial strain from 0% to 12% strain, in increments of 2% strain. Owing to the time delay inherent in locating and imaging the grid at each strain increment, a controlled three minutes wait period was taken between each imaging step for consistency.

Additional samples (N=3 in each group) were directly strained to 6% strain, returned to 0% and then strained to 12% strain and returned again to 0% strain. A single image was taken at each strain point after the grid has been relocated in focus and recover

calculated from the change in grid parameters at this point in time. The location and imaging process took roughly three minutes for each strain increment, and with previous studies indicating that 90% of any expected stress relaxation in a sample will have occurred within 1 minute [104, 108, 195], it is reasonable to assume that imaging took place after the majority of stress relaxation behaviour.

The local strains in both the radial and circumferential directions were calculated from the grid deformation, as described previously. Recovery calculations assessed the extent of grid deformation when strain was applied and the percentage of that recovered as the sample was returned to its starting strain.

5.5.2.3. Results of Micro strain measurements

The micro strain in all groups increased with the applied strain, but as seen in the meso strain analysis, the micro strains were notably smaller than the applied strains in the circumferential loading direction. (**Fig.5- 9** a). Comparing the three different treatment groups, no significant differences were found between groups in the circumferential direction. However, the large error bars in the buffer control and digested group data suggests that there was notable variability between samples. In the radial direction, fresh control and buffer control samples behaved very similarly, with local strains closely approximating applied values. However, the local strains were significantly smaller in the digested group, at around 50% of applied values at 12% applied strain (**Fig.5- 9** b).

It was notable that in both the circumferential and radial directions, the samples in all three group recovered to values in excess of 100%, indicating that the grid had returned beyond its starting conditions. This over-recovery was particularly evident after the application of 12% strain (**Fig.5- 9** c). No significant differences were found in the recovery of different groups in the circumferential direction. However, in the radial direction, samples in the digested group show significant more over recovery than other samples (**Fig.5- 9** d)

Circumferential direction Radial direction

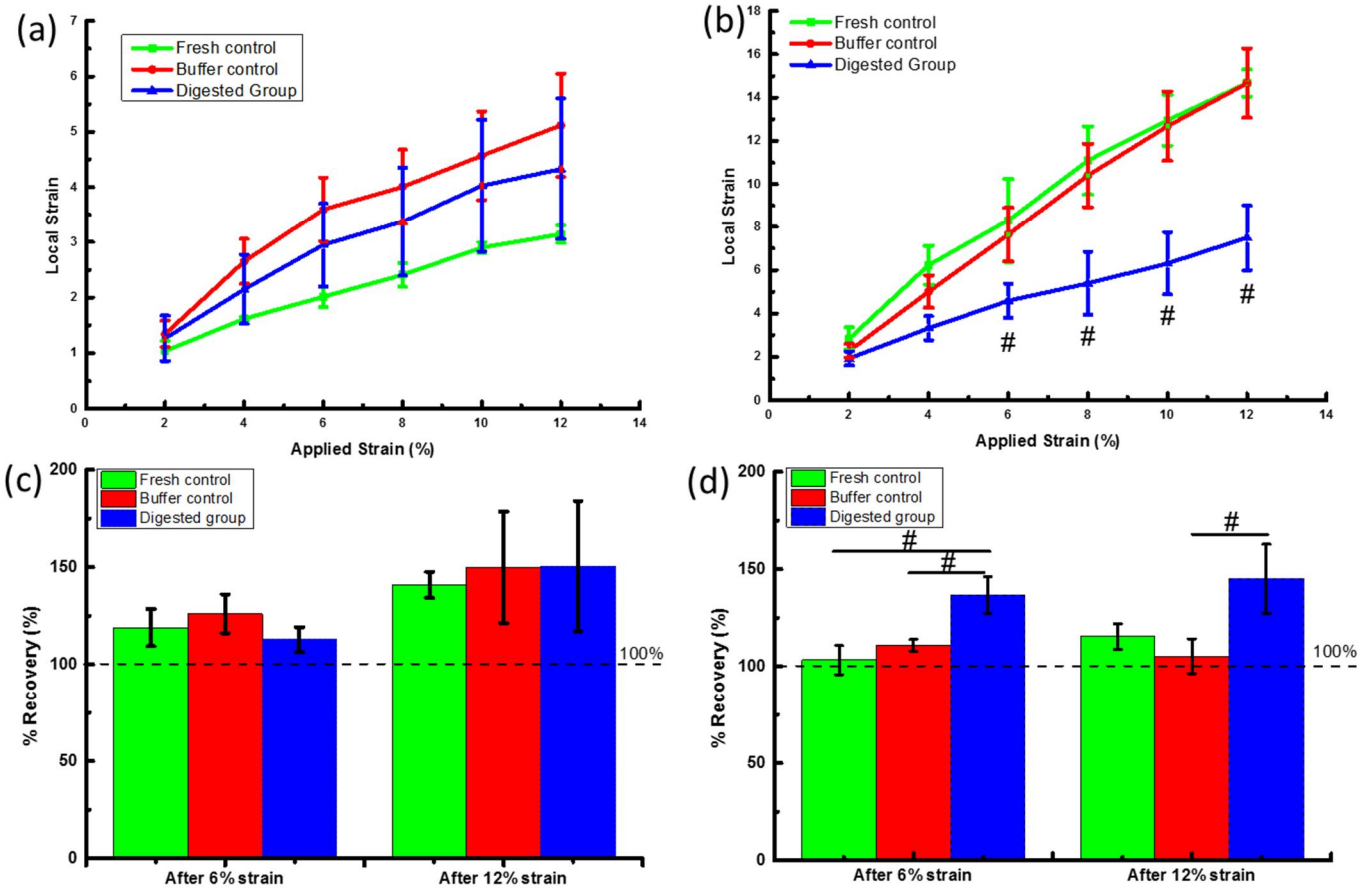

Fig.5- 9. The relationship between applied strains and local strains in fresh, buffer incubated and GAG digested samples, in the circumferential (a) and radial (b)

direction. The samples all showed over recovery (over 100%) in all groups, both in the (c) circumferential and (d) radial directions (statistical significant: # $p < 0.05$).

5.7. Discussion

In this study, macro and micro strains across the AV when subjected to equibiaxial loading were investigated. Firstly, the ability of the rig to uniformally strain samples was confirmed, after which DIC was adopted to more closely map meso strains across the valve. Finally, methods to investigate micro strains across the AV were investigated, and the photobleaching of grids adopted to measure local strains and sample recovery.

DIC is a non-contact optical correlation method used to measure full-field displacements on the surface of an object. In the present study, the samples were sprayed with a thin layer of face paint, to give them an artificial granular appearance that is similar to optical speckle. Strains across the sample surface could then be studied without other processing. The results confirmed that the strains across the whole leaflet were heterogeneous, especially in the radial direction where the region closest to the free edge was stiffer. It could be speculated that is important for the foundation of aortic valve leaflets. The stiffer edge region in radial strips could help the valve to withstand pressure during diastole to keep it closed, whilst lower stiffness nearer the basal attachment could help minimise damage from bending during valve

closing and opening.

In this study, the role of GAGs on the mechanical properties of the AV leaflets were also studied. Biaxial strain data reflects the results seen under uniaxial conditions. Fresh and buffer control samples showed anisotropy between the radial and circumferential response to the strain, and the leaflets were stiffer in the circumferential than radial direction. Once the GAGs were removed from the leaflets, comparable local strains were evident across the radial and circumferential direction, (**Fig.5- 9** a-b). It can be speculated that the GAGs play an important role in maintain the distribution of strains across the leaflet.

The resolution of DIC depends on the image size [239] and the quality of the artificial granular pattern on the sample surface used to provide strain markers during imaging. Both the DIC and the photo-bleaching were able to measure the strains in the tissues during loading. However, the DIC used macro-scale markers to obtain more global measures of change across the tissue surface while photo-bleached lines were a micro-measure, taken was more deep into the tissue. The images used to measure strain with the DIC approach were taken by camera, and the whole sample was imaged, make the analysis areas were 10×10 mm^2. By contrast, the images used to measure strain with photo-bleached lines were taken on a confocal microscope and the size of the imaged region was 1.5×1.5mm^2, so the photo-bleaching method was better to measure the local strains and the results represent the changes of local strains

while the DIC was better to be used to compare different changes across the samples.

Concerning recoverability, it was notable that all samples spring back from the applied strain to a position actually beyond the starting coordinates. This indicates highly elastic mechanics within the samples. However, the GAG digested samples shown significantly larger recovery ability again, particularly in the radial direction (**Fig.5- 9** d). The negatively charged GAGs have the ability to bind water molecules [108], therefore, GAG are generally thought to acts as a damper, to reduce the impact created by sudden changes in pressure gradient during systole. It is therefore likely that removing the GAGs eliminated the majority of damping behaviour in the valves, and the radially aligned elastin subsequently controlled the elastic recoil of the valve, leading to excess recoil. The interaction of collagen, elastin and GAGs appear critical for the effective function of the valve.

In conclusion, results indicate that strain distributions across the valve are heterogeneous and GAGs play a direct role in strain transfer through aortic valves, especially in the radial direction. Data also supports the importance of the spongiosa as a buffer layer between the ventricularis and fibrosa, as removal of the spongiosa led to homogenous strains across the valve leaflet, and over recovery from loading, factors which will alter the function of the AV in vivo.

Chapter Six

Discussion and Future Work

6.1 Introduction

The role of GAGs on structure-function relationships within the AV were investigated in this study. The quasi-static mechanical behaviour of the AV was characterised at both tissue and micro levels, and both uniaxial and biaxial studies were adopted to investigate local strain transfer through the leaflets. The distribution of GAGs through the aortic valve and their contribution to tissue level behaviour were experimentally investigated. In chapter 3, cyclic preconditioning and uniaxial tests to failure were used to investigate AV mechanics at the macro level, while in chapter 4, a custom designed rig was used to the measured the local strain distributions across the AV leaflet at a micro level. To compliment the uniaxial studies, biaxial studies were carried out in chapter 5, developing methods to investigate the strain distributions across the AV leaflet under equibiaxial strain. Data from the present study confirms some results from other studies and also brings new findings.

The negatively charged glycosaminoglycans (GAGs), which are composed of linear long chains of repeating disaccharide units [96], take an important role in the function of a tissue due of their ability to attract water [240]. In the AV leaflet, it is thought that the GAGs can absorb shear and cushion shock as the valve flexes and strains [54]. However, the role of GAGs on the mechanical properties of the AV is not clear.

The primary findings of the thesis are summarised as a series of points.

At the tissue level:

1. In agreement with previous studies, the mechanical behaviour of the AV is anisotropic, and the leaflet is stiffer in the circumferential direction. In freshly dissected samples, the maximum modulus in the circumferential direction is 19.65 ± 2.43 MPa, while in the radial direction, it is 2.19 ± 0.26 MPa. The leaflet has a higher failure strain and lower ultimate tensile strength (UTS) in the radial direction. Circumferentially, the failure strain is 31.02 ± 1.48 % with a UTS of 2.85 ± 0.48 MPa, while, radially, the failure strain is 53.12 ± 3.69 % and the UTS is 0.32 ± 0.05 MPa. Removal of GAGs from the leaflet had no significant effect on the anisotropic properties of leaflets in either the radial or circumferential direction.

2. During cyclic loading, the hysteresis drop was greatest in the first cycle, after which it remained at around 20-30%. There were no significant differences in peak load, modulus, or hysteresis between fresh or GAG digested samples, suggesting that digesting the GAG from the leaflets had no influence on any valve mechanical properties at a gross level.

3. However, data suggested that the removal GAGs may influence the preloading condition of the samples. All samples were taken to a tare load of 0.1N before testing begun. In digested samples, considerably larger extensions were required to reach the preload in the circumferential direction, while the strains to reach the preload in the radial direction were smaller in the digested group. The consistency of these data does suggest that GAG may influence the initial low stiffness behaviour of the AV at a macro level in a highly anisotropic manner.

At the micro level:

1. The AV is composed mainly of collagen, elastin and GAGs, all with specific orientations and locations. The collagen is mainly circumferential while elastin is radial. Collagen exists throughout the AV and is the main loading bearing component. The radially aligned elastin is localized in the ventricularis. Although GAGs are present throughout the leaflet, they are mainly in the spongiosa. The distribution of GAGs is heterogeneous across the leaflet, especially in the radial direction.

2. Local strain measurements revealed variations in local valve mechanical properties across the radial loading direction in both the fibrosa and ventricularis layers. Under uniaxial strain, local strains in the basal attachment

region were larger than those in the free edge region, suggesting that the free edge region is stiffer. This property may be important to keep the AV closed during diastole, but ensure it remains sufficiently flexible to stay fully open during systole. Local strains in the circumferential direction were relatively homogenous along the strip, with no significant differences in either the ventricularis or fibrosa.

3. The response of the AV to applied strain was layer specific and removal of the GAGs from the leaflet had the greatest effect on the mechanical properties of the fibrosa layer, both in the radial and circumferential direction. After digesting GAGs, inhomogeneity in the strain distribution across the fibrosa was reduced. However, no significant differences were found in the ventricularis layer.

4. During straining, strain values transverse to the loading direction were different in the circumferential and radial direction. Negative Poisson's ratios, which indicate an expansion of the sample width upon the application of strain, were seen in both the left and right regions of the circumferential strips while small, but positive Poisson's ratios was seen in the middle region. In contrast, only positive Poisson's ratio were seen transverse to loading in the radial direction.

5. The aortic valve response to the strain was different in the fibrosa and ventricularis. For native samples, in radial strips, local strains transverse to the loading direction showed significant differences between the fibrosa and ventricularis at the free edge area, where a Poisson's ratio of 0 was measured in the fibrosa layer, while the ventricularis contracted. In the circumferential strips, only negative Poisson's ratios were measured across the ventricularis while both positive and negative Poisson's ratios were measured in the fibrosa.

6.2. Discussion

6.2.1. The distribution of extracellular matrix

The AV has been shown to perform extremely complex and sophisticated functions, which depend critically on its specific cellular and ECM components [108]. Under the microscope, the AV leaflet consists of three distinct different layers. The ventricularis layer faces the left ventricle and is composed primarily of radially aligned elastin and collagen [89, 178, 188]; the middle layer, the spongiosa, is primarily composed of glycosaminoglycans (GAGs) and proteoglycans [241, 242]; On the opposite face of the valve is the fibrosa layer, which is composed predominantly of a dense network of type I collagen fibers, which exhibit macroscopic crimp and are aligned primarily in the circumferential direction. Although each layer has more predominant ECM

components, all ECM components exist across all the three layers. GAGs are primarily located in the spongiosa, but are present in all three layers (**Fig.4- 13**). A typical Miller's elastic stain image of the AV leaflet is shown in **Fig.6- 1**, clearly showing collagen throughout the leaflet, but the majority of elastin more localized to the ventricularis, and radially aligned. The varied content of ECM in each layer leads to their different mechanical properties. The overall mechanical behaviour is a summation of the mechanics of each of the individual layers within the valve leaflet.

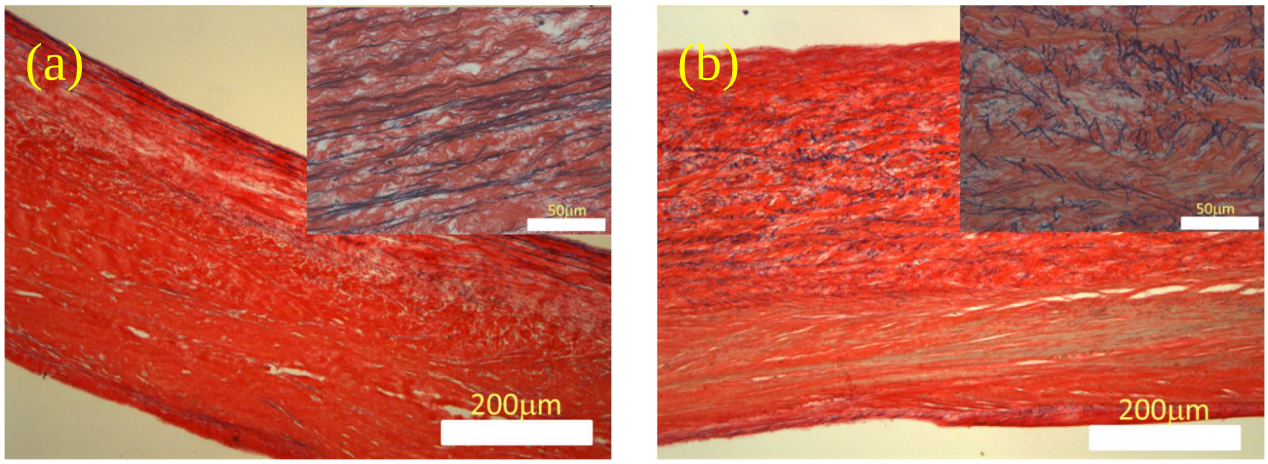

Fig.6- 1. Typical images of a (a) radial strip and (b) circumferential strip of the aortic valves stained with Miller's elastic staining. Elastin is stained black and collagen red.

Previous studies have focused on either quantifying the varied concentrations of GAGs within the different layers [88, 101] or quantifying distributions of each kind of GAG (**Table 1- 3**) [101, 102], but few studies have focused on the regional distribution of GAGs within each layer and how GAGs affect tissue mechanics [195].

In the present study, the regional distributions of the GAGs across the AV leaflet were

qualitative investigated via histology and related to tissue micromechanics. The results suggest that the content of the GAG is negatively correlated with the stiffness of the AV leaflets, as increased GAG content lead to reduced stiffness of the AV. This is perhaps not surprising, as the negatively charged GAGs have the ability to bind water molecules [108], meaning, GAG rich areas are generally highly hydrated, with less collagen to resist applied loads.

6.2.2. The effect of glycosaminoglycans on AV macromechanics and the preload condition.

Many studies have reported a marked anisotropy in the mechanical behaviour of the AV [9, 87, 99, 173, 181, 184]. The AV leaflets exhibit anisotropic strains because the collagen is predominantly aligned in the circumferential direction, providing greater tensile strength circumferentially than in the radial direction [9, 98, 155]. However, aligned in the radial direction are mainly highly extensible elastic fibres [87, 89, 92]. Such anisotropic properties of the valve leaflets are important for proper valve functioning. The high radial compliance of the leaflet allows leaflets to stretch during diastole and fully seal the valve against the backflow of blood. Circumferential stiffness is important for supporting the high transvalvular pressures to keep the valves closed during diastole.

A typical stress-strain curve for an AV is nonlinear (**Fig.1- 13** and **Fig.1- 16**). When

the AV leaflet is stretched circumferentially, the circumferential stresses rise rapidly with a minor increase in strain. However, the leaflet response in the radial direction demonstrates a much larger toe region, in which a small change in tensile stress causes a large deformation. The observed nonlinear stress-strain curve was previously speculated to result from the structural re-organization of the extracellular matrix (ECM) [166, 172].

In the present study, the anisotropic behaviour of the AV was confirmed in chapter 3. The failure strain, ultimate tensile strength (UTS) and maximum modulus were all significantly different when straining in the circumferential than radial direction (**Fig.3- 8**), with the elastin facilitating far more extensibility and less stiffness radially than circumferentially. Data also suggests that the GAGs have little effect on the macro tensile properties of the AV, as no significant differences were found between samples before and after GAG removal in either the circumferential or radial direction (**Fig.3- 6** and **Fig.3- 8**).

Whilst very few changes in gross AV mechanics were evident in response to GAG depletion, in the current study, there is some indication that the amount of sample extension required to reach the tare load at the start of tests may vary with GAG removal. The degree of extension to reach a tare load of 0.1 N, termed ΔL, was significantly different between treatment groups. Comparing ΔL for the two different loading directions, unsurprisingly ΔL was larger in the radial direction than the

circumferential direction in all samples group (**Fig.3- 4** b). However, as shown in **Fig.3- 4** a, ΔL was significant larger after GAG digestion in the circumferential direction but was reduced by GAG digestion in the radial direction. These data indicated that the initial low stiffness behaviour of the valve may have been altered by the GAG digestion, increasing stiffness in the radial direction while reducing stiffness in the circumferential direction.

Care must be taken when interpreting these data, as small variations in the initial laxity of the sample will potentially affect this parameter, making it hard to draw any conclusive conclusions. However, with practice, all samples were loaded into grips in an identical manner, and the relatively small error bars concerning sample extension to reach the tare load, indicate consistency in the approach, and lends confidence to attempts to carry out a tentative comparison of treatment groups.

Previous studies have suggested that GAG digestion reduces hysteresis in the low load response of the AV leaflet under biaxial loading [104]. Overall, data suggests that GAGs may be important in modulating stiffness and providing a damping mechanism to reduce leaflet flutter when the leaflet is not under high tensile stress [104]. The interactions between GAGs and the fibrous matrix do not appear to be significant enough to affect the failure strain, ultimate tensile strength (UTS) or maximum modulus, but are significant enough to affect preload conditions.

Many previous studies do not report a tare load, but those which do, use a tare load from 0.01N to 0.3N in uniaxial studies [13, 98, 99, 165, 166] or about 0.5g (size of samples were not clear) in biaxial studies [9, 184]. Currently, no studies have focus on the effect of preload on AV mechanics, and no standard preload protocol exists, hence the effects of tare load on sample mechanics should be investigated in the future.

6.2.3. The layer specific response to applied strain in the aortic valve.

Most articles reviewing aortic valve mechanics highlight the compositional differences between the layers of the valve and relate these to a specific mechanical function in each layer. Vesely et at (1992) carried out some of the pioneering work investigating the layer specific micromechanical properties of the fibrosa and ventricularis. They separated the fibrosa and the ventricularis in fresh leaflets via manual micro dissection and tested them individually. Comparing the fibrosa and the ventricularis, circumferentially the fibrosa was almost twice as stiff as the ventricularis, while there were no significant differences in stiffness in the radial direction. For extensibility, no difference was found between the fibrosa and ventricularis circumferentially while radially the ventricularis was more than twice as extensible as the fibrosa [90]. In a second study of mechanics in the isolated fibrosa and ventricularis, under biaxial loading, the fibrosa was less extensible than the ventricularis in the radial direction while the ventricularis showed a very large toe

region in the radial direction [9]. These data provide important insights into the properties of the fibrosa and ventricularis respectively. However, the interactivity between layers cannot considered in these type of experiments, so it is difficult to infer how the mechanically distinct fibrosa and ventricularis may function as part of the AV during loading.

The data collected in chapter four can be analysed to address this, and establish more about the distinct mechanics of each valve layer and how the layers interact during loading. To more fully probe the different response to applied strain between the fibrosa and ventriclularis, these data are reorganized in this chapter, to focus on a layer to layer comparison.

Fig.6- 2 once again looks at the local strain results in the loading direction ($\boldsymbol{S_L}$) for radial strips, but in this instance, strains in equivalent regions of the fibrosa and ventricularis are directly compared. Concerning the buffer control group, local strains varied somewhat across the width of the strip, but were reasonably consistent between layers, suggesting little relative movement between fibrosa and ventricularis. After GAG digestion, strain magnitudes across the fibrosa became more uniform as described in chapter 4, however, this lead to greater variability between the two layers, with larger strains in the ventricularis than in the fibrosa.

Considering strains transverse to the loading direction ($\boldsymbol{S_T}$), in either the buffer control

or digested group, local strains were found not to be significantly different in the regions closest to the basal attachment and middle (**Fig.6- 3**). By contrast, in the region closest to the free edge, $\boldsymbol{S_T}$ barely altered with applied strain in the fibrosa while it decreased in a linear manner in the ventricularis in the buffer control group. Notably, after GAG digestion, this differences between layers was lost, and both layers showed a small reduction in width on the application of load (**Fig.6- 3**).

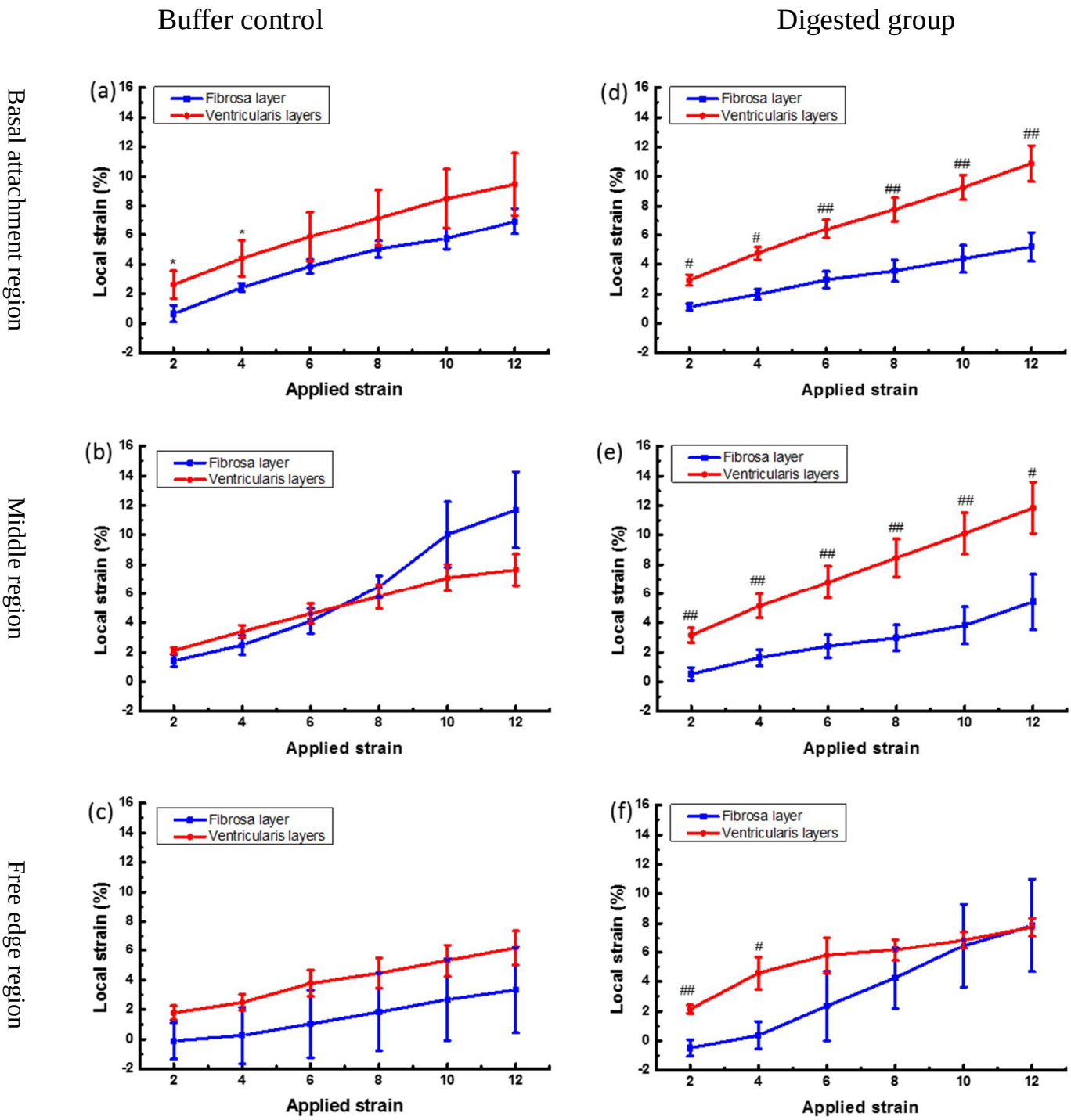

Fig.6- 2. Radial strips, showing local strain in the loading direction (S_L) at different applied strains, directly comparing the response in different valve layers, for buffer control (a-c) and digested samples (d-f), as measured in the region closest to the basal attachment (B), the middle (central) region (M) and the region closest to the free edge (F). Statistical significance, *: $p < 0.1$, #: $p < 0.05$, ##: $p < 0.01$.

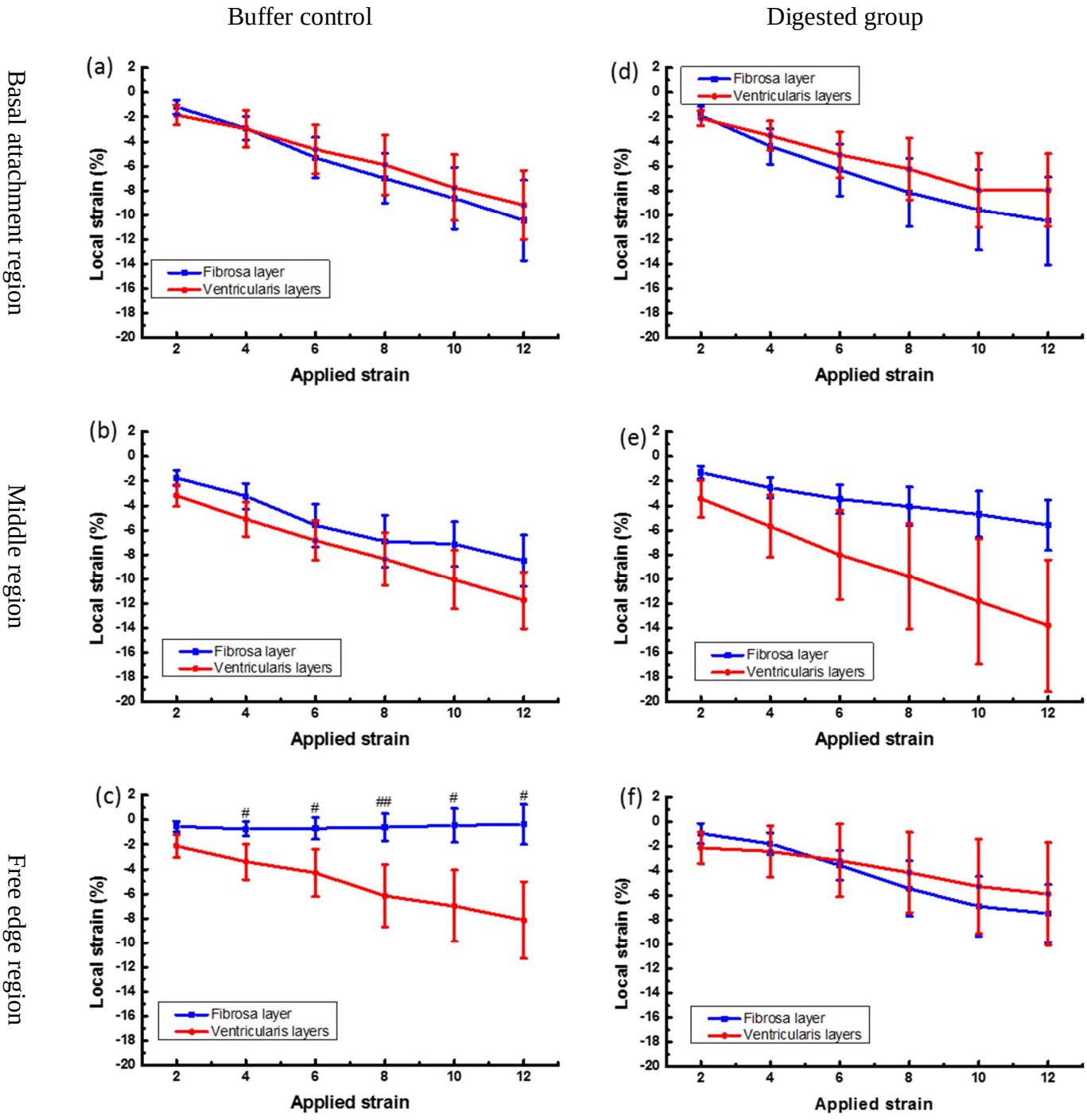

Fig.6- 3. Radial strips, showing local strain in the transverse to the loading direction (S_T) at different applied strains, directly comparing the response in different valve layers, for buffer control (a-c) and digested samples (d-f), as measured in the region closest to the basal attachment (B), the middle (central) region (M) and the region closest to the free edge (F). Statistical significance, *: $p < 0.1$, #: $p < 0.05$, ##: $p < 0.01$

Fig.6- 4 directly compares $\boldsymbol{S_L}$ in equivalent regions of the fibrosa and ventricularis for the circumferential strips. It was notable that in the fibrosa layer, all local strains were smaller than applied strains, across all sample regions in both the buffer control and freshly loaded samples, but there were also no significant differences in local longitudinal strains between any regions of the ventricularis and fibrosa, either before or after GAG digestion (**Fig.6- 4**). However, when considering the strains transverse to the loading direction ($\boldsymbol{S_T}$) in the buffer control group, clear differences were found between strains across the fibrosa and ventricularis, localized to the middle and right regions as shown in **Fig.6- 5**. The Poisson's ratio in buffer control samples was consistently negative in the ventricularis (**Fig.6- 5** a-c), indicating an expansion of the sample width upon the application of strain, while the fibrosa responded with a more conventional reduction in sample diameter upon loading. The Poisson's ratio of approximately -0.5 was highly consistent across the regions of ventricularis. By contrast, Poisson's ratios across the fibrosa side of radial strips were all positive but also more varied (**Fig.6- 5** a-c). Large Poisson's ratios, greater than 1, were seen in the middle of the fibrosa, with values around 0.3-0.5 at either side (**Fig.6- 5** a-c). After removing the GAG from these samples, all differences in Poisson's ratio between the fibrosa and ventricularis disappeared and $\boldsymbol{S_T}$ was very similar in these layers in all regions. However, it was also interesting to note that the previous ventricularis behaviour dominated and all regions of the strip showed negative Poisson's ratios.

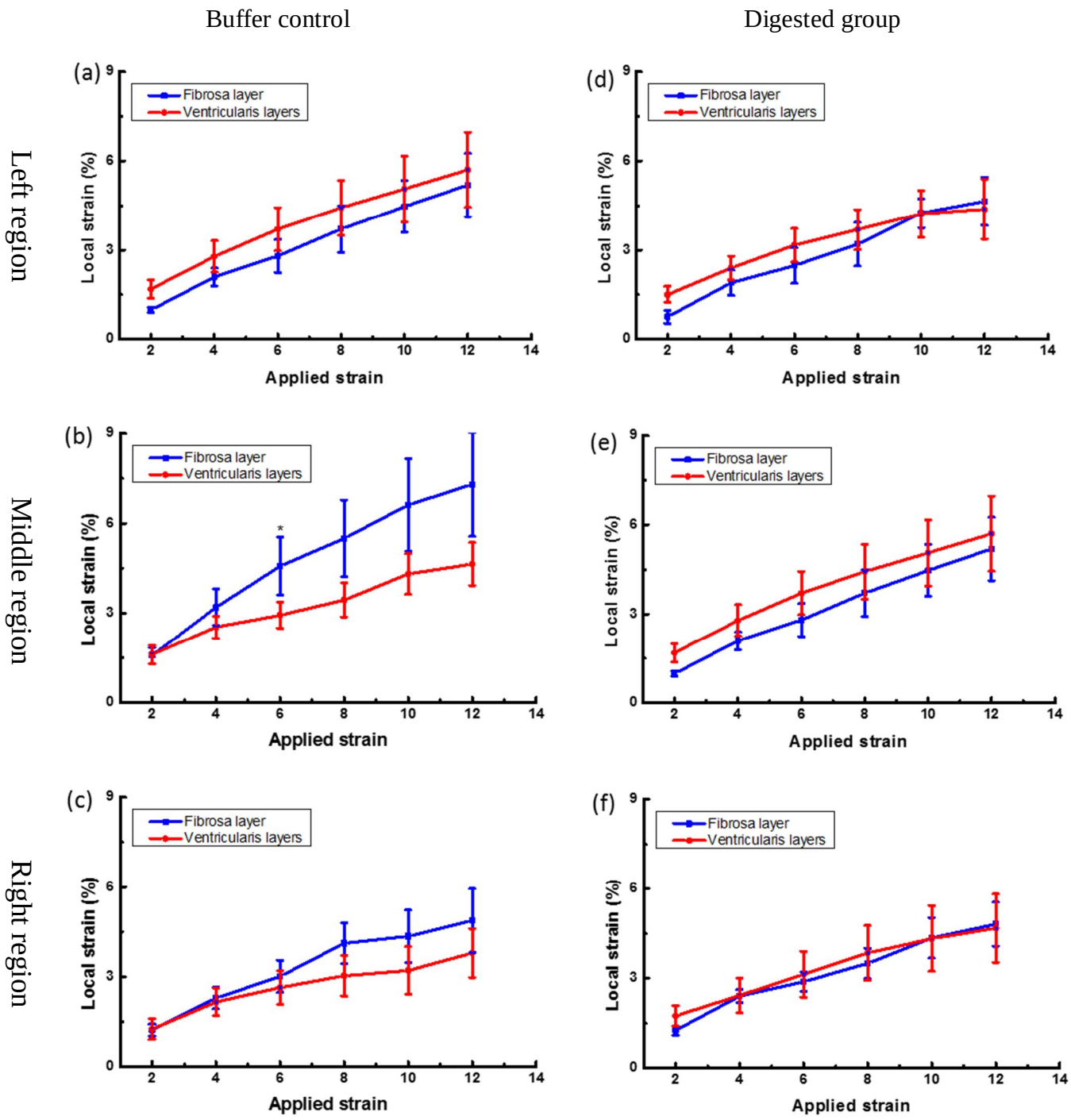

Fig.6- 4. Circumferential strips, showing local strain in the loading direction (S_L) at different applied strains, directly comparing the response in different valve layers, for buffer control (a-c) and digested samples (d-f), as measured in the middle (central) region (M) and the regions left (L) and right (R) of the middle. Statistical significance, *: $p < 0.1$, #: $p < 0.05$, ##: $p < 0.01$.

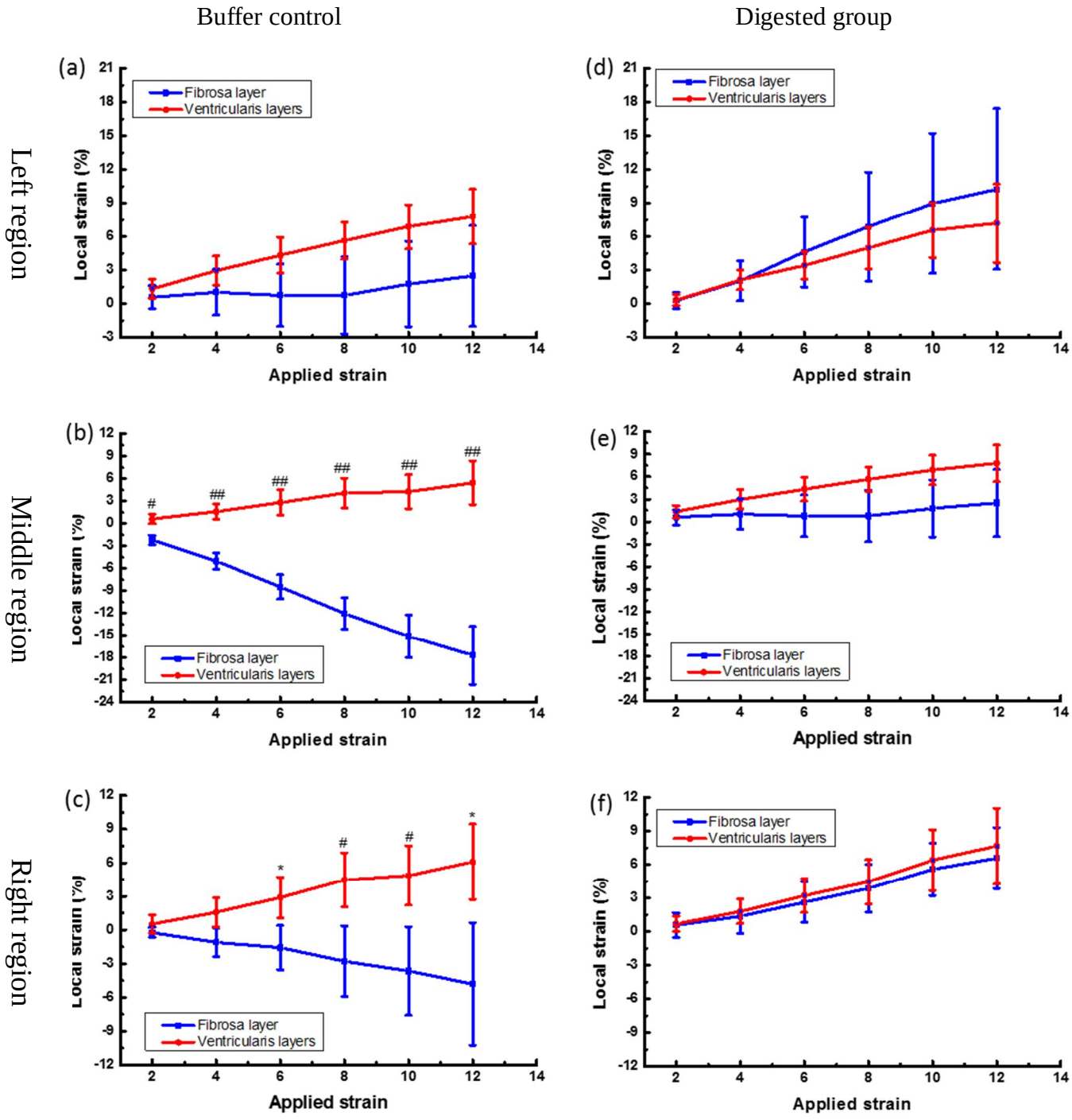

Fig.6- 5. Circumferential strips, showing local strain in the transverse to the loading direction (S_T) at different applied strains, directly comparing the response in different valve layers, for buffer control (a-c) and digested samples (d-f), as measured in the middle (central) region (M) and the regions left (L) and right (R) of the middle. Statistical significance, *: $p < 0.1$, #: $p < 0.05$, ##: $p < 0.01$.

The difference of Poisson's ratio measured in native and GAG digested samples suggest that the elastin holds the valve in a pre-stressed state assisted by the GAG rich spongiosa. When a circumferential strip is removed from the leaflet, the elastin is immediately able to contract the strip. However, once the strip is strained in the circumferential direction, the movement of collagen resists that contraction, and the strip will return to its original width, leading to an apparent negative Poisson's ratio as the sample width expands. In this scenario particularly, the buffering effect of the spongiosa between the ventricularis and fibrosa is very evident. In the intact valve, it is only the ventricularis that shows the contraction and subsequent expansion of leaflet strips upon loading with the spongiosa enabling a more classic response within the fibrosa. However, once the GAGs have been digested, this effect propagates through all layers of the valve, and the same strain behaviour can be seen in the fibrosa.

These results are surprising, as a direct comparison of the data in **Fig.6- 2** and **Fig.6- 5**, suggests the spongiosia can either interconnect the fibrosa and ventricularis and reduce interlayer movement (**Fig.6- 2**), or act as buffer between the layers and allow them to move independently (**Fig.6- 5**). Perhaps the GAGs can crosslink collagen and elastin in different manners, generating stiffer linkages in circumstances where the fibrosa and ventricularis behave similarly, but less stiff linkages between layers where GAGs are required to enable relative movement of the outer two layers of the valve as it opens or closes through internal shearing [6, 99, 109]. This facility may be critical

as the loading environment includes tension, flexion, pressure, and shear stress [5, 6, 99].

A Kelvin-Voigt model has been developed to describe AV viscoelasticity based on the three morphological layers of the valve [99]. In this approach, the non-linear stress–strain behaviour observed in the AV can be described and explained with a tri-layered structural model using a spring and dashpot configuration, with two springs representing the elasticity of the ventricularis and fibrosa layers, while the dashpot represents the spongiosa layer. Notably the spongiosa was able to buffer the fibrosa and ventricularis and allow them to strain independently [99] with the model providing a good fit to typical AV stress-strain behaviour. However, the model was empirical in nature, so did not consider true valve structure, and could therefore not model a true buffering effect.

Another study referring to the buffering effect of the spongiosa was conducted by Anssari-Benam and Screen (2012) [194]. In their study, the aortic valve interstitial cells (AVICs) were used to map the local strains within the fibrosa and ventricularis, and they demonstrated that there can be shearing between layers in the loading direction. They speculated that the buffering effect of the spongiosa was due to the GAGs [99, 155, 194]. However, these studies didn’t consider local strain transverse to the load direction nor look to see how GAG removal may influence buffering.

The present study suggests there were significant differences in local stifffnesses and mechanics between the fibrosa and ventricularis, requiring the relative movement between these two layers on the application of the strain, with GAGs playing different roles in enabling this behaviour. Considering radial strips, the macro-crimp is in the loading direction, and largely confined to the fibrosa. As such, when the strip is strained, the ventricularis tends to show larger strains than the fibrosa, as it is loaded more rapidly. In this loading direction, the spongiosa appears to help couple the layers, as the difference between ventricularis and fibrosa strains only really becomes significant after the GAGs are digested.

Previous studies suggest that collagen fibrils are relatively short and arranged as a discontinuous fibril network [216, 220]. As such there is an active debate regarding how collagen fibrils are effectively cross-linked and/or interwoven to provide structural integrity and how the collagen fibrils and their surrounding matrix transfer forces between neighbouring fibrils.

Scott and Vesely (1995) proposed a mechanism by which the collagen fibres were interconnected by the elastin, which stores energy as the collagen is stretched from its original conformation, and return it to the collagen fibre structure when unloaded [87]. In this model, elastic springs run from one collagen crimp to the next. As the tissue is initially stretched, the elastin undergoes tension while the collagen develops small bending forces as the bundles straighten. Once straight, the stiff collagen fibres take

up a larger proportion of the load in tension. When the load is released, the elastin acts to return the collagen to its undeformed geometry.

Other studies have hypothesized that GAGs act like cross- linking elements between collagen fibrils to transfer forces [197, 218, 229], and GAG digestion has been shown to affect the tensile and viscoelastic properties of aortic valves [108, 196] and other collagenous tissues [197, 217, 218, 229]. However, this theory is disputed, with other studies showing evidence against GAG mediated collagen interactions [104, 220, 221].

6.2.4. The role of GAGs on the strain distribution across the aortic valve leaflet.

Previous studies have suggested that strains distributions across the aortic valve are inhomogeneous. Michael et al (2011) reported a regional variation in dynamic deformation characteristics of AV leaflets at a tissue level [100]. Here, ink dot marked heart valves were sutured into a heart simulator and subjected to normal hemodynamic conditions. Stretch magnitudes across the surface the AV were determined by tracking the ink marks. The authors found higher stretch magnitudes in the free edge region and region close to the basal attachment. By contrast, a previous study in the host lab has suggested that the distribution of macrostrains across the AV was generally homogenous, correlating strongly with the applied strains in both

loading directions and both fibrosa and ventricularis [194], However, this study was uniaxial and on strip samples only.

In the present study, the strain distributions across the AV were investigated both on the macro and micro levels. DIC is a non-contact optical correlation method used to measure full-field displacements on the surface of an object which is easily conducted to investigate the strain distribution at a tissue level. Further, using the fluorescent dye, DTAF, it was also possible to completely stain samples and then photobleach a grid within different layers of the valves which can be viewed under a confocal microscopy to view microstrains. Our custom designed rigs enable us to incrementally load aortic valve samples in a controlled manner, whilst visualizing grid deformation, in order to understand the in situ micromechanical environment of the samples. Instead of using cell nuclei as strain markers, these methods allow one to image the deformation of ECM directly [197, 198, 229-232].

Both DIC and micro-strain analysis showed that strains across the AV were heterogeneous, which agreed with the previous studies [100, 155, 194, 227], but both methods also indicated that the free edge was stiffer than other regions of the AV. This is surprising as it is in direct contrast to the findings of Michael et al (2011) [100], but the very different test conditions make it difficult to directly to compare data. In the study by Michael et al, aortic roots were excised and mounted on a mock flow loop, such that whole surface of the AV was viewed [100], while a 5mm wide strip in the

centre of the leaflet was used in the present study. To secure the sample in the grips of the rig, regions at the end of the strips could not be viewed, such that a length of only 10 mm in the centre of the strip were tested during each experiment. Furthermore, Michael et al tested the AV leaflets under pulsatile hemodynamic and flow conditions, so the deformation of the valve included tension, flexion, pressure, and shear stress [18, 34, 48], whilst in the present study, only tensile strain was applied during the experiment. Whilst the more physiologically representative experiments of Michael et al are more appropriate for characterising the situ behaviour of the valve, the simple uniaxial conditions adopted here are more appropriate for looking at simple variations in stiffness across the material. Indeed, a stiffer free edge may be necessary to help the valve withstand pressure during diastole to keep it closed, whilst lower stiffness nearer the basal attachment could help minimise damage from bending during valve closing and opening.

As outlined in chapter 4, when straining the strip circumferentially, the central region in the fibrosa deformed the most both in the loading direction and transverse to this, indicating that the lowest circumferential stiffness was seen in the centre of the sample. The lower stiffness in the middle of a circumferential strip was speculated to be due to the reorganization of the collagen [184]. Fibres, running from the left and right edges of the leaflet meet in the middle [184], so there are fewer collagen fibres directly spanning this middle region to resist tensile load.

The effects of heterogeneous strain distribution across the AV are not clear. The valve interstitial cells represent a dynamic population of cells and the phenotype of valve cells is influenced by both complex genetic programming and the local hemodynamic factors [25, 48, 49]. AVICs can move from one phenotype to another during the lifespan of a cell, allowing them to adapt [45, 46], and are responsive [52] to their mechanical environment. Studies have shown that the base of the leaflet and the coaptation line of the valve are more prone to calcification than the belly region of the leaflet [243]. The correlation of regional distribution strain and the calcification is one direction of future study.

6.4. Future work

In this dissertation, focus was placed on GAGs and their role in the mechanical properties of the AV leaflet. Local strains were measured in sample before and after GAG removal. Other studies suggested that GAG removal resulted in significant morphological and functional tissue alterations, including decreases in cuspal thickness, reduction of water content and diminution of rehydration capacity [206]. However, the long-term damage to the ECM from GAG digestion remains unclear. To investigate these properties, tissue culture should be conducted.

Recently, a straining chamber was developed in the host lab, enabling AV strips to be

maintained and mechanical stimulated for up to 72 hours (**Fig.7- 1**). The chambers (up to 16 at a time) are connected to a single actuator arm and secured within a BOSE loading frame housed in an incubator, to maintain samples in 5% CO_2 at 37°C. In these chambers, structural damage from long-term fatigue loading of samples, or gene expression in response to the loading can be investigated.

In the future, this system could be used to study:

1) Structural changes to the AV in response to fatigue loading resulting from GAG removal, focusing on the effects of GAGs on sample response to differing loading regimes.

2) Gene expression of the cells, especially inflammatory factors, secretion of ECM components and the calcium metabolism of VICs, under physiological and over load conditions.

Other areas for future work may include

1) Possible correlations between the regional distribution of strain and the areas at risk of calcification.

2) The role of GAGs in other valves, such as the PV or MV.

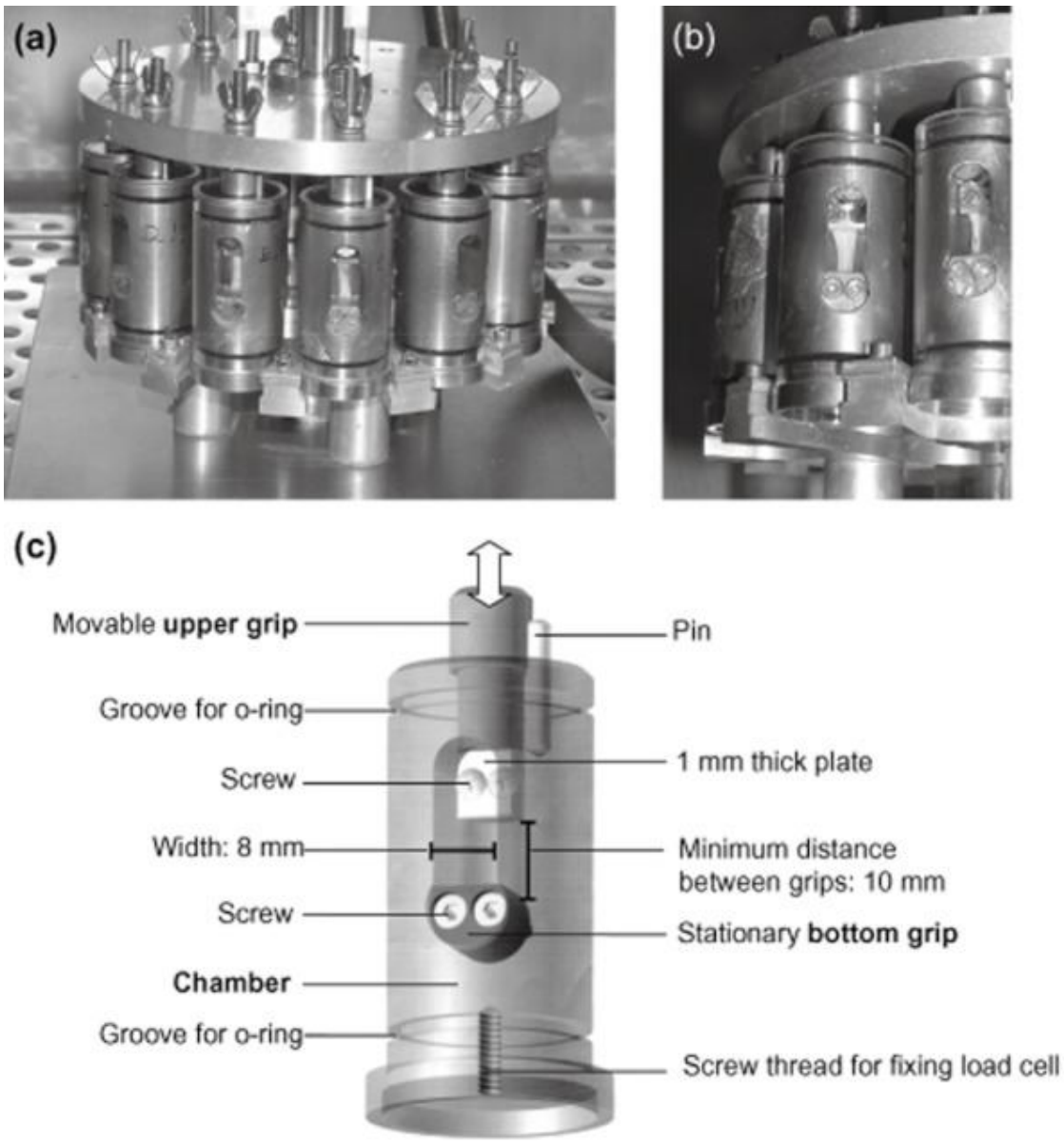

Fig.7- 1. (a) Complete straining system; (b) close up of an individual loading chamber; (c) drawing of the loading chamber highlighting the components.

From a broader perspective, on ultimate goal of studies investigating structure-function relationships in biological tissues and characterisation of the micromechanical environment within their ECM is to implement the gained knowledge into strategies that would lead to tissue-engineered replicates of the subject tissue. This is further encouraged in the case of AV, as none of the current

valve substitutes, i.e. the prosthetic and bioprosthetic valves, are reliable long-term alternatives to the dysfunctional native valve.

References

[1] Naeije R, Chesler N. Pulmonary Circulation at Exercise. Compr Physiol 2012;2:711-41.

[2] Kluckow M. Low systemic blood flow and pathophysiology of the preterm transitional circulation. Early human development 2005;81:429-37.

[3] Seymour RS, Hargens AR, Pedley TJ. The heart works against gravity. Am J Physiol 1993;265:R715-20.

[4] Misfeld M, Sievers HH. Heart valve macro- and microstructure. Philos Trans R Soc Lond B Biol Sci 2007;362:1421-36.

[5] Sacks MS, Yoganathan AP. Heart valve function: a biomechanical perspective. Philos Trans R Soc Lond B Biol Sci 2007;362:1369-91.

[6] Sacks MS, David Merryman W, Schmidt DE. On the biomechanics of heart valve function. Journal of Biomechanics 2009;42:1804-24.

[7] Yacoub MH, Kilner PJ, Birks EJ, Misfeld M. The aortic outflow and root: a tale of dynamism and crosstalk. Ann Thorac Surg 1999;68:S37-43.

[8] Balguid A, Rubbens MP, Mol A, Bank RA, Bogers AJJC, van Kats JP, et al. The Role of Collagen Cross-Links in Biomechanical Behavior of Human Aortic Heart Valve Leaflets—Relevance for Tissue Engineering. Tissue Engineering 2007;13:1501-11.

[9] Stella JA, Sacks MS. On the Biaxial Mechanical Properties of the Layers of the Aortic Valve Leaflet. Journal of Biomechanical Engineering 2007;129:757.

[10] Yoganathan AP, He Z, Casey Jones S. Fluid mechanics of heart valves. Annu Rev Biomed Eng 2004;6:331-62.

[11] Wells SM, Sacks MS. Effects of fixation pressure on the biaxial mechanical behavior of porcine bioprosthetic heart valves with long-term cyclic loading. Biomaterials 2002;23:2389-99.

[12] Merryman WD, Bieniek PD, Guilak F, Sacks MS. Viscoelastic Properties of the Aortic Valve Interstitial Cell. Journal of Biomechanical Engineering 2009;131:041005.

[13] Thubrikar M, Piepgrass WC, Bosher LP, Nolan SP. The elastic modulus of canine

aortic valve leaflets in vivo and in vitro. Circ Res 1980;47:792-800.

[14] Gundiah N, Kam K, Matthews PB, Guccione J, Dwyer HA, Saloner D, et al. Asymmetric Mechanical Properties of Porcine Aortic Sinuses. The Annals of Thoracic Surgery 2008;85:1631-8.

[15] Ni Leidhin C, Moran S, MacLean A. Cardiac tamponade--still a difficult clinical diagnosis. N Z Med J 2014;127:93-6.

[16] Rangayyan RM, Lehner RJ. Phonocardiogram signal analysis: a review. Crit Rev Biomed Eng 1987;15:211-36.

[17] Vasquez P, Marco MM, Mattsson E, Mandersson B. Application of the Empirical Mode Decomposition in the study of murmurs from Arteriovenous fistula stenosis. Conf Proc IEEE Eng Med Biol Soc 2010;2010:947-50.

[18] Arjunon S, Rathan S, Jo H, Yoganathan AP. Aortic valve: mechanical environment and mechanobiology. Ann Biomed Eng 2013;41:1331-46.

[19] Chester AH, El-Hamamsy I, Butcher JT, Latif N, Bertazzo S, Yacoub MH. The living aortic valve: From molecules to function. Glob Cardiol Sci Pract 2014;2014:52-77.

[20] Hurle JM, Colvee E, Fernandezteran MA. The Surface Anatomy of the Human Aortic-Valve as Revealed by Scanning Electron-Microscopy. Anat Embryol 1985;172:61-7.

[21] Butcher JT, Penrod AM, Garcia AJ, Nerem RM. Unique morphology and focal adhesion development of valvular endothelial cells in static and fluid flow environments. Arterioscler Thromb Vasc Biol 2004;24:1429-34.

[22] Deck JD. Endothelial cell orientation on aortic valve leaflets. Cardiovascular research 1986;20:760-7.

[23] Cheung WY, Young EW, Simmons CA. Techniques for isolating and purifying porcine aortic valve endothelial cells. J Heart Valve Dis 2008;17:674-81.

[24] Johnson DL, Rose ML, Yacoub MH. Immunogenicity of human heart valve endothelial cells and fibroblasts. Transplantation proceedings 1997;29:984-5.

[25] Davies PF, Passerini AG, Simmons CA. Aortic valve: turning over a new leaf(let) in endothelial phenotypic heterogeneity. Arterioscler Thromb Vasc Biol 2004;24:1331-3.

[26] Farivar RS, Filsoufi F, Adams DH. Mechanisms of Gal alpha 1-3Gal beta

1-4GlcNAc-R (alpha Gal) expression on porcine valve endothelial cells. J Thorac Cardiov Sur 2003;125:306-14.

[27] Poggianti E, Venneri L, Chubuchny V, Jambrik Z, Baroncini LA, Picano E. Aortic valve sclerosis is associated with systemic endothelial dysfunction. Journal of the American College of Cardiology 2003;41:136-41.

[28] Muller AM, Cronen C, Kupferwasser LI, Oelert H, Muller KM, Kirkpatrick CJ. Expression of endothelial cell adhesion molecules on heart valves: up-regulation in degeneration as well as acute endocarditis. J Pathol 2000;191:54-60.

[29] O'Brien KD. Pathogenesis of calcific aortic valve disease: a disease process comes of age (and a good deal more). Arterioscler Thromb Vasc Biol 2006;26:1721-8.

[30] O'Brien KD, Reichenbach DD, Marcovina SM, Kuusisto J, Alpers CE, Otto CM. Apolipoproteins B, (a), and E accumulate in the morphologically early lesion of 'degenerative' valvular aortic stenosis. Arterioscler Thromb Vasc Biol 1996;16:523-32.

[31] Nicosia MA, Cochran RP, Einstein DR, Rutland CJ, Kunzelman KS. A coupled fluid-structure finite element model of the aortic valve and root. Journal of Heart Valve Disease 2003;12:781-9.

[32] Yip CYY, Simmons CA. The aortic valve microenvironment and its role in calcific aortic valve disease. Cardiovascular Pathology 2011;20:177-82.

[33] Weinberg EJ, Mack PJ, Schoen FJ, Garcia-Cardena G, Kaazempur Mofrad MR. Hemodynamic environments from opposing sides of human aortic valve leaflets evoke distinct endothelial phenotypes in vitro. Cardiovascular engineering 2010;10:5-11.

[34] Balachandran K, Sucosky P, Yoganathan AP. Hemodynamics and mechanobiology of aortic valve inflammation and calcification. Int J Inflam 2011;2011:263870.

[35] Yap CH, Saikrishnan N, Tamilselvan G, Yoganathan AP. Experimental measurement of dynamic fluid shear stress on the aortic surface of the aortic valve leaflet. Biomech Model Mechanobiol 2012;11:171-82.

[36] Yap CH, Saikrishnan N, Yoganathan AP. Experimental measurement of dynamic fluid shear stress on the ventricular surface of the aortic valve leaflet. Biomech Model Mechan 2012;11:231-44.

[37] Sucosky P, Balachandran K, Elhammali A, Jo H, Yoganathan AP. Altered shear stress stimulates upregulation of endothelial VCAM-1 and ICAM-1 in a BMP-4- and TGF-beta1-dependent pathway. Arterioscler Thromb Vasc Biol 2009;29:254-60.

[38] Bischoff J, Aikawa E. Progenitor cells confer plasticity to cardiac valve endothelium. J Cardiovasc Transl Res 2011;4:710-9.

[39] Pahakis MY, Kosky JR, Dull RO, Tarbell JM. The role of endothelial glycocalyx components in mechanotransduction of fluid shear stress. Biochem Biophys Res Commun 2007;355:228-33.

[40] Latif N, Sarathchandra P, Taylor PM, Antoniw J, Brand N, Yacoub MH. Characterization of molecules mediating cell-cell communication in human cardiac valve interstitial cells. Cell biochemistry and biophysics 2006;45:255-64.

[41] Taylor PM, Batten P, Brand NJ, Thomas PS, Yacoub MH. The cardiac valve interstitial cell. The international journal of biochemistry & cell biology 2003;35:113-8.

[42] Filip DA, Radu A, Simionescu M. Interstitial cells of the heart valves possess characteristics similar to smooth muscle cells. Circ Res 1986;59:310-20.

[43] Mulholland DL, Gotlieb AI. Cell biology of valvular interstitial cells. Can J Cardiol 1996;12:231-6.

[44] Della Rocca F, Sartore S, Guidolin D, Bertiplaglia B, Gerosa G, Casarotto D, et al. Cell composition of the human pulmonary valve: a comparative study with the aortic valve--the VESALIO Project. Vitalitate Exornatum Succedaneum Aorticum labore Ingegnoso Obtinebitur. Ann Thorac Surg 2000;70:1594-600.

[45] Rabkin-Aikawa E, Farber M, Aikawa M, Schoen FJ. Dynamic and reversible changes of interstitial cell phenotype during remodeling of cardiac valves. The Journal of heart valve disease 2004;13:841-7.

[46] Liu AC, Joag VR, Gotlieb AI. The emerging role of valve interstitial cell phenotypes in regulating heart valve pathobiology. Am J Pathol 2007;171:1407-18.

[47] Bairati A, DeBiasi S. Presence of a smooth muscle system in aortic valve leaflets. Anat Embryol (Berl) 1981;161:329-40.

[48] Butcher JT, Simmons CA, Warnock JN. Mechanobiology of the aortic heart valve.

J Heart Valve Dis 2008;17:62-73.

[49] Simmons CA, Grant GR, Manduchi E, Davies PF. Spatial heterogeneity of endothelial phenotypes correlates with side-specific vulnerability to calcification in normal porcine aortic valves. Circ Res 2005;96:792-9.

[50] Masters KS, Shah DN, Leinwand LA, Anseth KS. Crosslinked hyaluronan scaffolds as a biologically active carrier for valvular interstitial cells. Biomaterials 2005;26:2517-25.

[51] Messier RH, Bass BL, Aly HM, Jones JL, Domkowski PW, Wallace RB, et al. Dual Structural and Functional Phenotypes of the Porcine Aortic-Valve Interstitial Population - Characteristics of the Leaflet Myofibroblast. Journal of Surgical Research 1994;57:1-21.

[52] Gupta V, Grande-Allen KJ. Effects of static and cyclic loading in regulating extracellular matrix synthesis by cardiovascular cells. Cardiovascular research 2006;72:375-83.

[53] Leask RL, Jain N, Butany J. Endothelium and valvular diseases of the heart. Microsc Res Tech 2003;60:129-37.

[54] Sacks MS, Schoen FJ, Mayer JE. Bioengineering Challenges for Heart Valve Tissue Engineering. Annual Review of Biomedical Engineering 2009;11:289-313.

[55] Enser M, Avery NC. Mechanical and chemical properties of the skin and its collagen from lean and obese-hyperglycaemic (ob/ob) mice. Diabetologia 1984;27:44-9.

[56] Jor JW, Nielsen PM, Nash MP, Hunter PJ. Modelling collagen fibre orientation in porcine skin based upon confocal laser scanning microscopy. Skin research and technology : official journal of International Society for Bioengineering and the Skin 2011;17:149-59.

[57] Turner CH, Burr DB. Orientation of collagen in osteonal bone. Calcified tissue international 1997;60:90.

[58] Ignatius A, Blessing H, Liedert A, Schmidt C, Neidlinger-Wilke C, Kaspar D, et al. Tissue engineering of bone: effects of mechanical strain on osteoblastic cells in type I collagen matrices. Biomaterials 2005;26:311-8.

[59] Kjaer M, Langberg H, Heinemeier K, Bayer ML, Hansen M, Holm L, et al. From mechanical loading to collagen synthesis, structural changes and function in human tendon. Scandinavian journal of medicine & science in sports 2009;19:500-10.

[60] Silver FH, Freeman JW, Seehra GP. Collagen self-assembly and the development of tendon mechanical properties. J Biomech 2003;36:1529-53.

[61] Silver FH, Christiansen DL, Snowhill PB, Chen Y. Role of storage on changes in the mechanical properties of tendon and self-assembled collagen fibers. Connective tissue research 2000;41:155-64.

[62] Yamamoto E, Hayashi K, Yamamoto N. Mechanical properties of collagen fascicles from the rabbit patellar tendon. J Biomech Eng 1999;121:124-31.

[63] Klein JA, Hukins DW. Collagen fibre orientation in the annulus fibrosus of intervertebral disc during bending and torsion measured by x-ray diffraction. Biochim Biophys Acta 1982;719:98-101.

[64] Berthet-Colominas C, Miller A, Herbage D, Ronziere MC, Tocchetti D. Structural studies of collagen fibres from intervertebral disc. Biochim Biophys Acta 1982;706:50-64.

[65] Wan C, Hao Z, Wen S, Leng H. A quantitative study of the relationship between the distribution of different types of collagen and the mechanical behavior of rabbit medial collateral ligaments. PLoS One 2014;9:e103363.

[66] Amiel D, Nimni ME. The collagen in normal ligaments. The Iowa orthopaedic journal 1993;13:49-55.

[67] Cheheltani R, McGoverin CM, Rao J, Vorp DA, Kiani MF, Pleshko N. Fourier transform infrared spectroscopy to quantify collagen and elastin in an in vitro model of extracellular matrix degradation in aorta. The Analyst 2014;139:3039-47.

[68] Koch RG, Tsamis A, D'Amore A, Wagner WR, Watkins SC, Gleason TG, et al. A custom image-based analysis tool for quantifying elastin and collagen micro-architecture in the wall of the human aorta from multi-photon microscopy. J Biomech 2014;47:935-43.

[69] Dahiya R, Ganguly NK, Majumdar S, Chakravarti RN. Collagen types in normal and atherosclerotic human aorta. Indian heart journal 1983;35:326-8.

[70] Schmut O. The organization of tissues of the eye by different collagen types. Albrecht von Graefes Archiv fur klinische und experimentelle Ophthalmologie Albrecht von Graefe's archive for clinical and experimental ophthalmology 1978;207:189-99.

[71] Collins D, Lindberg K, McLees B, Pinnell S. The collagen of heart valve. Biochim Biophys Acta 1977;495:129-39.

[72] Handler CE, Child A, Light ND, Dorrance DE. Mitral valve prolapse, aortic compliance, and skin collagen in joint hypermobility syndrome. British heart journal 1985;54:501-8.

[73] Kastelic J, Galeski A, Baer E. The multicomposite structure of tendon. Connective tissue research 1978;6:11-23.

[74] Coward LA, Sun R. Hierarchical approaches to understanding consciousness. Neural networks : the official journal of the International Neural Network Society 2007;20:947-54.

[75] Jesudason R, Sato S, Parameswaran H, Araujo AD, Majumdar A, Allen PG, et al. Mechanical forces regulate elastase activity and binding site availability in lung elastin. Biophysical journal 2010;99:3076-83.

[76] Schellenberg JC, Liggins GC, Kitterman JA, Lee CC. Elastin and collagen in the fetal sheep lung. II. Relationship to mechanical properties of the lung. Pediatric research 1987;22:339-43.

[77] Pierce JA, Resnick H, Henry PH. Collagen and elastin metabolism in the lungs, skin, and bones of adult rats. The Journal of laboratory and clinical medicine 1967;69:485-93.

[78] Mikawa Y, Hamagami H, Shikata J, Yamamuro T. Elastin in the human intervertebral disk. A histological and biochemical study comparing it with elastin in the human yellow ligament. Archives of orthopaedic and traumatic surgery Archiv fur orthopadische und Unfall-Chirurgie 1986;105:343-9.

[79] Oxlund H, Manschot J, Viidik A. The role of elastin in the mechanical properties of skin. J Biomech 1988;21:213-8.

[80] Tavis MJ, Thornton JW, Harney JH, Danet RT, Woodroof EA, Bartlett RH.

Mechanism of skin graft adherence: collagen, elastin, and fibrin interactions. Surgical forum 1977;28:522-4.

[81] Jiang X, Luttrell I, Li DY, Yang CC, Chitaley K. Altered bladder function in elastin-deficient mice at baseline and in response to partial bladder outlet obstruction. BJU international 2012;110:413-9.

[82] Murakumo M, Ushiki T, Abe K, Matsumura K, Shinno Y, Koyanagi T. Three-dimensional arrangement of collagen and elastin fibers in the human urinary bladder: a scanning electron microscopic study. The Journal of urology 1995;154:251-6.

[83] Kim KM, Kogan BA, Massad CA, Huang YC. Collagen and elastin in the obstructed fetal bladder. The Journal of urology 1991;146:528-31.

[84] Lillie MA, Gosline JM. Mechanical properties of elastin along the thoracic aorta in the pig. J Biomech 2007;40:2214-21.

[85] Sherebrin MH, Song SH, Roach MR. Mechanical anisotropy of purified elastin from the thoracic aorta of dog and sheep. Canadian journal of physiology and pharmacology 1983;61:539-45.

[86] Schliwa M. Guidebook to the Extracellular-Matrix and Adhesion Proteins - Kreis,T, Vale,R. Nature 1994;367:32-.

[87] Scott M, Vesely I. Aortic valve cusp microstructure: the role of elastin. The Annals of Thoracic Surgery 1995;60:S391-4.

[88] Tseng H, Grande-Allen KJ. Elastic fibers in the aortic valve spongiosa: A fresh perspective on its structure and role in overall tissue function. Acta Biomaterialia 2011;7:2101-8.

[89] Vesely I. The role of elastin in aortic valve mechanics. Journal of Biomechanics 1998;31:115-23.

[90] Vesely I, Noseworthy R. Micromechanics of the fibrosa and the ventricularis in aortic valve leaflets. J Biomech 1992;25:101-13.

[91] Vesely I, Lozon A. Natural preload of aortic valve leaflet components during glutaraldehyde fixation: effects on tissue mechanics. J Biomech 1993;26:121-31.

[92] Lee TC, Midura RJ, Hascall VC, Vesely I. The effect of elastin damage on the

mechanics of the aortic valve. J Biomech 2001;34:203-10.

[93] Martin RB, Lau ST, Mathews PV, Gibson VA, Stover SM. Collagen fiber organization is related to mechanical properties and remodeling in equine bone. A comparison of two methods. J Biomech 1996;29:1515-21.

[94] Schoen FJ. Aortic valve structure-function correlations: role of elastic fibers no longer a stretch of the imagination. J Heart Valve Dis 1997;6:1-6.

[95] Grande-Allen KJ, Osman N, Ballinger ML, Dadlani H, Marasco S, Little PJ. Glycosaminoglycan synthesis and structure as targets for the prevention of calcific aortic valve disease. Cardiovascular research 2007;76:19-28.

[96] Prydz K, Dalen KT. Synthesis and sorting of proteoglycans. Journal of cell science 2000;113 Pt 2:193-205.

[97] Vesely I. Heart valve tissue engineering. Circulation Research 2005;97:743-55.

[98] Anssari-Benam A, Bader DL, Screen HR. Anisotropic time-dependant behaviour of the aortic valve. J Mech Behav Biomed Mater 2011;4:1603-10.

[99] Anssari-Benam A, Bader DL, Screen HR. A combined experimental and modelling approach to aortic valve viscoelasticity in tensile deformation. J Mater Sci Mater Med 2011;22:253-62.

[100] Weiler M, Hwai Yap C, Balachandran K, Padala M, Yoganathan AP. Regional analysis of dynamic deformation characteristics of native aortic valve leaflets. Journal of Biomechanics 2011;44:1459-65.

[101] Stephens EH, Chu CK, Grande-Allen KJ. Valve proteoglycan content and glycosaminoglycan fine structure are unique to microstructure, mechanical load and age: Relevance to an age-specific tissue-engineered heart valve. Acta Biomater 2008;4:1148-60.

[102] Latif N, Sarathchandra P, Taylor PM, Antoniw J, Yacoub MH. Localization and pattern of expression of extracellular matrix components in human heart valves. J Heart Valve Dis 2005;14:218-27.

[103] Eriksen HA, Satta J, Risteli J, Veijola M, Vare P, Soini Y. Type I and type III collagen synthesis and composition in the valve matrix in aortic valve stenosis. Atherosclerosis 2006;189:91-8.

[104] Eckert CE, Fan R, Mikulis B, Barron M, Carruthers CA, Friebe VM, et al. On the biomechanical role of glycosaminoglycans in the aortic heart valve leaflet. Acta Biomater 2013;9:4653-60.

[105] Mol A, Bouten CVC, Baaijens FPT, Zund G, Turina MI, Hoerstrup SP. Tissue engineering of semilunar heart valves: current status and future developments. The Journal of heart valve disease 2004;13:272-80.

[106] Hasan A, Ragaert K, Swieszkowski W, Selimovic S, Paul A, Camci-Unal G, et al. Biomechanical properties of native and tissue engineered heart valve constructs. J Biomech 2014;47:1949-63.

[107] Vesely I. Heart valve tissue engineering. Circ Res 2005;97:743-55.

[108] Borghi A, New SE, Chester AH, Taylor PM, Yacoub MH. Time-dependent mechanical properties of aortic valve cusps: effect of glycosaminoglycan depletion. Acta Biomater 2013;9:4645-52.

[109] Sacks MS, Schoen FJ, Mayer JE. Bioengineering challenges for heart valve tissue engineering. Annu Rev Biomed Eng 2009;11:289-313.

[110] Schenke-Layland K, Riemann I, Opitz F, Konig K, Halbhuber KJ, Stock UA. Comparative study of cellular and extracellular matrix composition of native and tissue engineered heart valves. Matrix Biol 2004;23:113-25.

[111] Luckhaupt SE, Calvert GM. Prevalence of coronary heart disease or stroke among workers aged <55 years--United States, 2008-2012. MMWR Morb Mortal Wkly Rep 2014;63:645-9.

[112] Otto CM, Prendergast B. Aortic-valve stenosis--from patients at risk to severe valve obstruction. N Engl J Med 2014;371:744-56.

[113] Go AS, Mozaffarian D, Roger VL, Benjamin EJ, Berry JD, Blaha MJ, et al. Heart disease and stroke statistics--2014 update: a report from the American Heart Association. Circulation 2014;129:e28-e292.

[114] Iung B, Vahanian A. Epidemiology of acquired valvular heart disease. Can J Cardiol 2014;30:962-70.

[115] Siu SC, Silversides CK. Bicuspid aortic valve disease. J Am Coll Cardiol 2010;55:2789-800.

[116] Yuan SM, Jing H. The bicuspid aortic valve and related disorders. Sao Paulo Med J 2010;128:296-301.

[117] Karp N, Grosse-Wortmann L, Bowdin S. Severe aortic stenosis, bicuspid aortic valve and atrial septal defect in a child with Joubert Syndrome and Related Disorders (JSRD) - a case report and review of congenital heart defects reported in the human ciliopathies. Eur J Med Genet 2012;55:605-10.

[118] Ait-Ali L, Foffa I, Festa P, Graziaandreassi M. [Bicuspid aortic valve: epidemiology, genetics and clinics]. Recenti Prog Med 2012;103:589-95.

[119] Lawrie GM. Role of transcatheter aortic valve implantation (TAVI) versus conventional aortic valve replacement in the treatment of aortic valve disease. Methodist Debakey Cardiovasc J 2012;8:4-8.

[120] De Mozzi P, Longo UG, Galanti G, Maffulli N. Bicuspid aortic valve: a literature review and its impact on sport activity. Br Med Bull 2008;85:63-85.

[121] Ward C. Clinical significance of the bicuspid aortic valve. Heart 2000;83:81-5.

[122] Bowler MA, Merryman WD. In vitro models of aortic valve calcification: solidifying a system. Cardiovasc Pathol 2014.

[123] David Merryman W. Mechano-potential etiologies of aortic valve disease. J Biomech 2010;43:87-92.

[124] Roberts WC, Ko JM. Frequency by decades of unicuspid, bicuspid, and tricuspid aortic valves in adults having isolated aortic valve replacement for aortic stenosis, with or without associated aortic regurgitation. Circulation 2005;111:920-5.

[125] Rocha SM, Moura LM, Rocha-Goncalves F. [Bicuspid aortic valve and aortic disease: past, present and future]. Rev Port Cardiol 2010;29:1727-36.

[126] Nishimura RA. Cardiology patient pages. Aortic valve disease. Circulation 2002;106:770-2.

[127] Mathieu P, Boulanger MC. Basic Mechanisms of Calcific Aortic Valve Disease. Canadian Journal of Cardiology 2014;30:982-93.

[128] El-Hamamsy I, Balachandran K, Yacoub MH, Stevens LM, Sarathchandra P, Taylor PM, et al. Endothelium-dependent regulation of the mechanical properties of aortic valve cusps. J Am Coll Cardiol 2009;53:1448-55.

[129] Li C, Xu S, Gotlieb AI. The progression of calcific aortic valve disease through injury, cell dysfunction, and disruptive biologic and physical force feedback loops. Cardiovascular pathology : the official journal of the Society for Cardiovascular Pathology 2013;22:1-8.

[130] Schoen FJ, Levy RJ. Calcification of tissue heart valve substitutes: Progress toward understanding and prevention. Annals of Thoracic Surgery 2005;79:1072-80.

[131] Cloyd KL, El-Hamamsy I, Boonrungsiman S, Hedegaard M, Gentleman E, Sarathchandra P, et al. Characterization of porcine aortic valvular interstitial cell 'calcified' nodules. PLoS One 2012;7:e48154.

[132] Mohler ER, 3rd, Gannon F, Reynolds C, Zimmerman R, Keane MG, Kaplan FS. Bone formation and inflammation in cardiac valves. Circulation 2001;103:1522-8.

[133] Guerraty M, Mohler Iii ER. Models of aortic valve calcification. J Investig Med 2007;55:278-83.

[134] Rajamannan NM, Subramaniam M, Rickard D, Stock SR, Donovan J, Springett M, et al. Human aortic valve calcification is associated with an osteoblast phenotype. Circulation 2003;107:2181-4.

[135] Mahler GJ, Farrar EJ, Butcher JT. Inflammatory cytokines promote mesenchymal transformation in embryonic and adult valve endothelial cells. Arterioscler Thromb Vasc Biol 2013;33:121-30.

[136] Nadlonek NA, Lee JH, Weyant MJ, Meng X, Fullerton DA. ox-LDL induces PiT-1 expression in human aortic valve interstitial cells. J Surg Res 2013;184:6-9.

[137] Linefsky JP, O'Brien KD, Katz R, de Boer IH, Barasch E, Jenny NS, et al. Association of serum phosphate levels with aortic valve sclerosis and annular calcification: the cardiovascular health study. J Am Coll Cardiol 2011;58:291-7.

[138] Cote N, El Husseini D, Pepin A, Guauque-Olarte S, Ducharme V, Bouchard-Cannon P, et al. ATP acts as a survival signal and prevents the mineralization of aortic valve. J Mol Cell Cardiol 2012;52:1191-202.

[139] Hutcheson JD, Chen J, Sewell-Loftin MK, Ryzhova LM, Fisher CI, Su YR, et al. Cadherin-11 regulates cell-cell tension necessary for calcific nodule formation by valvular myofibroblasts. Arterioscler Thromb Vasc Biol 2013;33:114-20.

[140] Pibarot P, Dumesnil JG. Prosthetic heart valves: selection of the optimal prosthesis and long-term management. Circulation 2009;119:1034-48.

[141] Singhal P, Luk A, Butany J. Bioprosthetic Heart Valves: Impact of Implantation on Biomaterials. ISRN Biomaterials 2013;2013:14.

[142] Tillquist MN, Maddox TM. Cardiac crossroads: deciding between mechanical or bioprosthetic heart valve replacement. Patient Prefer Adherence 2011;5:91-9.

[143] Rippel RA, Ghanbari H, Seifalian AM. Tissue-engineered heart valve: future of cardiac surgery. World J Surg 2012;36:1581-91.

[144] Kim WG, Park JK, Lee WY. Tissue-engineered heart valve leaflets: an effective method of obtaining acellularized valve xenografts. Int J Artif Organs 2002;25:791-7.

[145] Dube J, Bourget JM, Gauvin R, Lafrance H, Roberge CJ, Auger FA, et al. Progress in developing a living human tissue-engineered tri-leaflet heart valve assembled from tissue produced by the self-assembly approach. Acta Biomater 2014;10:3563-70.

[146] Morsi YS. Bioengineering strategies for polymeric scaffold for tissue engineering an aortic heart valve: an update. Int J Artif Organs 2014;37:651-67.

[147] Hutcheson JD, Aikawa E, Merryman WD. Potential drug targets for calcific aortic valve disease. Nat Rev Cardiol 2014;11:218-31.

[148] Xing Y, Warnock JN, He Z, Hilbert SL, Yoganathan AP. Cyclic pressure affects the biological properties of porcine aortic valve leaflets in a magnitude and frequency dependent manner. Ann Biomed Eng 2004;32:1461-70.

[149] Xing Y, He Z, Warnock JN, Hilbert SL, Yoganathan AP. Effects of constant static pressure on the biological properties of porcine aortic valve leaflets. Ann Biomed Eng 2004;32:555-62.

[150] Haerten K, Dohn G, Dohn V, Seipel L, Loogen F. [Natural history of patients with severe aortic valve disease under medical therapy (author's transl)]. Z Kardiol 1980;69:757-62.

[151] Sun L, Rajamannan NM, Sucosky P. Defining the role of fluid shear stress in the expression of early signaling markers for calcific aortic valve disease. PLoS One 2013;8:e84433.

[152] Hoehn D, Sun L, Sucosky P. Role of Pathologic Shear Stress Alterations in Aortic

Valve Endothelial Activation. Cardiovasc Eng Tech 2010;1:165-78.

[153] David Merryman W, Shadow Huang H-Y, Schoen FJ, Sacks MS. The effects of cellular contraction on aortic valve leaflet flexural stiffness. Journal of Biomechanics 2006;39:88-96.

[154] Corden J, David T, Fisher J. In vitro determination of the curvatures and bending strains acting on the leaflets of polyurethane trileaflet heart valves during leaflet motion. Proc Inst Mech Eng H 1995;209:243-53.

[155] Lewinsohn AD, Anssari-Benham A, Lee DA, Taylor PM, Chester AH, Yacoub MH, et al. Anisotropic strain transfer through the aortic valve and its relevance to the cellular mechanical environment. Proceedings of the Institution of Mechanical Engineers, Part H: Journal of Engineering in Medicine 2011;225:821-30.

[156] Gould RA, Chin K, Santisakultarm TP, Dropkin A, Richards JM, Schaffer CB, et al. Cyclic strain anisotropy regulates valvular interstitial cell phenotype and tissue remodeling in three-dimensional culture. Acta Biomater 2012;8:1710-9.

[157] Thubrikar MJ, Aouad J, Nolan SP. Patterns of Calcific Deposits in Operatively Excised Stenotic or Purely Regurgitant Aortic Valves and Their Relation to Mechanical-Stress. American Journal of Cardiology 1986;58:304-8.

[158] Otto CM, Kuusisto J, Reichenbach DD, Gown AM, O'Brien KD. Characterization of the early lesion of 'degenerative' valvular aortic stenosis. Histological and immunohistochemical studies. Circulation 1994;90:844-53.

[159] Martin C, Pham T, Sun W. Significant differences in the material properties between aged human and porcine aortic tissues. European Journal of Cardio-Thoracic Surgery 2011;40:28-34.

[160] Balachandran K, Bakay MA, Connolly JM, Zhang X, Yoganathan AP, Levy RJ. Aortic Valve Cyclic Stretch Causes Increased Remodeling Activity and Enhanced Serotonin Receptor Responsiveness. The Annals of Thoracic Surgery 2011;92:147-53.

[161] Balachandran K, Konduri S, Sucosky P, Jo H, Yoganathan AP. An Ex Vivo Study of the Biological Properties of Porcine Aortic Valves in Response to Circumferential Cyclic Stretch. Annals of Biomedical Engineering 2006;34:1655-65.

[162] Billiar KL, Sacks MS. Biaxial Mechanical Properties of the Native and

Glutaraldehyde-Treated Aortic Valve Cusp: Part II---A Structural Constitutive Model. Journal of Biomechanical Engineering 2000;122:327-35.

[163] Mirnajafi A, Raymer JM, McClure LR, Sacks MS. The flexural rigidity of the aortic valve leaflet in the commissural region. J Biomech 2006;39:2966-73.

[164] Stella JA, Liao J, Sacks MS. Time-dependent biaxial mechanical behavior of the aortic heart valve leaflet. J Biomech 2007;40:3169-77.

[165] Rousseau EP, Sauren AA, van Hout MC, van Steenhoven AA. Elastic and viscoelastic material behaviour of fresh and glutaraldehyde-treated porcine aortic valve tissue. J Biomech 1983;16:339-48.

[166] Sauren AA, van Hout MC, van Steenhoven AA, Veldpaus FE, Janssen JD. The mechanical properties of porcine aortic valve tissues. J Biomech 1983;16:327-37.

[167] Jiao T, Clifton RJ, Converse GL, Hopkins RA. Measurements of the effects of decellularization on viscoelastic properties of tissues in ovine, baboon, and human heart valves. Tissue Eng Part A 2012;18:423-31.

[168] Hoerstrup SP, Sodian R, Daebritz S, Wang J, Bacha EA, Martin DP, et al. Functional living trileaflet heart valves grown in vitro. Circulation 2000;102:III44-9.

[169] White JF, Werkmeister JA, Hilbert SL, Ramshaw JAM. Heart valve collagens: cross-species comparison using immunohistological methods. The Journal of heart valve disease 2010;19:766-71.

[170] Aldous IG, Veres SP, Jahangir A, Lee JM. Differences in collagen cross-linking between the four valves of the bovine heart: a possible role in adaptation to mechanical fatigue. American journal of physiology Heart and circulatory physiology 2009;296:H1898-906.

[171] Grashow JS, Yoganathan AP, Sacks MS. Biaixal stress-stretch behavior of the mitral valve anterior leaflet at physiologic strain rates. Annals of Biomedical Engineering 2006;34:315-25.

[172] Mavrilas D, Missirlis Y. An approach to the optimization of preparation of bioprosthetic heart valves. J Biomech 1991;24:331-9.

[173] Clark RE. Stress-strain characteristics of fresh and frozen human aortic and mitral leaflets and chordae tendineae. Implications for clinical use. J Thorac

Cardiovasc Surg 1973;66:202-8.

[174] Missirlis YF, Chong M. Aortic valve mechanics--Part I: material properties of natural porcine aortic valves. J Bioeng 1978;2:287-300.

[175] Stradins P, Lacis R, Ozolanta I, Purina B, Ose V, Feldmane L, et al. Comparison of biomechanical and structural properties between human aortic and pulmonary valve. European journal of cardio-thoracic surgery : official journal of the European Association for Cardio-thoracic Surgery 2004;26:634-9.

[176] Sun W, Sacks MS, Scott MJ. Effects of Boundary Conditions on the Estimation of the Planar Biaxial Mechanical Properties of Soft Tissues. Journal of Biomechanical Engineering 2005;127:709.

[177] Sacks M. Biaxial Mechanical Evaluation of Planar Biological Materials. Journal of Elasticity 2000;61:199-246.

[178] Sacks MS. A Method for Planar Biaxial Mechanical Testing That Includes In-Plane Shear. Journal of Biomechanical Engineering 1999;121:551-5.

[179] Waldman SD, Michael Lee J. Boundary conditions during biaxial testing of planar connective tissues. Part 1: Dynamic Behavior. Journal of Materials Science: Materials in Medicine 2002;13:933-8.

[180] Waldman SD, Sacks MS, Lee JM. Boundary conditions during biaxial testing of planar connective tissues Part II :Fiber orientation. Journal of Materials Science Letters 2002;21:1215-21.

[181] Christie GW, Barratt-Boyes BG. Mechanical properties of porcine pulmonary valve leaflets: how do they differ from aortic leaflets? Ann Thorac Surg 1995;60:S195-9.

[182] Christie GW, Barratt-Boyes BG. Age-dependent changes in the radial stretch of human aortic valve leaflets determined by biaxial testing. Ann Thorac Surg 1995;60:S156-8; discussion S9.

[183] Christie GW, Barratt-Boyes BG. Biaxial mechanical properties of explanted aortic allograft leaflets. Ann Thorac Surg 1995;60:S160-4.

[184] Billiar KL, Sacks MS. Biaxial mechanical properties of the natural and glutaraldehyde treated aortic valve cusp--Part I: Experimental results. J Biomech Eng

2000;122:23-30.

[185] Chong M, Eng M, Missirlis YF. Aortic valve mechanics. Part II: a stress analysis of the porcine aortic valve leaflets in diastole. Biomaterials, medical devices, and artificial organs 1978;6:225-44.

[186] Gloeckner DC, Billiar KL, Sacks MS. Effects of mechanical fatigue on the bending properties of the porcine bioprosthetic heart valve. ASAIO J 1999;45:59-63.

[187] Thubrikar M, Piepgrass WC, Deck JD, Nolan SP. Stresses of Natural Versus Prosthetic Aortic-Valve Leaflets Invivo. Annals of Thoracic Surgery 1980;30:230-9.

[188] Vesely I, Boughner D. Analysis of the bending behaviour of porcine xenograft leaflets and of natural aortic valve material: bending stiffness, neutral axis and shear measurements. Journal of Biomechanics 1989;22:655-71.

[189] Ragaert K, De Somer F, Somers P, De Baere I, Cardon L, Degrieck J. Flexural mechanical properties of porcine aortic heart valve leaflets. J Mech Behav Biomed Mater 2012;13:78-84.

[190] Sauren AA, Rousseau EP. A concise sensitivity analysis of the quasi-linear viscoelastic model proposed by Fung. J Biomech Eng 1983;105:92-5.

[191] Doehring TC, Carew EO, Vesely I. The effect of strain rate on the viscoelastic response of aortic valve tissue: a direct-fit approach. Ann Biomed Eng 2004;32:223-32.

[192] Carew EO, Garg A, Barber JE, Vesely I. Stress relaxation preconditioning of porcine aortic valves. Ann Biomed Eng 2004;32:563-72.

[193] Robinson PS, Tranquillo RT. Planar biaxial behavior of fibrin-based tissue-engineered heart valve leaflets. Tissue Eng Part A 2009;15:2763-72.

[194] Anssari-Benam A, Gupta HS, Screen HRC. Strain Transfer Through the Aortic Valve. J Biomech Eng-T Asme 2012;134.

[195] Tseng H, Kim E, Connell P, Ayoub S, Shah J, Grande-Allen KJ. The Tensile and Viscoelastic Properties of Aortic Valve Leaflets Treated with a Hyaluronidase Gradient. Cardiovasc Eng Tech 2013;4:151-60.

[196] Rigozzi S, Muller R, Snedeker JG. Local strain measurement reveals a varied regional dependence of tensile tendon mechanics on glycosaminoglycan content. J

Biomech 2009;42:1547-52.

[197] Thorpe CT, Klemt C, Riley GP, Birch HL, Clegg PD, Screen HRC. Helical sub-structures in energy-storing tendons provide a possible mechanism for efficient energy storage and return. Acta Biomaterialia 2013;9:7948-56.

[198] Cheng VWT, Screen HRC. The micro-structural strain response of tendon. Journal of Materials Science 2007;42:8957-65.

[199] Blakeslee D, Baines MG. Immunofluorescence using dichlorotriazinylaminofluorescein (DTAF). I. Preparation and fractionation of labelled IgG. Journal of immunological methods 1976;13:305-20.

[200] Szczesny SE, Edelstein RS, Elliott DM. DTAF Dye Concentrations Commonly Used to Measure Microscale Deformations in Biological Tissues Alter Tissue Mechanics. PLoS ONE 2014;9:e99588.

[201] Upton ML, Gilchrist CL, Guilak F, Setton LA. Transfer of macroscale tissue strain to microscale cell regions in the deformed meniscus. Biophysical journal 2008;95:2116-24.

[202] Michalek AJ, Buckley MR, Bonassar LJ, Cohen I, Iatridis JC. Measurement of local strains in intervertebral disc anulus fibrosus tissue under dynamic shear: contributions of matrix fiber orientation and elastin content. J Biomech 2009;42:2279-85.

[203] Huyghe JM, Jongeneelen CJ. 3D non-affine finite strains measured in isolated bovine annulus fibrosus tissue samples. Biomech Model Mechanobiol 2012;11:161-70.

[204] Jones CW, Smolinski D, Keogh A, Kirk TB, Zheng MH. Confocal laser scanning microscopy in orthopaedic research. Progress in histochemistry and cytochemistry 2005;40:1-71.

[205] Grande-Allen KJ, Calabro A, Gupta V, Wight TN, Hascall VC, Vesely I. Glycosaminoglycans and proteoglycans in normal mitral valve leaflets and chordae: association with regions of tensile and compressive loading. Glycobiology 2004;14:621-33.

[206] Lovekamp JJ, Simionescu DT, Mercuri JJ, Zubiate B, Sacks MS, Vyavahare NR.

Stability and function of glycosaminoglycans in porcine bioprosthetic heart valves. Biomaterials 2006;27:1507-18.

[207] Hall ML, Krawczak DA, Simha NK, Lewis JL. Effect of dermatan sulfate on the indentation and tensile properties of articular cartilage. Osteoarthritis and cartilage / OARS, Osteoarthritis Research Society 2009;17:655-61.

[208] Henninger HB, Underwood CJ, Ateshian GA, Weiss JA. Effect of sulfated glycosaminoglycan digestion on the transverse permeability of medial collateral ligament. J Biomech 2010;43:2567-73.

[209] Al Jamal R, Roughley PJ, Ludwig MS. Effect of glycosaminoglycan degradation on lung tissue viscoelasticity. American journal of physiology Lung cellular and molecular physiology 2001;280:L306-15.

[210] Lovekamp J, Vyavahare N. Periodate-mediated glycosaminoglycan stabilization in bioprosthetic heart valves. J Biomed Mater Res 2001;56:478-86.

[211] Anssari-Benam A, Bader DL, Screen HRC. A combined experimental and modelling approach to aortic valve viscoelasticity in tensile deformation. Journal of Materials Science: Materials in Medicine 2011;22:253-62.

[212] Garcia Paez JM, Carrera A, Jorge E, Millan I, Cordon A, Rocha A, et al. Hysteresis of a biomaterial: influence of sutures and biological adhesives. J Mater Sci Mater Med 2007;18:715-24.

[213] Grande-Allen KJ, Mako WJ, Calabro A, Shi Y, Ratliff NB, Vesely I. Loss of chondroitin 6-sulfate and hyaluronan from failed porcine bioprosthetic valves. J Biomed Mater Res A 2003;65:251-9.

[214] Talman EA, Boughner DR. Effect of altered hydration on the internal shear properties of porcine aortic valve cusps. Ann Thorac Surg 2001;71:S375-8.

[215] Dainese L, Guarino A, Micheli B, Biagioli V, Polvani G, Maccari F, et al. Aortic valve leaflet glycosaminoglycans composition and modification in severe chronic valve regurgitation. J Heart Valve Dis 2013;22:484-90.

[216] Cribb AM, Scott JE. Tendon response to tensile stress: an ultrastructural investigation of collagen:proteoglycan interactions in stressed tendon. Journal of anatomy 1995;187 (Pt 2):423-8.

[217] Liao J, Vesely I. Skewness angle of interfibrillar proteoglycans increases with applied load on mitral valve chordae tendineae. J Biomech 2007;40:390-8.

[218] Redaelli A, Vesentini S, Soncini M, Vena P, Mantero S, Montevecchi FM. Possible role of decorin glycosaminoglycans in fibril to fibril force transfer in relative mature tendons--a computational study from molecular to microstructural level. J Biomech 2003;36:1555-69.

[219] Lujan TJ, Underwood CJ, Henninger HB, Thompson BM, Weiss JA. Effect of dermatan sulfate glycosaminoglycans on the quasi-static material properties of the human medial collateral ligament. Journal of orthopaedic research : official publication of the Orthopaedic Research Society 2007;25:894-903.

[220] Fessel G, Snedeker JG. Evidence against proteoglycan mediated collagen fibril load transmission and dynamic viscoelasticity in tendon. Matrix Biol 2009;28:503-10.

[221] Marturano JE, Arena JD, Schiller ZA, Georgakoudi I, Kuo CK. Characterization of mechanical and biochemical properties of developing embryonic tendon. Proceedings of the National Academy of Sciences of the United States of America 2013;110:6370-5.

[222] Lujan TJ, Underwood CJ, Jacobs NT, Weiss JA. Contribution of glycosaminoglycans to viscoelastic tensile behavior of human ligament. Journal of applied physiology 2009;106:423-31.

[223] Millesi H, Reihsner R, Hamilton G, Mallinger R, Menzel EJ. Biomechanical properties of normal tendons, normal palmar aponeuroses and palmar aponeuroses from patients with Dupuytren's disease subjected to elastase and chondroitinase treatment. Connective tissue research 1995;31:109-15.

[224] Legerlotz K, Riley GP, Screen HR. GAG depletion increases the stress-relaxation response of tendon fascicles, but does not influence recovery. Acta Biomater 2013;9:6860-6.

[225] Screen HR, Chhaya VH, Greenwald SE, Bader DL, Lee DA, Shelton JC. The influence of swelling and matrix degradation on the microstructural integrity of tendon. Acta Biomater 2006;2:505-13.

[226] Buchanan RM, Sacks MS. Interlayer micromechanics of the aortic heart valve

leaflet. Biomech Model Mechanobiol 2014;13:813-26.

[227] Krishnamurthy VK, Guilak F, Narmoneva DA, Hinton RB. Regional structure–function relationships in mouse aortic valve tissue. Journal of Biomechanics 2011;44:77-83.

[228] Scott JE. Elasticity in extracellular matrix 'shape modules' of tendon, cartilage, etc. A sliding proteoglycan-filament model. The Journal of physiology 2003;553:335-43.

[229] Thorpe CT, Riley GP, Birch HL, Clegg PD, Screen HR. Effect of fatigue loading on structure and functional behaviour of fascicles from energy-storing tendons. Acta Biomater 2014;10:3217-24.

[230] Thorpe CT, Klemt C, Riley GP, Birch HL, Clegg PD, Screen HR. Helical sub-structures in energy-storing tendons provide a possible mechanism for efficient energy storage and return. Acta Biomater 2013;9:7948-56.

[231] Shepherd JH, Riley GP, Screen HR. Early stage fatigue damage occurs in bovine tendon fascicles in the absence of changes in mechanics at either the gross or micro-structural level. J Mech Behav Biomed Mater 2014;38:163-72.

[232] Thorpe CT, Riley GP, Birch HL, Clegg PD, Screen HR. Fascicles from energy-storing tendons show an age-specific response to cyclic fatigue loading. Journal of the Royal Society, Interface / the Royal Society 2014;11:20131058.

[233] Boerboom RA, Driessen NJB, Bouten CVC, Huyghe JM, Baaijens FPT. Finite Element Model of Mechanically Induced Collagen Fiber Synthesis and Degradation in the Aortic Valve. Annals of Biomedical Engineering 2003;31:1040-53.

[234] Driessen NJ, Bouten CV, Baaijens FP. Improved prediction of the collagen fiber architecture in the aortic heart valve. Journal of Biomechanical Engineering 2005;127:329-36.

[235] Tung S-H, Sui C-H. Application of digital-image-correlation techniques in analysing cracked cylindrical pipes. Sadhana 2010;35:557-67.

[236] Caro-Bretelle AS, Gountsop PN, Ienny P, Leger R, Corn S, Bazin I, et al. Effect of sample preservation on stress softening and permanent set of porcine skin. J Biomech 2015.

[237] Kershaw JD, Misfeld M, Sievers HH, Yacoub MH, Chester AH. Specific regional and directional contractile responses of aortic cusp tissue. J Heart Valve Dis 2004;13:798-803.

[238] Screen HR, Lee DA, Bader DL, Shelton JC. Development of a technique to determine strains in tendons using the cell nuclei. Biorheology 2003;40:361-8.

[239] Tung SH, Sui CH. Application of digital-image-correlation techniques in analysing cracked cylindrical pipes. Sadhana 2010;35:557-67.

[240] Basappa, Rangappa KS, Sugahara K. Roles of glycosaminoglycans and glycanmimetics in tumor progression and metastasis. Glycoconjugate journal 2014;31:461-7.

[241] Vesely I, Boughner D. Analysis of the bending behaviour of porcine xenograft leaflets and of natural aortic valve material: bending stiffness, neutral axis and shear measurements. J Biomech 1989;22:655-71.

[242] Talman EA, Boughner DR. Internal shear properties of fresh porcine aortic valve cusps: Implications for normal valve function. Journal of Heart Valve Disease 1996;5:152-9.

[243] Thubrikar MJ, Aouad J, Nolan SP. Patterns of calcific deposits in operatively excised stenotic or purely regurgitant aortic valves and their relation to mechanical stress. American Journal of Cardiology;58:304-8.

[244] Wang W, Parker KH. The effect of deformable porous surface-layers on the motion of a sphere in a narrow cylindrical tube. J Fluid Mech 1995;283:287-305.